A view to a kill: using cutting edge microscopy to study predatory bacteria

Emma Elizabeth Brock

Doctor of Philosophy

University of York

Physics, Engineering and Technology

September 2022

Abstract

Bdellovibrio bacteriovorus (*B. bacteriovorus*) are a promising tool in the fight against antimicrobial resistance. With a predatory lifestyle and a wide range of prey, including antibiotic drug resistant pathogens, they are novel solution to the growing issues presented by antimicrobial resistant bacteria. Despite the proven importance of motility to *B. bacteriovorus* predation efficiency, their swimming behaviour remained little understood. The key characteristics of their motility including their re-orientation mechanisms were unknown.

This study has utilised digital inline holographic microscopy (DIHM), a novel three-dimensional and high speed imaging technique, to shed new light on *B. bacteriovorus* swimming behaviour. The cells were tracked in a range of conditions including in bulk fluid, near to surfaces and in the presence of live prey cells. The resulting trajectories were analysed to quantify the key motility characteristics, patterns, and differences in behaviour dependent on condition changes.

I have shown, for the first time, that *B. bacteriovorus* have a complex bi-phasic swimming style with run-reverse-flick re-orientations. Their motility behaviour including swimming speeds, run lengths and re-orientation angles remains consistent over a co-culturing window of 19-24 hours. However, it changes radically near to surfaces showing a significant drop in swimming speed and no longer performing a run reverse flick style re-orientation. Instead, its behaviour becomes significantly more homogeneous in both run length distribution and re-orientation angle. In contrast, in the presence of live prey cells *B. bacteriovorus* retain the run reverse flick behaviour but increase their swimming speed. This is likely a mechanism to increase predation efficiency in areas of high prey density. These results represents the first in-depth three-dimensional study of *B. bacteriovorus* motility.

ACKNOWLEDGMENTS

I would like to thank everyone who has contributed to this thesis and supported me and my research over the last four years. It has been tough going at times and without you all I would not have gotten to this stage.

Firstly, I would like to thank my supervisors Dr Laurence Wilson and Dr Christoph Baumann for their help, patience, support and advice throughout my PhD.

I would also like to thank my wider Physics of Life family at York. For all the help and support, the coffees, kindness and cake-Wednesday chats. Doing a PhD hasn't been easy but you've made it a lot more fun. A special shout out goes to Dr Adam Wollman for giving undergrad me the chance to try a biological project and setting me off down this path.

To all my wonderful friends I am so lucky to have you in my life. Ellie, Alice, Becki, Lily, Louise, Martha, and Suzy, thank you for always being there. From much appreciated puppy visits, to watching sitcoms in blanket forts, unexpected care packages, crafting sessions and copious cups of tea. You have kept me sane through these trying few years. Let's never stop going for brunch.

Max, Norbert and Stanley, I love you. (And watch out. I will have a lot more time now to crochet novelty hats).

Most of all I would like to thank my family for their endless support, especially my parents. From foundation year to PhD. There is no question, I would not be here without you.

AUTHOR'S DECLARATION

I declare that the work in this thesis was carried out in accordance with the requirements of the University's Regulations and Code of Practice for Research Degree Programmes and that it has not been submitted for any other academic award. Except where indicated by specific reference in the text, the work is the candidate's own work. Work done in collaboration with, or with the assistance of, others, is indicated as such. Any views expressed in the thesis are those of the author.

SIGNED:  DATE: 28/09/2022

'There is no point in being stupid unless you show it'

Kay Frost

CONTENTS

List of Tables

List of Figures

CHAPTER 1

INTRODUCTION

1.1 Antimicrobial resistance

Antimicrobial resistance (AMR) is a significant and growing issue and so forms the key motivation behind this research project. In particular, AMR of bacterial pathogens is associated with high mortality rates which are predicted to increase significantly in the coming years [1, 2]. Investment into new and novel solutions to AMR is urgently needed if we are to avoid a global health care disaster [1–7].

Antimicrobial resistance refers to the ability of microorganisms, such as bacteria and fungi, to evolve immunity to antimicrobial agents, for example drugs such as penicillin. This resistance is due to natural selection and adaptation, and is a normal consequence of evolution [8, 9]. In simple terms, bacteria are able to quickly and consistently adapt to varied pressures within their environment. This ability is part of what makes them such pervasive and successful organisms. The environmental pressures they encounter can include changes in temperature, food sources, or the introduction of new or harmful chemicals such as antibiotic drugs. Cells with traits that allow them to successfully adapt to these changes are more likely to survive and reproduce. Therefore these traits get passed on from one generation to the next [9]. In addition to direct genetic transfer from parent to daughter cells, bacteria are able to perform horizontal gene transfer [8]. This transfer can happen in one of four main ways: conjugation, transduction, transformation or mutation [3]. These processes can be seen in more detail in Fig. 1.1 All three processes result in the indirect gain (not from parent cells) of small quantities of DNA [8]. Horizontal gene transfer makes bacterial popula-

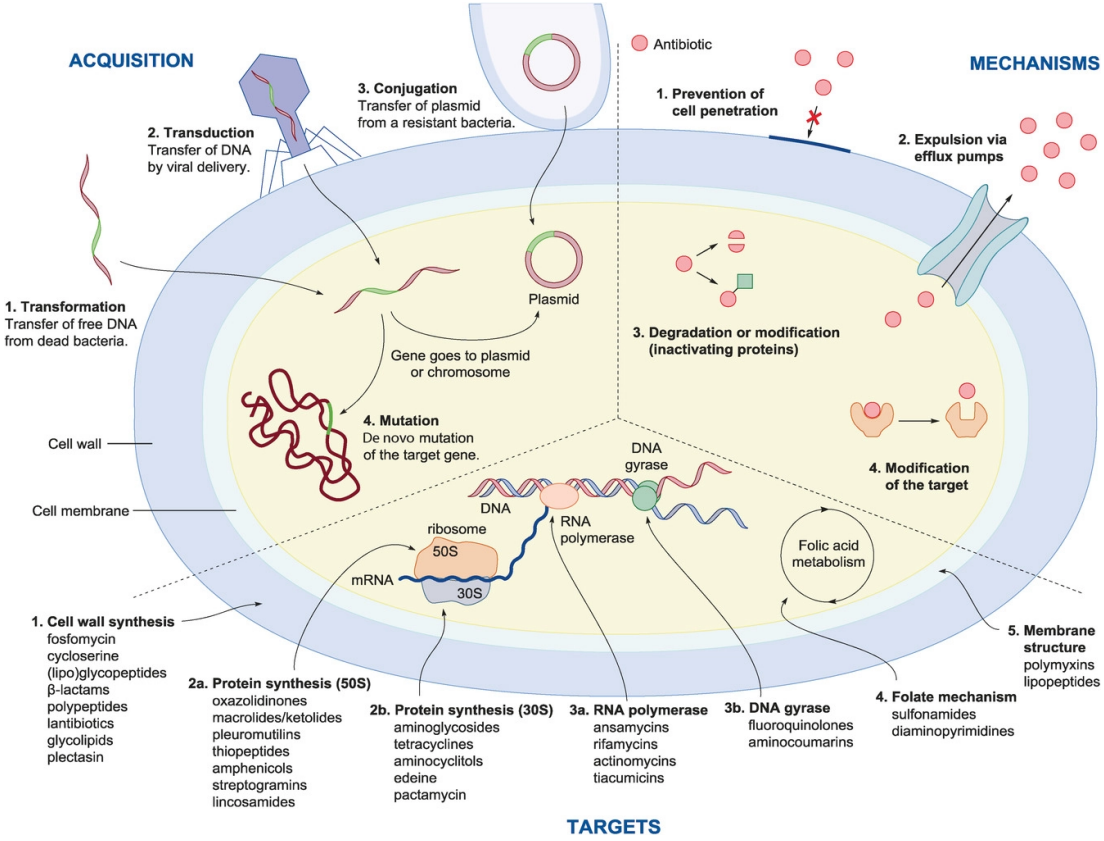

Figure 1.1: Diagram showing the five main targets for antibiotic treatments, the four main mechanisms of bacterial resistance and the four key ways bacteria acquire that resistance. Taken from [3].

tions particularly robust and is considered a more significant contributor to the development of antibiotic resistance than direct gene transfer [3, 8, 10].

The information encoded by the horizontally gained DNA enable bacteria to employ a variety of mechanisms to resist antibiotic treatments [3]. One of the key distinctions between different antibiotic treatments is if they are bactericidal or bacteriostatic. Bactericidal antibiotics kill the bacteria within the body. Bacteriostatic drugs do not kill them. Instead they stop the bacteria from growing, relying on the immune system to remove the infection [11]. Different antibiotics target different essential cell mechanisms in order to disrupt the bacterium's life cycle [12]. A range of antibiotic targets can be seen in Fig. 1.1. These targets can be structural cell features such as membrane structure or cell wall synthesis. They can also be biochemical pathway targets such as protein synthesis or RNA polymerase [3]. Bacterial cells combat these treatments in a number of different ways. This can include preventing the drug from entering the cell in the first place, expelling the drug from the cell using efflux pumps, degrading or modifying the drug once it is inside the cell or modifying the initial drug target molecule or

system [3, 13].

Whilst acquisition of AMR is a natural process, human practices have significantly accelerated AMR rates over recent years. Two of the key human driven contributors to AMR are; over-prescription of antibiotics in clinical settings and extensive use of antibiotics in intensive farming [14]. Antibiotics revolutionised medicine when they were discovered in the 1900's [15]. They proved to be very effective at combating previously untreatable conditions and continue to be a cornerstone of modern medicine. This is reflected in the fact that antibiotic consumption by daily defined doses increased 65% between the years 2000 and 2015[16]. Unfortunately the knock on effect of this greater antibiotic use is an increase in AMR. The link between antibiotic consumption and resulting AMR has been well studied, showing association across various healthcare settings in numerous countries [16]. For a specific example; in one study of urban poor in the USA, it was shown that people were significantly more likely to be colonised with methicillin-resistant *Straphylococcus aureus* (MRSA) if they had used antibiotics within the last year [17]. However, it is important to note that increases in AMR cannot be simply attributed to greater medicinal antibiotic use alone. Studies have found that a combination of factors in tandem exacerbate the problem, including lower spending on public healthcare and higher rates of private healthcare [18].

In addition to medicinal overuse of antibiotics, industrial scale use of antibiotics in farming is having a serious, negative impact. Global demand for animal protein as a food source is continuing to rise at unprecedented rates [19]. This demand is driving an increase in the use of antibiotics for the health and productivity of livestock - approximately 80% of antibiotics in the USA are utilised in farming, agriculture and aquaculture [20–22]. This is in turn causing an increase in AMR pathogens in farm animals. Concerningly these pathogens are then able to spread easily from the animals to interconnected environments including water systems, soil and humans [23, 24].

These human practices, coupled with a lack of research into new antibiotics, has caused a significant rise in problematic infections or 'super-bugs' that are resistant to several widely used antibiotics [25]. Well known examples include MRSA, *Clostridium difficle* (C. diff) and multi-drug-resistant *Tuberculosis* (MDR TB). This poses significant risks both to global health care and the economy. A recent study has shown that in 2019 1.27 million deaths were a direct result of antimicrobial resistant bacterial infection [26]. In addition, it showed a further 3.68 million deaths were due to illness in which bacterial AMR contributed,

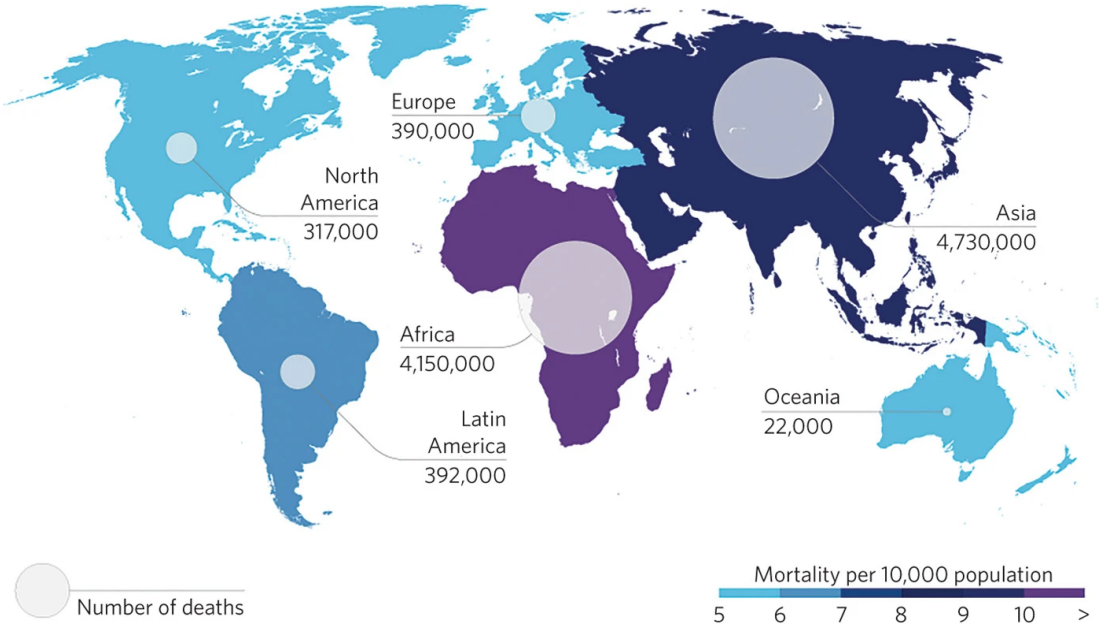

Figure 1.2: Map showing the deaths attributable to AMR every year by 2050 (per continent). Taken from [4].

making AMR one of the leading causes of death globally, in all age groups. A previous review has estimated that by 2050 around 10 million people could die per year due to AMR infections [7]. It is most likely that of these deaths an unequal portion will occur in less affluent countries as can be seen in Fig. 1.2 [4, 27]. Apart from the obvious health care disaster this poses, it is likely to have a significant, negative impact on the global economy, including food supply.

In order to tackle AMR there will need to be a global and multifaceted approach. This includes actions such as tracking AMR infections, implementing prevention and containment strategies and investment into new vaccines and diagnostic testing methods [5, 27]. Perhaps most crucially, it will be necessary to develop new and novel antimicrobial drugs and therapeutics [25]. One exciting possible alternative to traditional antibiotics is the use of living antibiotics such as predatory bacteria. A key candidate set of organisms for this is *Bdellovibrio bacteriovorus* and like organisms (BALOs). *Bdellovibrio bacteriovorus* (*B. bacteriovorus*) has be shown to be effective at predating a wide range of pathogenic bacteria including concerning multi-drug-resistant strains [28]. In addition, studies suggest that the nature of the predation cycle prevents pathogens from being able to develop a genetically stable resistance to predation, making long term resistance unlikely and giving this form of treatment a significant advantage over traditional antibiotic drugs [29, 30].

1.2 *B. bacteriovorus*

B. bacteriovorus was first discovered by Stolp and Petzold in 1962, whilst attempting to isolate bacteriophages from soil [31]. Since then *B. bacteriovorus* and like organisms (BALOs) have been found in a variety of environments including freshwater, seawater and digestive tracts [32]. *B. bacteriovorus* is a type of δ-proteobacterium (Gram negative). They are particularly small at approximately 0.8-1.2μm in length and 0.3-0.5μm wide [33] - considerably smaller than many of their prey. They are primarily obligate endobiotic predators, meaning they are reliant on prey for their life-cycle and predate by invading and replicating within prey cells [34]. *B. bacteriovorus* uses this method to predate on a wide range of Gram negative bacteria including common pathogens such as *Salmonella* and *E. coli* as can be seen in Fig. 1.3.

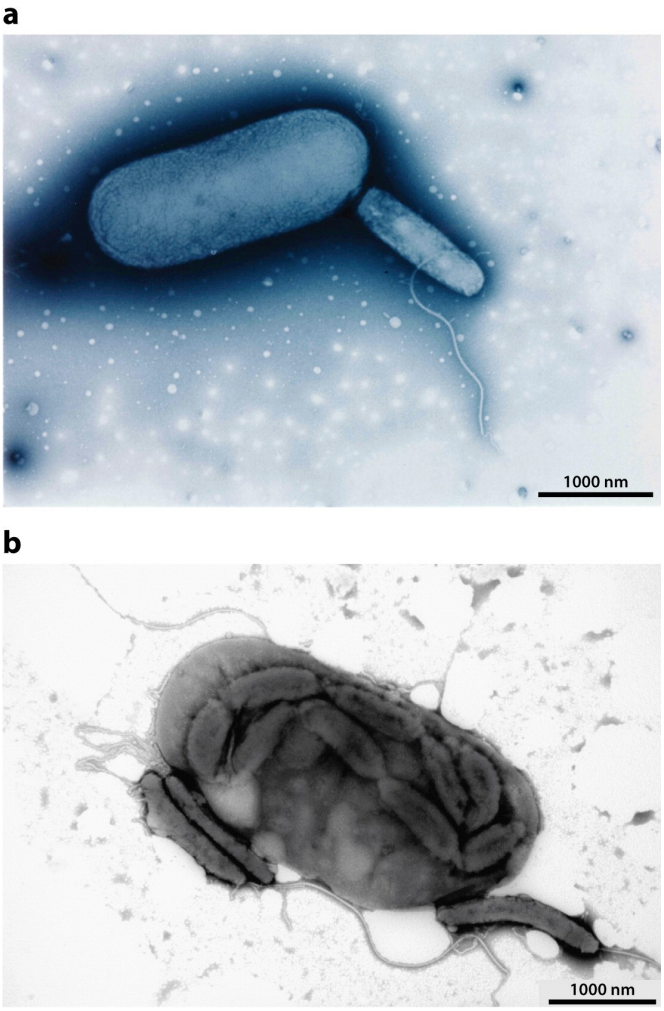

Figure 1.3: Electron micrographs showing a) Attachment of *B. bacteriovorus* to a prey cell of *E. coli* (where the larger cell is the prey), b) *B. bacteriovorus* replicating inside a prey cell, where the large grey oblong is the predator containing smaller rod-shaped *B. bacteriovorus* progeny. Taken from [35].

1.2.1 Application of *B. bacteriovorus* as an antibiotic

Awareness of AMR has grown over recent years, leading to an expanding demand for new and alternative antibiotic treatments. In particular, the idea of living antibiotics has increased in popularity. Predatory bacteria, such as *B. bacteriovorus*, are not the only players in this field, with the most notable alternative being bacteriophages. Using bacteriophages as antibiotics is not a new idea - they have been in use as a form of antibiotic since 1919 [36]. However, bacteriophages are highly specific to a strain of bacteria, requiring either detailed knowledge of infection type before treatment or a 'cocktail' of related phages in use together [37, 38]. Another significant problem with phage therapy is that prey bacteria readily evolve resistance to bacteriophages, similarly to evolving resistance to traditional antibiotics as discussed in section 1.1 [36–38]. In contrast, *B. bacteriovorus* are able to evolve alongside their prey with a heavy selection advantage going to those predators which evolve advantages in overcoming prey bacteria defences. An additional issue with phage therapy is its interaction with the human immune system. Studies have shown that the use of bacteriophages will illicit a response from the immune system. This response can vary depending on the phage in question. However it's general impact is to reduce the effectiveness of the phage overtime and with repeated use [39, 40]. This immune response can also have actively damaging impact including exacerbating existing illness such as collitis [41]. There needs to be further study of this impact of bacteriophages to fully understand the implications on use [39]. It may be possible that there are similar issues caused by the therapeutic use of *B.bacteriovorus*. However, as of yet, these type of problems have not been reported. Overall *B. bacteriovorus* has advantages over phage therapy both in terms of broad application and prevention of long term resistance.

B. bacteriovorus has become a model organism for the use of predatory bacteria in infection treatments. Therefore, it is important to note that whilst the primary motivation behind this research project is AMR in the setting of human healthcare, *B. bacteriovorus* have been found to have a wide variety of potential applications beyond this. This includes in environmental management, waste water treatment, food production and agriculture, [42–46]. This broadens the scope of the impact of this and similar research projects.

In focusing on *B. bacteriovorus*'s potential application in healthcare settings, there are some key considerations, foremost: their ability to predate pathogens and their safety of use within the human body, including interactions with the

immune system. As discussed, *B. bacteriovorus* has been shown to be effective at predating wide range of pathogenic bacteria. However, and crucially in the fight against AMR, it has also been shown to be effective at doing this within biofilms of antibiotic resistant bacteria [47, 48]. This includes biofilms formed of multi-drug resistant bacterium [49]. Biofilms are complex structures of bacterial colonies which show high resistance to antibiotics. They are known to help protect bacteria from the human immune system, giving rise to infection persistence particularly in medical settings [50]. Recent studies have shown that *B. bacteriovorus* can act as key modulators of biofilm formation in nature altering the structure and composition of films [51]. This ability to predate within and interact with biofilms makes *B. bacteriovorus* very promising for a variety of medical applications, such as minimising chronic infection on implanted medical devices.

In addition to biofilm formation, pathogenic bacteria use cell membrane modifications, including bacterial capsules, protect themselves from the human immune system. Bacterial capsules are layers which enclose the whole bacterial cell, typically coating the cell in long molecules such as long chain sugars [52]. They help to prevent detection and envelopment by immune cells in a variety of ways including physically shielding cell surface antigens and mimicking human cell surfaces [52, 53] These membrane modifications also enable them to evade bacteriophage infection and as such could also pose a challenge to detection and invasion by *B.bacteriovorus* [54, 55]. There have not been many studies to investigate the impact of bacterial capsules on *B.bacteriovorus* predation yet. The studies that have been conducted showed that *B.bacteriovorus* were still able to predate despite the presence of a capsule, as can be seen in Fig. 1.4 [56]. However, other studies have shown that some bacterial S-layers can impact predation [57]. Whilst more studies need to be done into the impact of bacterial membrane modifications and capsules on *B.bacteriovorus* predation, the results so far are promising.

Further to broad application to AMR bacterium, *B.bacteriovorus* have been tested on a range of specific human disease relevant pathogens. This includes showing their effective predation of bacteria from cystic fibrosis isolates [58] - a debilitating and often terminal lung disease that is exacerbated by bacterial infection - and predation of bacteria associated with periodontal (gum) disease. It was found that although predation efficiency decreased with the complexity of mix of bacterium from samples, they were able to predate two key dental infection pathogens (*Fusobacterium nucleatum*, and *Aggregatibacter actinomycetemcomitans*) from *ex vivo* samples [59]. This is small snapshot of *B. bacteriovorus* potential for treating human disease.

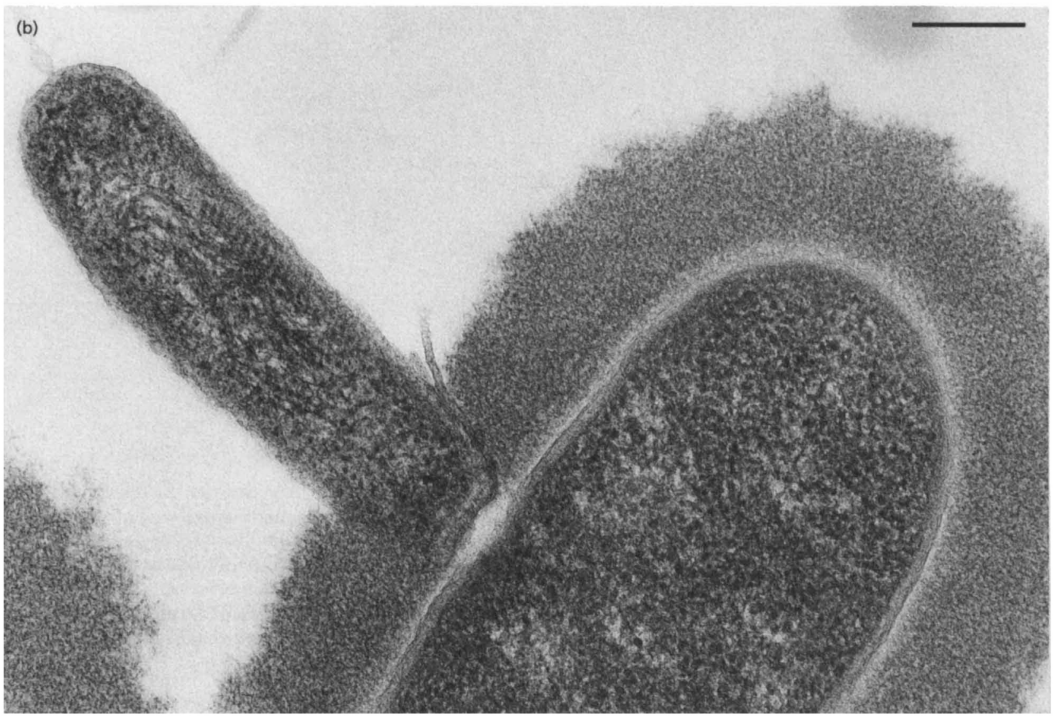

Figure 1.4: Electron micrograph showing a thin section of a capsulated *E.coli* K29 cell (the larger cell) with an attached *B.bacteriovorus* which has penetrated the capsule. Scale bar 200 nm. Taken from [56].

Beyond predating relevant pathogens *in vitro* lab settings studies have also been done *in vivo* on animal models. This includes in zebra fish larvae where *B.bacteriovorus* worked in tandem with the host immune system to get rid of *Shigella* infection [60]. Similarly, they have been shown to be safe for use in mouse models, including respiratory and intravenous inoculation, with the mouse body clearing the *B. bacteriovorus* quickly and efficiently after predation [61]. They have also been found to be non-toxic to rabbit ocular surfaces [62]. Further studies will be needed in a variety of animal models to establish their safety of use, and better understand the immune response to *B.bacteriovorus* treatment. However, studies so far have had promising results. Perhaps even more excitingly to testing in animal models, *B. bacteriovorus* have been tested on five different human cell lines and were shown to be non-cytotoxic in all cases, i.e. they did not trigger inflammation [63].

As the above examples demonstrate, the potential for application of *B. bacteriovorus* in medical settings is clear. However, the use of *B. bacteriovorus* as a treatment in human patients requires a deep understanding of their behaviour including all stages of their complex life cycle and the mechanisms they use for predation. There are still gaps in our understanding which require further study.

1.2.2 *B. bacteriovorus* life cycle and predation mechanisms

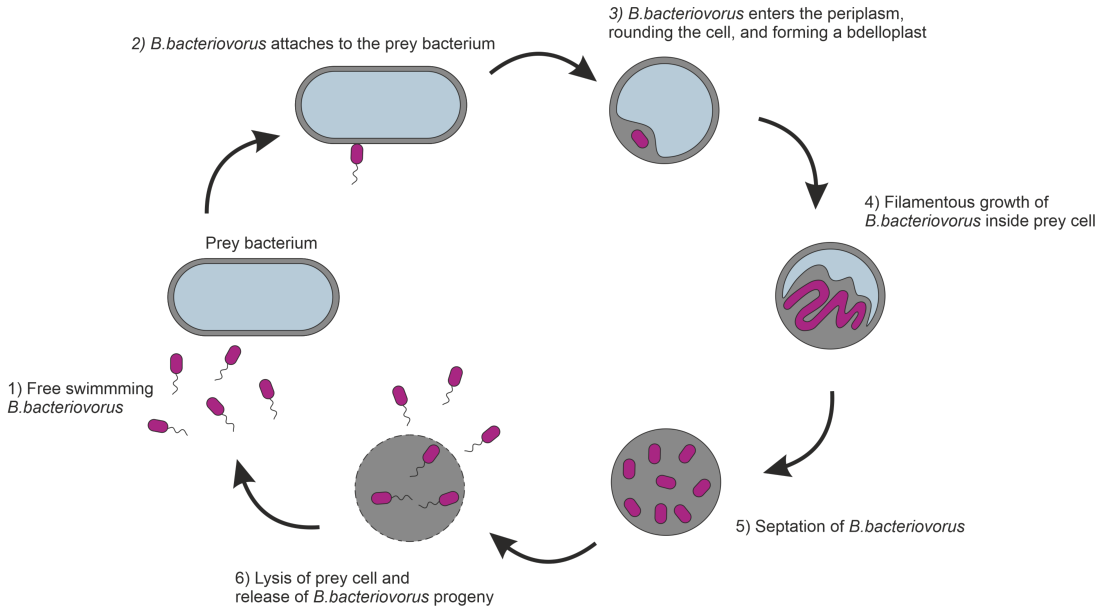

Figure 1.5: Schematic diagram depicting the predatory lifecycle of *B. bacteriovorus*. The key stages include: 1) Free swimming attack phase cells, 2) Attachment to prey cell membrane, 3) Prey cell invasion and bdelloplast formation, 4) Prey consumption and *B. bacteriovorus* growth, 5) Septation of daughter progeny cells, 6) Lysis of prey cell and release of progeny.

The basis to *B. bacteriovorus*'s application as an antibiotic is its fascinating predatory life cycle, as can be seen in Figs. 1.5 and 1.6. All BALOs have a predatory aspect to their life cycle. Some strains of *B. bacteriovorus*, such as *Tiberius*, can alternate between slow axenic growth and predation. However, most are obligate predators (including the HD100 strain used throughout this study) [32].

The *B. bacteriovorus* life cycle starts with free swimming attack phase cells. These cells navigate through their environment until they encounter a prey cell. When an attack phase *B. bacteriovorus* makes contact with a prey cell it attaches itself to the outside of the cell surface, this is reversible initially - there is a short, 1-5 min recognition period during which *B. bacteriovorus* is able to distinguish between living Gram negative prey cells and other elements in its environment such as dead cells, Gram positive cells or debris [64]. If it detects a live prey cell it will permanently attach to the outside of the prey membrane, if not, it will detach and swim off to find viable prey [65] [64]. This attachment process takes approximately 10-30 min [66].

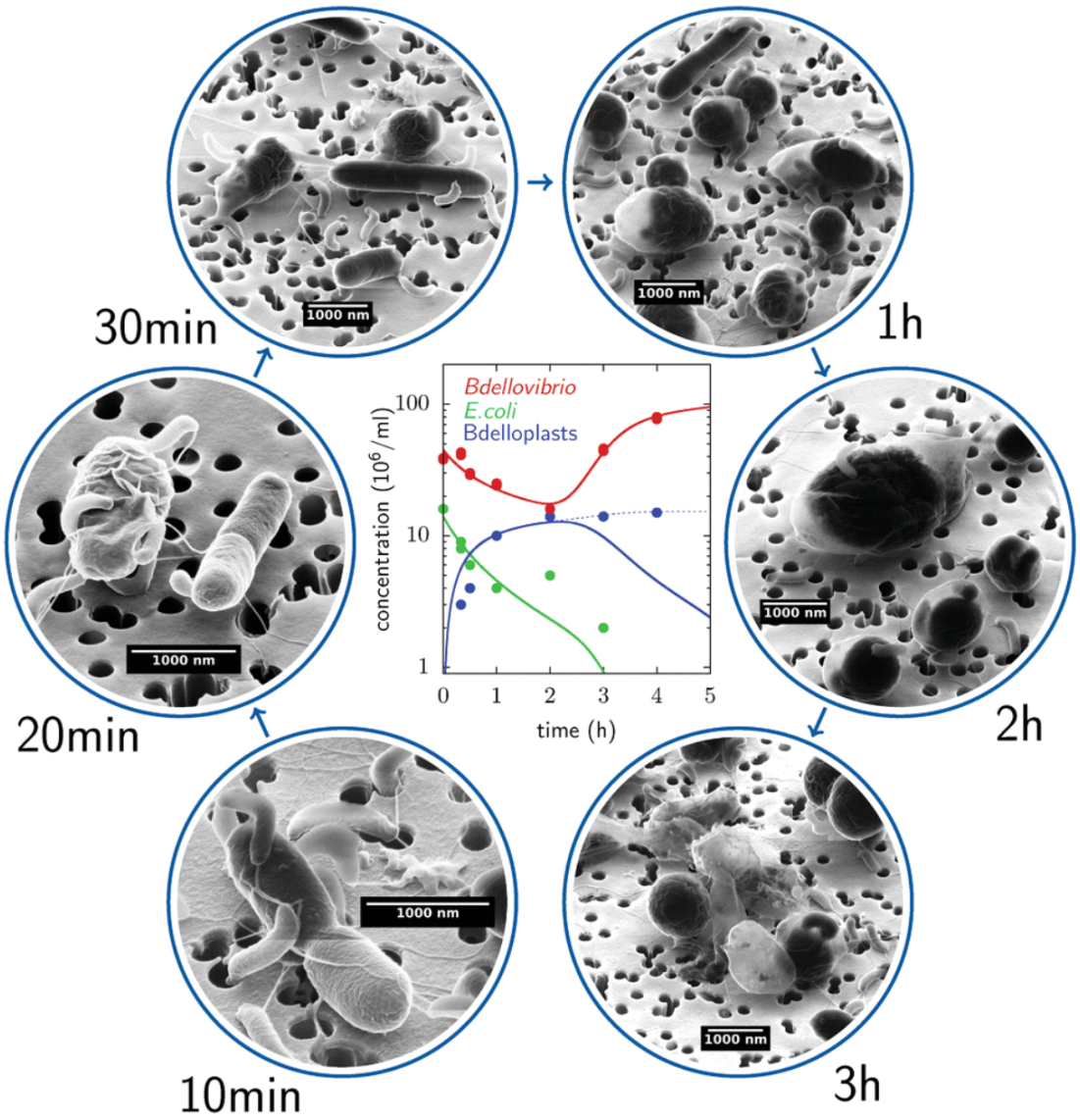

Figure 1.6: Helium-ion microscopy (HIM) images showing the *B. bacteriovorus* life cycle, whilst predating *E. coli*. Images clearly show the attachment of *B. bacteriovorus* to prey cells (10-30min), the formation and evolution of B. bacteriovorusplasts (1h) and the consumption and lysis of prey cells (2-3h). The plot in the centre shows the predation process predicted by a numerical model (solid lines) fitted to the cell count by counting cells in phase-contrast micrographs, where the dashed line is the sum of intact and already lysed bdelloplasts in the model. Taken from [66].

Once attached to the cell surface *B. bacteriovorus* begins the process of penetrating into the prey cell membrane. It uses a secretion of hydrolytic enzymes to create a small pore (around 200 nm diameter) in the prey cell membrane through which it squeezes itself [35, 67]. The predator then locates itself between the prey cell membrane layers within the periplasm. This process is remarkably fast taking only 1-2 min [35]. Various studies have shown that *B. bacteriovorus* have type IV pili which are essential to this process of prey cell attachment and invasion, likely aiding in surface adhesion and potentially using twitching or ratcheting mechanisms to help force the predator through the pore opening [65, 67, 68]. Once within the periplasm layer the *B. bacteriovorus* neatly seals the pore behind it using a form of LPS plug which is not yet well understood [35].

Once safely inside the prey cell periplasm *B. bacteriovorus* attaches itself to the cytoplasmic membrane causing the cell to round, forming a spherical structure known as a bdelloplast [69]. The bdelloplast becomes the home for the predator as it uses a sequential, orchestrated arsenal of predatory hydrolytic enzymes and nucleases to degrade the contents of the prey cell including DNA [70–72]. The degraded cell contents serves as a source of energy and nutrients which *B. bacteriovorus* uses to grow filamentously [69].

After the prey cell has been fully consumed the predator septates into multiple daughter progeny cells, typically between 4-6 cells per prey cell [73]. These daughter progeny cells grow their own flagellum, exit the prey cell membrane through discrete pores, leaving behind a ghost cell [73]. The daughter progeny are initially shorter than mature attack phase cells, however they lengthen and mature, and subsequently continue the predatory cycle [73] . As can be seen from Fig. 1.6 the entire life cycle from attachment to prey lysis takes about 3 h.

Genetic studies of *B. bacteriovorus*, looking at the predation abilities of a variety of mutants, have highlighted some key components to *B. bacteriovorus* predation. Two of the most significant genes groups for predation efficiency are for pilus and motility [74]. However, *B. bacteriovorus* free swimming motility remains poorly understood. The basic characteristics of their swimming, such as re-orientation mechanisms, are largely unknown and so any impact these characteristics have on *B. bacteriovorus* ability to find prey cells within their environment are also unknown. The focus of this project was to study *B. bacteriovorus* motility in previously unseen detail. The aim was to shed light on their swimming characteristics, contributing to the overall understanding of their predatory behaviour.

1.3 Bacterial motility

There is a fascinating diversity in bacterial motility, including swimming, crawling and swarming behaviours. These behaviours play an important role in the life cycle of bacteria, such as aiding in biofilm formation, finding nutrients in their environments and dispersal of progeny cells [75].

This section introduces the key concepts that underlie bacterial swimming behaviour including Reynolds numbers, Brownian motion, bacterial flagella and chemotaxis. It also outlines what we already know about *B. bacteriovorus* swimming behaviour and the areas to be investigated.

1.3.1 Micro-scale swimming and Reynolds numbers

One of the most significant differences between swimming on the microscale of bacteria compared to the macroscale of organisms such as fish is the relationship between the inertial forces (necessary to accelerate masses) and the viscous forces (the resistance of fluids to shear). This relationship can be described using a dimensionless parameter called the Reynolds number (R), where:

$$R = \frac{LV\zeta}{\eta}, \tag{1.1}$$

where L is the linear size of the particle (in the case of a bacterium the length of the cell), V is the velocity of the particle, ζ is the specific gravity of the fluid and η is its viscosity [76].

Crucially, bacteria experience very low Reynolds numbers compared to those at the macroscale. Macroscale organisms such as medium sized fish (for example a dogfish) experience Reynolds numbers of $R \approx 10^5$ whereas bacterium experience $R \approx 10^{-5}$ [76–78]. In terms of the forces involved this shows that there is negligible inertia meaning that bacteria cannot coast - i.e. when they stop actively propelling themselves forward they almost immediately stop travelling in that direction [76]. This, amongst other effects, has important implications for bacterial swimming strategies. For example, the symmetry of the flow around a bacterium makes that flow effectively reversible. Therefore, in order to make 'progress' at low Reynolds numbers bacteria must have an asymmetrical element to their swimming pattern [79, 80].

1.3.2 Brownian motion and diffusion

Brownian motion is named after the man who first observed the phenomenon - the botanist, Robert Brown. In 1828 he spotted that when pollen grains are suspended in water they move perpetually, appearing to dance around randomly [81]. At the time this was a controversial discovery and it wasn't until 1905, when Einstein related Brownian motion to the kinetic energy of a particle (in turn helping to confirm that matter consists of discrete particles), that the true significance of this discovery began to be appreciated [76].

Brownian motion causes particles in an aqueous medium to move in the motion of a random walk, i.e. there is an equal likelihood of them moving in any given direction over a chosen time step. The key here is that this random walk style Brownian motion causes diffusion. In turn, diffusion drives many biological processes and has a significant impact on bacterial swimming behaviour.

There are two types of diffusion relevant to bacterial motion: translational and rotational. Translational diffusion relates to the uniform movement in space of a particle (non-rotational), with the coefficient of this giving a measure of how quickly particles can disperse in a given medium. The translation diffusion coefficient (D_t) is given by:

$$D_t = \frac{k_B T}{f}, \tag{1.2}$$

where k_B is the Boltzmann constant, T is the absolute temperature, f is the frictional coefficient of the particle. The friction coefficient (f) of an object can be found using equation1.3 below:

$$f = \frac{\vec{F}}{\vec{v}}, \tag{1.3}$$

where $\vec{F}$ is the force and $\vec{v}$ is the velocity of the particle.

In the case of bacterial swimmers that exist in the regime of low Reynolds numbers, the inertia of a particle is negligible, meaning that the viscous drag is by far the most dominant force present and is approximately equal to the frictional coefficient. From hydrodynamics we can use Stokes' law to find this drag force and so the friction coefficient:

$$\vec{F_D} = 6\pi\eta\alpha\vec{v} \approx f\vec{v}, \tag{1.4}$$

where η is the viscosity of the medium and α is the radius of the particle.

Combining equations 1.2 and 1.4 gives us an equation for the translational diffusion coefficient of a particle known as the Stokes-Einstein equation which can be applied in biologically relevant settings:

$$D_t = \frac{k_B T}{6\pi\eta\alpha}. \tag{1.5}$$

The rotational diffusion of a particle can be calculated in a similar manner to the translational diffusion. However, instead of relating to the uniform movement of a particle in space, it relates to the rotation of that particle in space about a given axis. There is a slightly different frictional coefficient in this case [76], resulting in, for a spherical particle of radius α, a rotational diffusion coefficient (D_r) where:

$$D_r = \frac{k_B T}{8\pi\eta\alpha^3}. \tag{1.6}$$

It is important to note that the equations above describe the motion of a spherical object. A large number of bacteria are not spherical. Instead they are often rod or rod-like - the *B.bacteriovorus* cells used in this study are comma shaped and the *E.coli* prey cells are rod shaped. The diffusion and micro-hydrodynamics of anisotropic objects such as rods is significantly more complex than that of spheres. Their behaviour is dependent on variety of factors, including their shape parameters and the viscoelasticity of their surroundings [82, 83]. In the case of this study, the diffusion of spherical objects give a sufficient approximation of cell movement to enable successful trajectory analysis.

Both translational and rotational diffusion have a significant impact on the strategy bacteria use to survive. Not all bacteria are motile, some passively use diffusion to their advantage, others use active motility strategies to optimise their life cycles. The combination of low Reynolds number and diffusion means that there is little point to a bacterium searching its local environment for individual useful molecules, it will gain as much by passively waiting to bump into them. However, there is a point to finding an environment with higher concentrations of useful molecules - increasing your likelihood of encountering them [79]. In the case of *B. bacteriovorus*, where their source of nutrients may also have active swimming abilities, the situation becomes very much more complex.

1.3.3 Bacterial motility mechanisms

There are an assortment of mechanisms involved in bacterial motility. The majority of motile bacteria use some form of external appendage to enable movement, these include pili and flagellum. The most studied and well understood form of bacterial swimming is the planktonic state, where cells use one or more flagella to power their motion. Fig. 1.7 shows some examples of bacterial flagella including peritrichous (flagella all over the cell body), amphitrichous (one flagellum present at each pole end of the cell) and monotrichous (one flagellum at one pole end of the cell).

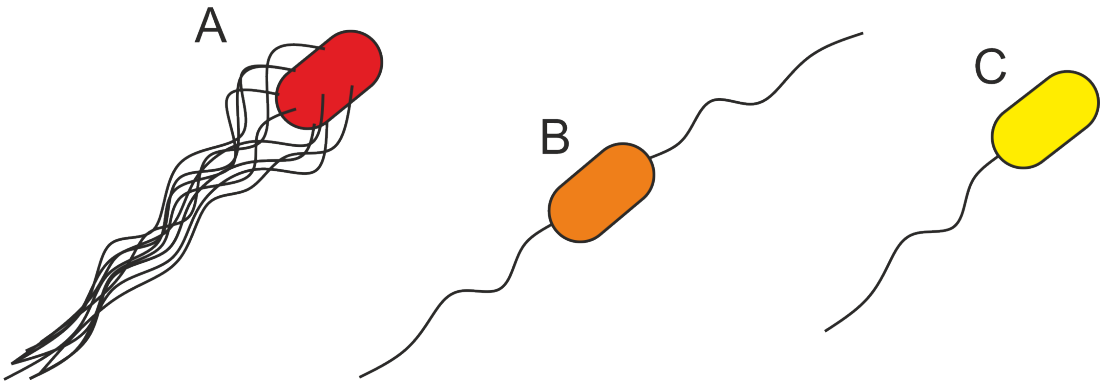

Figure 1.7: Diagram showing different types of bacterial flagellation. *A* Peritrichous: flagellum present all over the cell surface, for exaple *E. coli*. *B* Amphitrichous: two flagellum, one at each pole of the cell, for example *Campylobater jejuni*. *C* Monotrichous: a single flagellar location at one pole of the cell, for example *B. bacteriovorus*.

Bacterial flagella are formed of a long (up to 15 μm), thin (≈ 20nm), semi-rigid filament attached to the cell body via a flexible section known as a hook [84] . The base of the hook is joined to a rotary motor which is embedded in the cell body as can be seen in Fig. 1.8c. This rotary motor is often reversible and is typically driven by the movement of protons or sodium ions - know as the proton or sodium motive force [85–87].

Free swimming bacteria typically have a pattern of motion of a random walk - with long straight sections, known as runs, punctuated by re-orientation events (when the cells change direction). The style of re-orientation a bacterium performs is mostly dependent on the type and number of flagella it has. This leads to is a wide variety of swimming styles. Some bacterial cells, including *E.coli* and *Salmonella enterica serovar Typhimurium* (*S. Typhimurium*) can switch their flagella motor direction [88]. This motor switching causes the cell swimming direction to change and is driven by a system of sensory and signalling proteins within the cell [87]. This pattern is known as run and tumble swimming, and is illustrated in Fig. 1.8 a and b.

One interesting example of bacterial swimming that also employs switching direction of the flagellar motor is the 'darting' motion of *Campylobater jejuni* [89]. In this case, the bacterium are amphitrichously flagellated - have one flagellum at each pole of the cell. These opposing flagellum rotate, resulting in one wrapping around the cell body in the direction of travel. When they switch the rotor direction this flagellum wrapping switches - one unwraps and the other wraps causing a sharp change in direction [89].

An additional example of motor reversal driving a swimming pattern is the'run-reverse-flick' behaviour of *Vibrio alginolyticus* [90, 91]. Similarly to *B. bacteriovorus*, *Vibrio alginolyticus* are monotrichous, with their single flagellar located on a pole end of the cell. When the cell switches the direction of the motor, it reverses it's path. This puts a force on the hook section of the flagellum, which buckles and cause a secondary turn of approximately 90 °[90, 91].

In contrast to the above examples *Rhodobacter sphaeroides* can only rotate their flagellar in one direction - they have a unidirectional rotary motor [92]. They have one lateral flagellum which they intermittently stop rotating. This results in a run-stop-run swimming style. When the flagellum is not rotating the cell body will reorient in the environment due to Brownian motion. Interestingly, the coiling of their relaxed flagellum may also contribute to their angular position change [92].

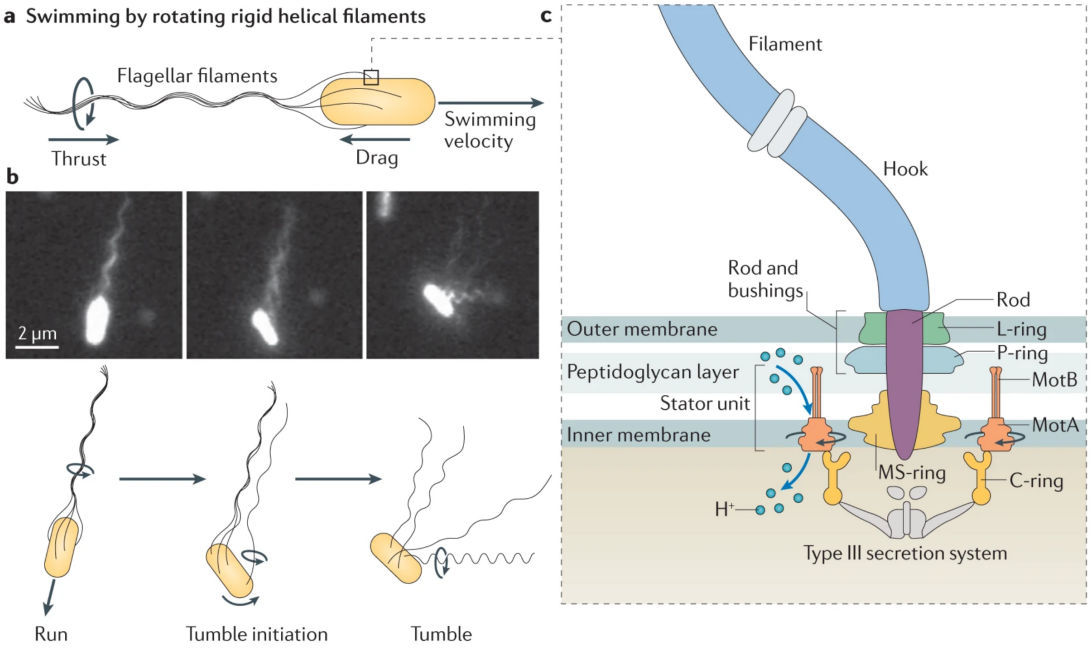

Figure 1.8: Series of diagrams illustrating *E. coli* swimming technique. *a:* Schematic diagram illustrating the swimming of a peritrichously flagellated bacterium such as *E. coli*. *b:* Set of epifluorescence images showing the 'run-to-tumble' transition. In frame one, all flagella rotate counterclockwise (CCW), resulting in the bundling of the flagellar filaments and therefore straight swimming. In frame two, one motor has switched from CCW to clockwise (CW), and the bundle is beginning to come apart. In frame three, the CW filament has transformed from normal to semicoiled and all the filaments have unbundled, resulting in a 'tumble' which is an active reorientation event. *c:* Schemtic diagram showing the architecture of the *E. coli* flagellar motor. Taken from [75]

Similarly to *Rhodobacter sphaeroides*, *Sinorhizobium meliloti* also have unidirectional roatry motors [93]. However, they have a bundle of flagellum, similar to *E.coli*. This results in them employing a different motility strategy to both *Rhodobacter sphaeroides* and *E.coli*. Instead of stopping their flagella motors or switching them, they asynchronously modulate their speed. This induces a slowing down of their swimming, resulting in a smooth turn which reorients the cell [93, 94].

In addition to these free swimming behaviours, a number of bacteria also use surface based motility including swarming, gliding and twitching. Swarming motility is a coordinated group movement across solid or semi-solid surfaces, that is mediated by flagellar [95]. It involves cell to cell communication, and often an increase in flagellar numbers, a change in cell shape and specific cell surface secretions [95]. The biological implications of swarming are still not well understood. However, it is known that swarming can increase antibiotic resistance

and is often linked to pathogenicity [95]. Gliding and twitching behaviour are also linked to pathogenicity, partly through their role in biofilm formation [96]. Twitching is mediated by the extension and retraction of pili on the cell surface, as is some types of gliding motility. However the mechanisms of gliding are generally less well characterised [97]. All three behaviours enable bacterial cells to spread across surfaces, with benefits for the bacterial colony.

Despite the wide variety of bacterial motility styles the overall outcome is similar - bacteria use motility to actively respond to their surroundings. This includes transient features such as chemical gradients and other stimuli including light. They are able to alter their behaviour to bias their motility based on such stimuli. In the case of free swimming cells they change the length of their runs (the frequency of their re-orientation events). For example *E. coli* will lengthen its runs in response to a gradient of nutrients in a fluid, causing the cells to swim up the gradient and populate the area of higher nutrient density [98, 99]. This type of behaviour is called chemotaxis and is found in many different bacterial species [100]. Bacteria can also show changes in motility in response to other chemical signals including oxygen (aerotaxis) or non-chemical stimuli such as light (phototaxis) [101].

In addition to active motility responses, bacterial cells can have their swimming behaviour passively changed by physical obstacles in their environments. In particular, it is known that bacterial cells have a tendency to congregate on or become trapped by surfaces and defects, such as large particles in their surroundings [102–106]. *E. coli* have been most studied and have been shown to swim in large circles on surfaces, repressing re-orientations and remaining in trajectories parallel to the trapping surface [103, 104]. A number of studies including simulations have been done to try to understand this surface trapping behaviour. Most concluded that this is primarily due to the hydrodynamic interactions between the bacterial cells and surfaces, including collisions with the surface, increased viscosity near to surfaces and Brownian motion [104, 107–109]. Others have gone on to suggest this surface trapping behaviour could be commandeered, using modified surfaces, to direct bacterial swimming [110].

1.3.4 Models of bacterial motility

Bacterial motility poses many biological questions which could benefit from modelling of physical characteristics. As such, various aspects of bacterial motility have been simulated and modelled; from bacterial behaviour at surfaces and the mechanics of flagellum motion, to space searching or foraging strategies [84, 107, 108, 111–116]. The later is of particular interest to this project. Similarly to other predatory organisms, there is significant pressure for *B.bacteriovorus* to optimise it's searching strategy to find prey more quickly and therefore increase it's predation efficiency. Whilst, the system of *B.bacteriovorus* swimming with a variety of motile prey is relatively complex, much research has been done into general foraging and searching strategies. These studies may help to give some insight into the underling physics governing *B.bacteriovorus* motility.

The basic premise of foraging theory is that organisms are aiming to maximise their intake of energy per unit time of searching [117]. In the case of *B.bacteriovorus*, maximising their number of encounters with prey cells in a given time. Organisms will achieve this by optimising the way they move through their environment - their searching patterns. In general, these patterns of movement are diffusive and can be described by a random walk. As briefly discussed in section 1.3.3, a random walk consists of straight sections (runs) punctuated by turning events where organisms will reorient randomly, with each run having a different direction [80]. Trying to model and understand this searching behaviour becomes more complicated when you consider that organisms have mechanisms by which they sense and respond to their environment and forms of memory of where they have been [118].

As discussed in section 1.3.2, diffusion mechanics are key to bacterial swimming behaviour. Bacterial swimming trajectories are generally referred to as anomalous diffusion or anomalous transport. Anomalous transport is a stochastic phenomenon that has non-normal diffusive motion (not Brownian motion) ie. the relationship between the mean squared displacement and time is non-linear [119–121]. The motion of active swimmers such as bacteria is super-diffusive anomalous transport - where the scaling exponent of mean squared displacement is between 1 and 2 (see section 2.7.5.3 for a detailed description of mean squared displacement).

A variety of different anomalous transport models have been investigated for their properties and applications. For an extensive list of examples see reference [121] The current leading model for foraging and searching behaviour in biological

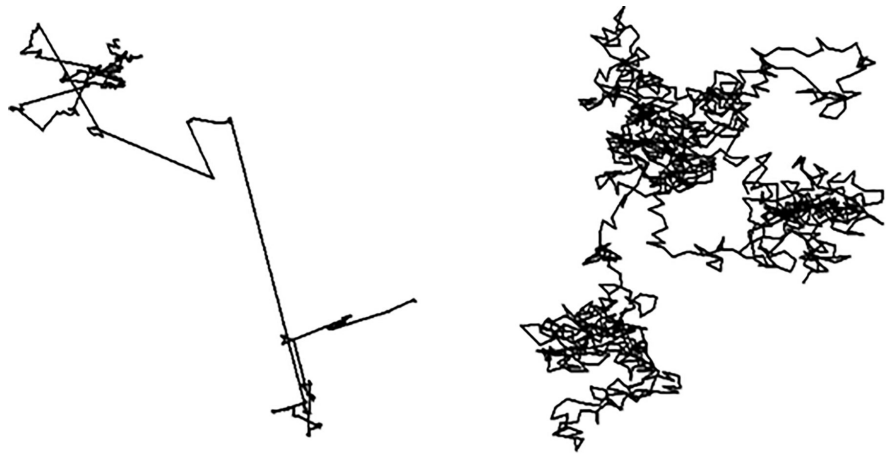

Figure 1.9: Example plots of a Lévy walk (left) and a Brownian walk (right). The Brownian walk is comprised of many similar length runs. In contrast the Lévy walk contains significantly greater range of run lengths which make a dominant contribution to the overall length of the movement pattern. Taken from [118]

settings, including bacterial motility, is Lévy walk [118].

Lévy walks, also known as Lévy flights, are patterns which were initially studied in a purely mathematical context [122]. It wasn't until the 1980's that their potential application in biological settings was recognised by Schlesinger and Klafter [123]. A Lévy walk is a random walk where the run times have a power law distribution with a heavy tail as described in equation 1.7 below:

$$P(l) \approx l^{-m} \tag{1.7}$$

where $1 < m < 3$ [124]. This power law distribution results in trajectories formed of clusters of many short runs interspersed with longer runs. This clustered pattern is repeated across all scales leading to fractal patterns that do not have a characteristic scale [118]. Fig. 1.9 shows examples of both a Brownian walk (right) and a Lévy walk (left). It clearly demonstrates the impact of this power law distribution - showing how the occasional longer run times make a significant contribution to the nature of the trajectory [118].

Lévy walks have been shown to have searching advantages over normal diffusive motility patterns due to their super-diffusive and scale free nature [125]. The pattern minimises the mean distance travelled before encountering a target (for example a prey cell), thereby optimising search efficiency [124, 126]. Lévy walk patterns of movement have been seen in a variety of macro-scale foraging and predatory organisms including, sea birds, honeybees, fruit fly, spider monkeys, and

jackals [126–130]. They have also been seen in microscopic organisms including swimming and swarming bacteria and plankton [124, 131–134]. In the case of swimming *E.coli* cells, the Lévy walk pattern has been shown to be a result of random fluctuations in the *E.coli* chemotaxis pathway, which increase its environmental searching efficiency [124, 131].

There has been some controversy around Lévy walks and their occurrence in biology. Some have suggested that organisms have evolved to have Lévy walk patterns to their motility because it is one of the most efficient ways to search an environment [125, 135]. However, others have argued that Lévy walk can emerge due to other innocuous process, and once achieved there is a selection pressure against losing it due to its advantages in searching and foraging [136]. Further research needs to be done to fully understand the true link between Lévy walks and biological foraging.

In general, the modelling discussed above gives some interesting insight into possible *B.bacteriovorus* environmental searching strategies. However, it is important to note they are typically based on idealised or simplified systems. In reality, if *B.bacteriovorus* is applied in the body, these systems become substantially more complex, with many interacting factors that will impact on cell behaviour.

1.3.5 *B. bacteriovorus* motility

B. bacteriovorus is highly motile, with average swimming speeds of between 30-60μms^{-1}, however it has been reported to swim as fast as 160μms^{-1} [137]. Its swimming is driven by rotation of a single, polar, membrane sheathed, flagellum composed of 6 key flagellar filament proteins (flagellins) [71, 137, 138]. This flagellum is approximately 28nm in thickness, and typically 3-4μm long [138, 139]. It has a complex dampened wave form morphology with an unusual tapered end section [138, 140]. It has been shown that, whilst not necessary for predation if applied directly to prey cells, *B. bacteriovorus* flagella are crucial to predation efficiency in free swimming environments, suggesting they play an important role in locating prey cells [137].

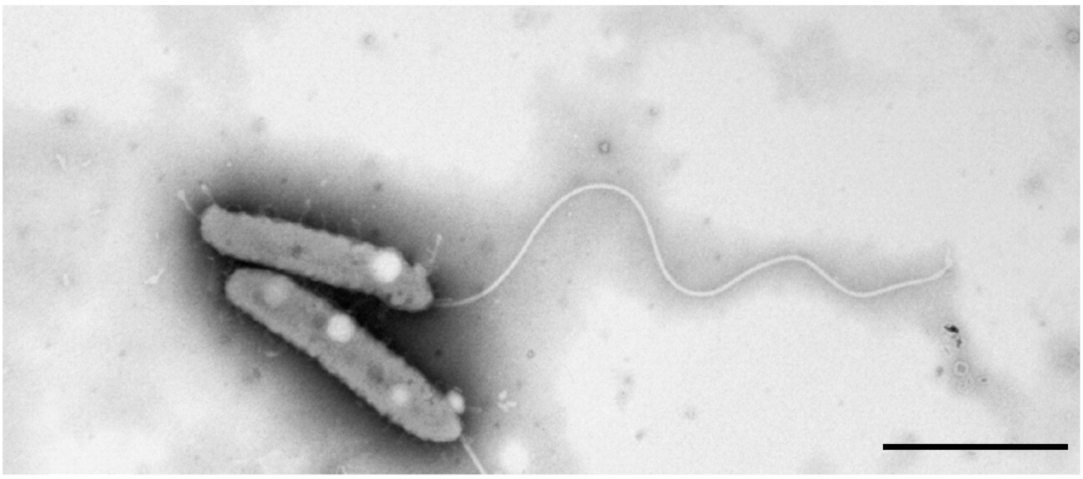

Figure 1.10: Electron microscopy image of *B. bacteriovorus* showing the flagellum. The bar represents 1 μm.Taken from [139].

There have been some interesting studies into *B. bacteriovorus* motility changes dependent on environmental viscosity, giving mixed results. One study using polyvinyl-pyrrolidone (PVP) showed that at high viscosities *B. bacteriovorus* swimming speed was reduced by about 20%. This caused a slight delay in predation, however, in total, similar amounts of predation were observed as in non-viscous media [141]. Another study using polyethyl-ene glycol (PEG) solutions and dextran found that the two different polymers (linear and branched respectively) had distinctly different effects. At low (1%) PEG concentrations *B. bacteriovorus* swimming speeds and predation rates significantly increased - the swimming speeds by 31%. However, at higher concentrations of PEG (5%) swimming speeds and predation were significantly negatively impacted with predation being completely stopped at the highest concentrations (10%) [142]. In contrast, the dextran solutions showed a simple decay in swimming speed and predation rates with viscosity increases [142]. The results from these studies are mixed, with the different polymer rheologies likely playing a part in this, however, the standout result is that swimming speeds are intrinsically linked to predation rates. In all cases, as swimming speeds increased so did predation rates and as they decreased so did predation rates. This very clearly demonstrates how essential motility is to the *B. bacteriovorus* predatory life-cycle.

Given how essential motility is to predation, there has been significant and ongoing debate as to how *B. bacteriovorus* find prey in their environment. This includes if they are passive or active hunters, i.e. if they swim around and randomly bump into prey cells, or if they use mechanisms to increase their chances of encountering prey, or even actively hunt individual cells. It is known that *B.*

bacteriovorus perform chemotaxis towards a variety of chemicals such as certain amino acids, yeast extract and various other molecules including acetate [143–145]. A study has also shown that methyl-accepting chemotaxis proteins (MCPs) do play a role in predation: mutant cells without the genes encoding for MCPs were less efficient predators [146]. In addition, a study of *B. bacteriovorus* moving on surfaces has suggested that they use slow gliding motility to scout for sessile prey on surfaces [147]. This evidence combined suggests that they do perform some form of chemotaxis driven active hunting, i.e. similar to *E. coli* seeking out high concentrations of nutrients, *B. bacteriovorus* seeks out high concentrations of prey cells. The benefit of this kind of behaviour in low nutrient environments would be significant [69]. However, a study of *B. bacteriovorus* chemotaxis towards live prey cells demonstrated that they only performed chemotaxis towards particularly high concentrations of other bacterial cells (whether prey or not), and not to low concentrations, concluding that they don't use chemical attractant to find prey [148]. A recent study agreed, showing that *B. bacteriovorus* do not perform chemotaxis towards individual prey cells, suggesting instead that they have a passive hunting method that capitalises on hydrodynamic effects [108]. The data from the study indicates that hydrodynamic forces cause prey and predator to co-localise onto surfaces and defects. This is turn increases the prey density and reduces *B.bacteriovorus* search from three to two dimensions [108]. The combined evidence suggests that both biochemical and hydrodynamic interactions are important to *B.bacteriovorus* predation in bulk fluid and surface environments.

It is clear that the flagellum and the resulting cell motility have a key role to play in the predation success of *B. bacteriovorus*. However, the nature of this role remains unclear. Many of the previous studies have focused on flagellum structure and all motility studies of free swimming *B. bacteriovorus* cells have only considered movement in two dimensions at any given time. This has typically been in the focal plane of the microscope without considering depth (z) information. The complexity of *B. bacteriovorus* motility including the fundamental characteristics of their swimming style are unknown. This project has aimed to reveal the fundamental characteristics of *B. bacteriovorus* motility by investigating its swimming behaviour in three dimensions using digital inline holographic microscopy.

CHAPTER 2

METHODS: MICROSCOPY TECHNIQUES AND IMAGE ANALYSIS

2.1 Introduction

The invention of microscopes has had an immeasurable impact upon science and society. From the discovery of micro-organisms, to the understanding of human physiology, microscopy continues to fuel and enable fascinating and useful research.

One of the earliest known microscopes was made by Dutch glasses maker, Zacharias Jannsenn (1580-1638) [149] . These early compound microscopes suffered from many abberations mostly due to the quality of the glass used. Antonie van Leeuwenhoek(1632-1723) bypassed some of these abberation issues by using single lens microscopes made from glass lenses he ground and polished himself [150]. The lens was of remarkable quality for the time and allowed him to observe a wide range of subjects previously unseen by the human eye. His work included observing plant and animal tissues such as feathers, scales and spermatozoa. Perhaps one of his most significant discoveries was the observation of microscopic organisms or as he called them "animalcules" [151].

Since then microscopy has developed significantly: from brightfield and dark-field illumination to fluorescence, electron, and holographic microscopy, scientists continue to push the boundaries of what is observable and therefore our knowledge of the world around us.

2.2 Brightfield illumination microscopy

Brightfield is one of the simplest forms of microscopy illumination. It was used by most early microscopes and continues to be a staple feature in biological and teaching laboratories. Brightfield techniques underlie a number of modern microscopy methods including holography.

At its most basic a brightfield microscope consists of three key lenses: a tube lens, an objective lens and an eyepiece lens. A bright light source shines light through a sample specimen and onto the objective lens. The objective lens magnifies the image of the sample, which then passes through the tube lens focusing the magnified image at an intermediate focal plane. The eyepiece lens allows the user to view this magnified image or, alternatively, the light can be directed to a camera for recording.

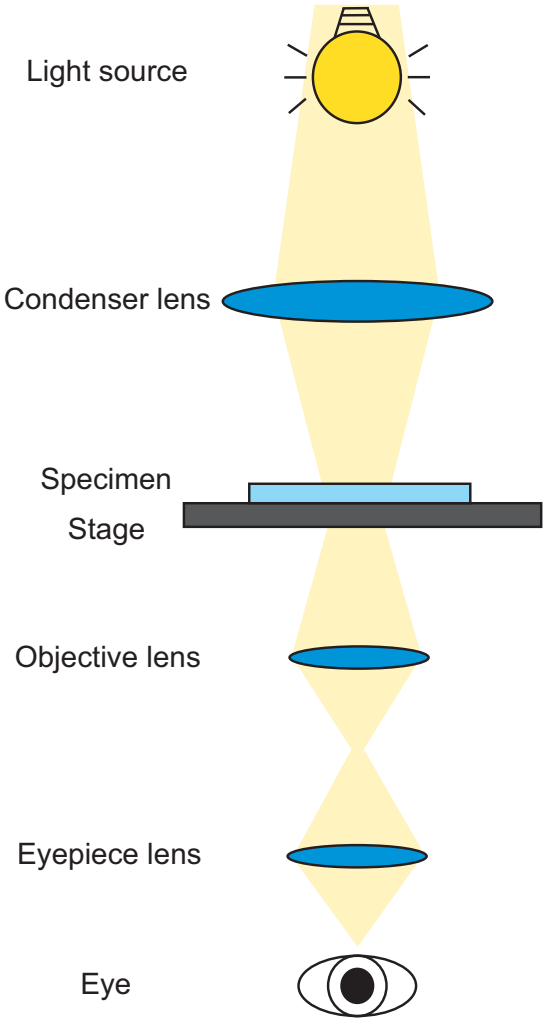

Figure 2.1: Schematic diagram showing the optical components and corresponding light path for a simple brightfield microscopy set up.

Typical modern laboratory set ups are as can be seen in Fig. 2.1, where the sample is placed between the objective lens and a condenser lens. The condenser lens changes the sample illumination from an approximately collimated beam to a ray cone, focusing the light onto the sample. This increases resolution of the microscope by allowing the objective to capture light rays from larger diffraction angles. Essentially the condenser lens increases the effective aperture of the imaging system (see section 2.3 for more detail on lens apertures and resolution) [152]. Using a condenser lens also enables precise control of the sample illumination - it is possible to focus the illumination light on a chosen section of a sample and to manipulate it to allow for alternative modes of imaging such as darkfield illumination.

In brightfield light microscopy the contrast in the image comes from the differences in optical density of the specimen and its surrounding medium ie. how much the light the specimen absorbs or scatters. Coloured specimens are at an advantage as the pigments give additional contrast. Unfortunately, a large proportion of biological samples are transparent and colourless – bacteria being a key example – which means brightfield microscopy may not be the best choice for imaging them. Stains, such as Gram stain, can be used to improve the contrast of the images. However, these stains can have a knock on physiological impact on the cells being imaged [153]. Techniques such as darkfield, phase contrast and fluorescence microscopy offer alternative imaging methods with improved contrast.

2.3 Resolution in microscopy

One key characteristic of any microscope is its resolution - the minimum distance between distinguishable objects in an image. The resolution of a microscope is dependent upon a variety of things, including the quality of the components within it. However, in light microscopy resolution is fundamentally limited by the wavelength of the light source used.

As light passes through the objective lens of a microscope it is diffracted and interferes with itself - particularly at the edges of the objective lens aperture. This process causes point sources in the sample to become diffuse spots, in a manner determined by the point spread function of the optics.

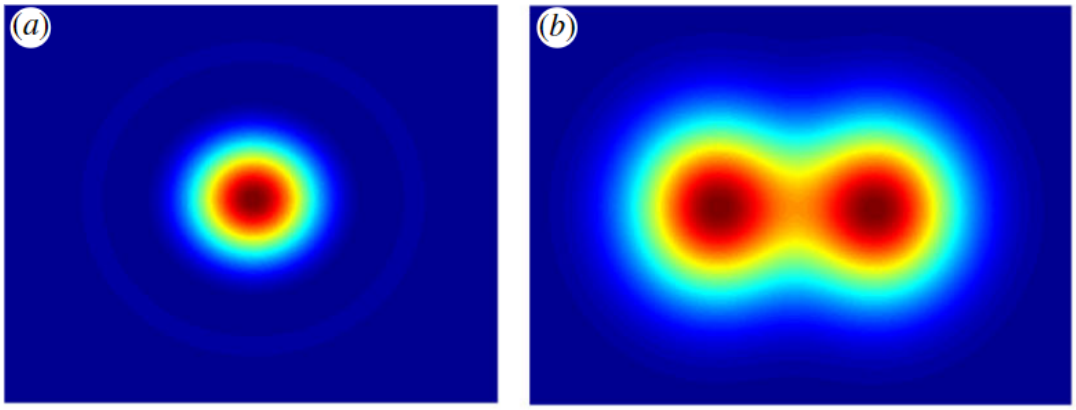

Figure 2.2: Mathematically generated point spread function images a) The Airy disc of a point source emitter imaged using a spherical lens, including the central spot and first ring, b) Two such Airy discs overlapping so they are not easily distinguishable as separate point sources. Taken from [154].

The point spread functions in an image can be mathematically approximated as Airy discs consisting of a central spot surrounded by concentric rings of decreasing intensity as can be seen in Fig. 2.2. The ability to distinguish between two objects in an image is dependent on how much their Airy discs overlap [155]. The size of an Airy disc for any given object (and so how likely it is to overlap with a neighbouring disc) is determined by the numerical aperture of the objective lens and wavelength of the light source being used.

The numerical aperture, NA, of a lens is:

$$NA = nsin(\theta), \tag{2.1}$$

where n is the refractive index of the medium between the objective lens and the sample (often air or oil) and θ is the aperture angle of the lens as can be seen in Fig. 2.3. In order to maximise the resolution of a microscope the aperture angle of the objective lens should be matched to the be aperture angle of the condenser lens. The working aperture of a microscope is a result of the sum of the condenser and objective lens aperture angles [152].

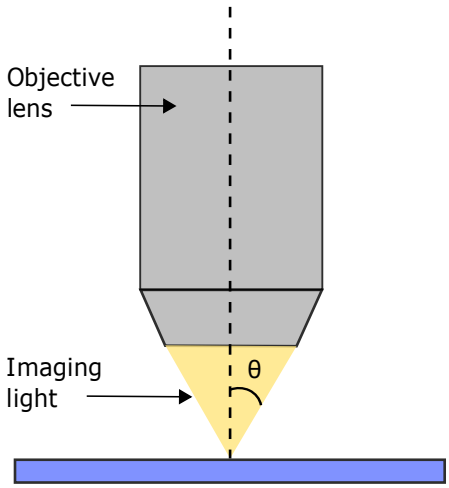

Figure 2.3: Schematic diagram of objective lens showing aperture angle (θ).

There are a number of ways to calculate the resolution of a microscope. Two of the most commonly used are the Abbe criterion and the Rayleigh criterion [152, 155]. Both combine the numerical aperture of the objective lens, with the wavelength of the light source to give a measure of the resolution. The Abbe criterion is based on finding the radius of the diffraction Airy disk in the image plane and can be calculated using equation 2.2 below:

$$R_A = \frac{o.5\lambda}{NA}, \tag{2.2}$$

where R_A is the Abbe resolution, λ is the wavelength of the light and NA is the numerical aperture of the objective lens [155].

The Rayleigh criterion can be calculated in a similar way, however, it defines the minimum distance between two resolvable objects as being when the central spots of the Airy discs do not overlap - i.e. the central spot of one disc may overlap with the first minimum of the second disc [155].

$$R_R = \frac{0.61\lambda}{NA} \tag{2.3}$$

where R_R is the Rayleigh resolution,

2.4 Köhler illumination

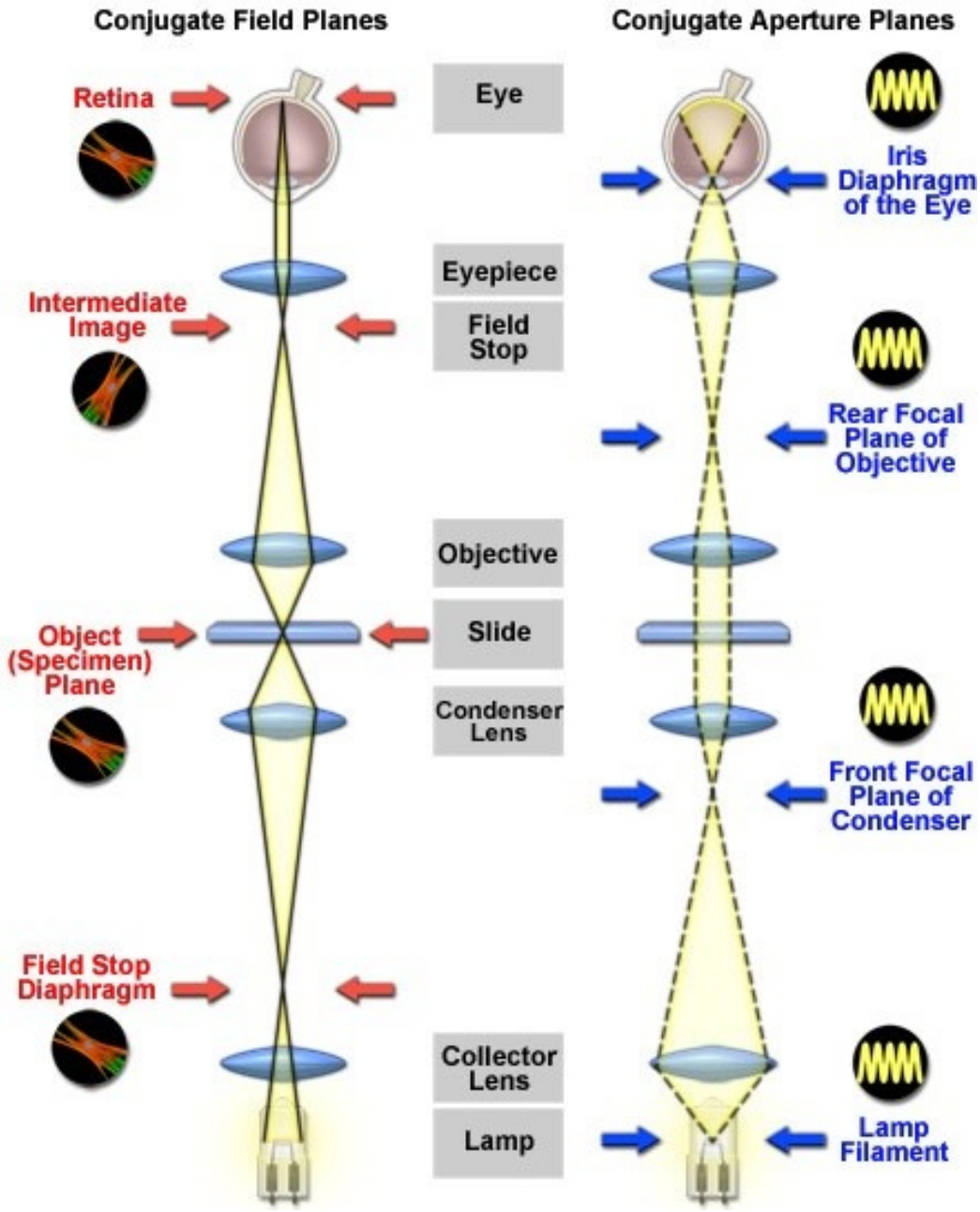

Figure 2.4: Schematic diagram showing the two conjugate planes for Köhler illumination [152].

For the optimisation of brightfield microscopy the additional step of Köhler illumination can be used. Köhler illumination is a method which helps to achieve an even and bright sample illumination which in turn will maximise spatial resolution and optimise image formation for use in a range of imaging modes [156]. It is achieved by creating two sets of conjugate planes - one containing the specimen image and the other an image of the lamp filament. This requires the addition of a field stop and a collector lens - the set up can be seen in Fig. 2.4.

The two sets of conjugate planes are created by properly aligning and focusing the microscope. The precise way to do this depends upon the make and set up of the microscope in use. However, in general, the basic requirements of Köhler illumination are fairly straightforward. The lamp housing has a collector lens which is set up to simultaneously focus the light onto the front aperture of the condenser lens whilst wholly filling that aperture with light. The condenser lens is then adjusted so that each of the conjugate planes is focused in specific locations along the optical path at the same time [155]. These locations can be seen in Fig. 2.4.

The key with these sets of conjugate planes is that they are both equal within themselves and reciprocal between the two sets ie. images in the same set of planes will all be in focus at once whilst the other set will all be out of focus [155]. This means that when you are viewing the aperture planes you will see only the lamp filament and when you are viewing the field planes you will see only the sample. This also means that you can manipulate the imaging process by adding additional components such as adjustable diaphragms which can change the sample illumination [155].

2.5 Darkfield illumination

Darkfield is an alternative to brightfield illumination which can offer improved contrast without staining. Darkfield illumination is particularly well suited for viewing transparent biological samples that have a refractive index close to aqueous medium and therefore achieve low contrast in typical brightfield imaging. This includes samples such as bacterium and cells in tissue culture [155].

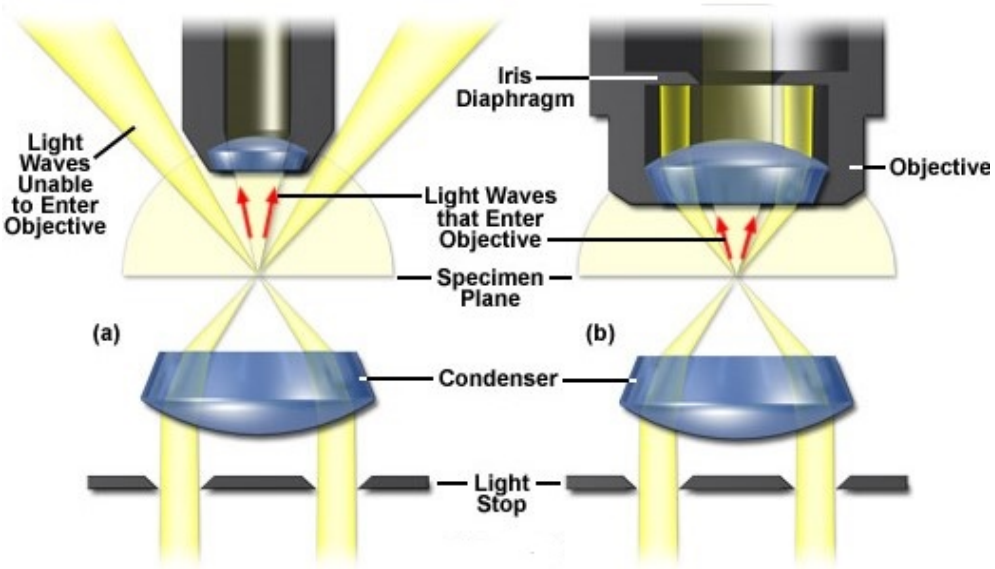

Figure 2.5: Schematic diagram showing two possible configurations for darkfield microscopy: a) Set up using a standard objective lens: b) Set up using a darkfield objective lens with an internal iris diaphragm [152].

The optical components and light path for darkfield microscopy can be seen in Fig. 2.5. A light stop is added to the path to obscure the central part of the light beam - this leaves a hollow cylinder of light to enter the condenser lens. This light is focused by the condenser onto the specimen, the hollow cylinder of light becomes a hollow cone, resulting in only high angle light hitting the specimen.

For a darkfield set up the numerical aperture of the condenser lens must be greater than that of objective lens [155]. This means that if no sample is present on the microscope stage all the light from the cone will cross at the specimen plane and will not enter the objective. This will result in a dark image. When a sample is placed at the specimen plane the oblique rays will pass through it and interact with the interfaces within it, such as bacterial cell membranes. This scattered light results in features in the sample appearing as bright on a dark background.

The key advantage of using darkfield is that only the weakly scattered light is visible - meaning objects that achieve low contrast in brightfield will be much more visible in darkfield. However, this is also the main source of issues with darkfield imaging - the quality of image can be significantly affected by contributions from unwanted weakly scattering elements in the field of view such as dust or dirt on the microscope slide. Thankfully this dust rarely moves and so for the purposes of this project this was not an issue.

Throughout this project darkfield microscopy was used as a method to check bacterial cultures had grown and were motile, as in Fig. 2.6. It also gave an approximate qualitative measure of sample density when preparing samples for holography.

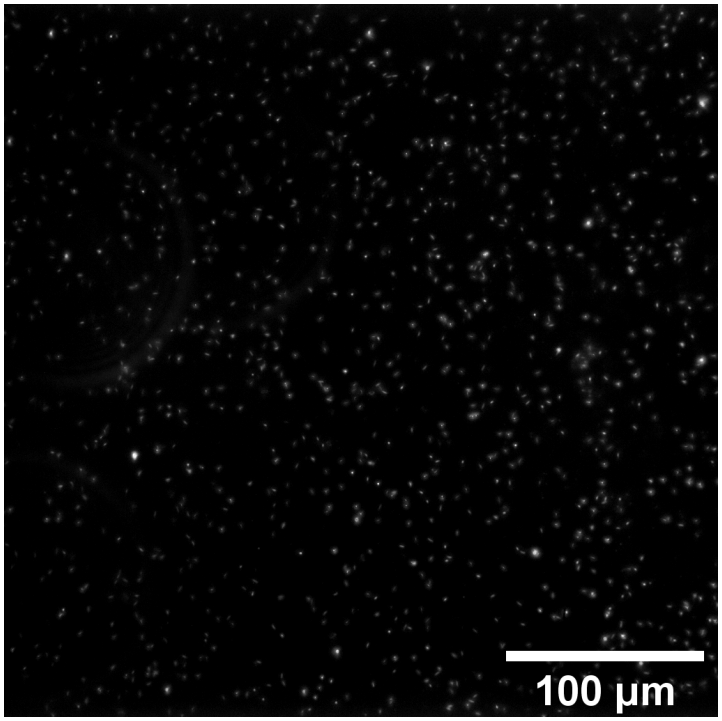

Figure 2.6: Example frame from a darkfield video of a *B. bacteriovorus* co-culture containing both *B. bacteriovorus* and *E. coli* prey cells. Where the larger spots in the image are the *E. coli* cells. Taken with a 40x air objective. Scale bar showing 100µm.

2.6 Microscopy for cell tracking

The main focus of this research project is to study the swimming behaviour of *B. bacteriovorus*. There are a wide variety of cell tracking microscopy and image analysis techniques used to study cell motility. These include both two dimensional (2D) and three dimensional (3D) methods.

Typically, 2D methods for cell tracking are easier to set up, and result in images which are simpler and faster to analyse, than 3D equivalents. These techniques are primarily based on taking a series of images or a video from which cell coordinates can be found in each frame, later stitching these coordinates together to find cell swimming trajectories (often using some form of computerisation or tracking software). *B. bacteriovorus* motility has previously been studied using 2D methods including behaviour in viscous fluids and on surfaces, see section 1.3.5 for details and examples [108, 137, 141–148]. For examples of 2D tracking of other bacteria see: [89, 99, 157–159]. The main problem with these 2D methods is that the microscopes used are optimised for high resolution over depth of view. This means that cells can only be seen (and therefore tracked) whilst they are in the focal plane of the microscope. In order to maximise time spent in the focal plane, cells are often imaged in droplets, on surfaces, or confined to small chambers and channels. Bacterial cells naturally inhabit 3D spaces and their behaviour near to or on surfaces can be significantly different to that in bulk [102–106, 160]. In addition, even in free-swimming set ups, the limited focal plane makes it difficult to take accurate measurements of key characteristics such as turning angle [161]. This is due to only being able to measure a projection of the turning angle on the focal plane (in x and y) meaning there is considerable ambiguity in any results. Without taking these various factors into account meaningful and interesting behaviour can be missed. In the case of *B. bacteriovorus, we know that both their free swimming behaviour in bulk liquids, and their behaviour at surfaces are important factors in their life-cycle. In order to properly characterise their motility behaviour, including size and distribution of turning angles, it was most appropriate to use a 3D cell tracking method for this project.*

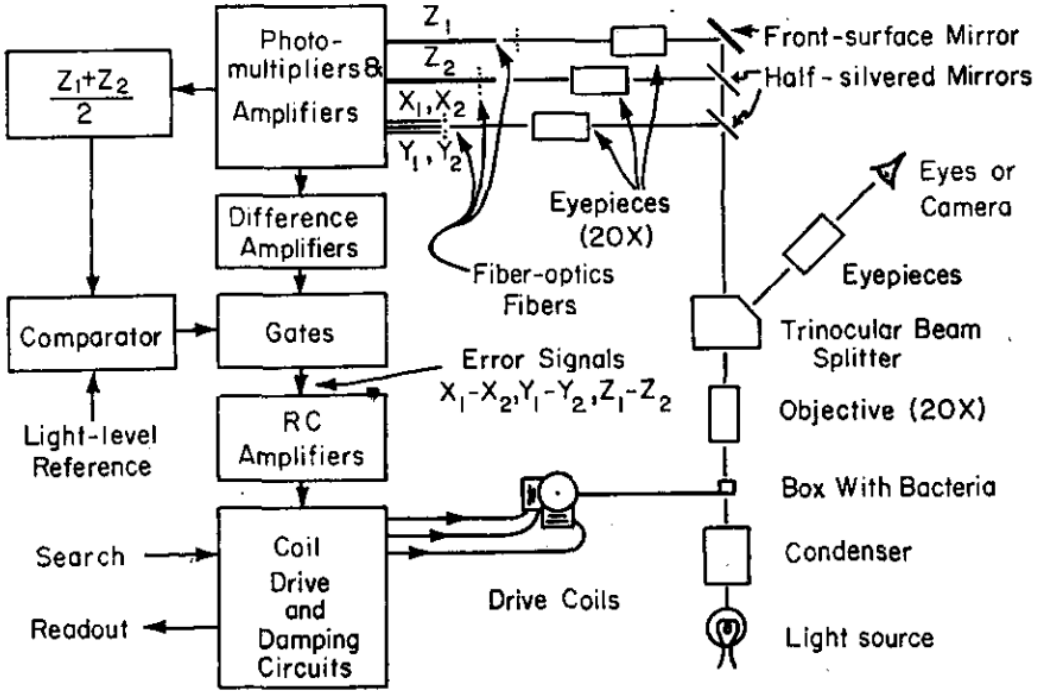

Figure 2.7: Original schematic diagram of Howard Berg's bacterial tracking microscope. Taken from [162].

The first method used to study bacterial swimming in 3D was developed by Howard Berg in 1971 [162]. Berg's microscope set up is shown in Fig. 2.7. It used a motorised sample stage which could be translated in the three planes, x-y-z, to maintain focus on a selected bacterial cell. The position of this stage was automatically controlled using a combination of phase contrast imaging, optical fibres and photomultipliers (PMTs). The optical fibres passed the phase contrast image to three pairs of PMTs: x_1, x_2, y_1, y_2, z_1 and z_2. When a cell moved in the positive x direction more light was transmitted by x_1 than by x_2 and the opposite if it moved in the negative x direction. The same applied also applied in the y and z dimensions. Finding the difference between the PMTs outputs, e.g. $x_1 - x_2$, gave a signal which was proportional to the cells displacement. This signal was filtered and amplified, and formed a feedback loop which was used to control the drive coils for the stage position. This system had a tracking range of approximately 1 mm in any direction and a position accuracy of around the diameter of a bacterial cell . If the cell it was tracking swam out of range of the stage, it would automatically refocus in it's centre position and wait for another cell to swim into the field of view [162]. Whilst this may appear a relatively simple concept overall, it was revolutionary in it's time. The results this microscope produced made a ground breaking contribution to understanding bacterial motility behaviour.

This method developed by Berg was initially used to study the swimming of *E. coli*, showing, for the first time, run and tumble swimming patterns. It has since been used to study other bacterial behaviour such as chemotaxis and swimming at surfaces [98, 102]. The main downside to this method is that it only allows the study of a single cell at a time, making it difficult to study population level dynamics or cell interactions.

Since Berg's initial discoveries, a number of different 3D cell tracking methods for simultaneously studying multiple swimming cells have been developed. Some, such as optimised dark-field 3D tracking, are only suitable for objects above 10μm in size - much larger than *B. bacteriovorus* [163]. Scanning-based methods such as fast scanning electric-piezo microscopy have been developed and used to study micro-swimming behaviour including spermatozoa. However, they are based on taking a stack of images within a time window, in the case of electric-piezo scanning giving a resulting video frequency of approximately 70Hz [164]. One of this issues with this technique is that it takes a 'rolling' scan of the sample volume, where the top z-slice will be taken at a different time to the bottom one, meaning that it does not give a true snapshot of what is happening at each time point. This technique can be effective for obtaining simultaneous swimming trajectories of cells, but only if they are relatively large and slow swimming such as sea urchin spermatozoa [164]. 2D studies of *B. bacteriovorus* have shown them to be fast swimmers, swimming on average 30-60μms^{-1}, meaning scanning methods are unsuitable for this study.

Defocused 3D imaging techniques bypass some of these issues, allowing tracking of multiple small objects (diameter <10μm), simultaneously at relatively high frequencies. These methods are based on using the relationship between the diameter of the largest diffraction ring of an object and it's distance from the focal plane to give an estimate of z position [165]. This method of tracking has been applied to study a variety bacterial behaviour including the collective cell dynamics of *E. coli*, *Caulobacter crescentus* swarming near surfaces and characterisation of the swimming behaviour of *Serratia marcescens* [109, 161, 166]. Defocussed techniques, have two main types - those using a fluorescent set up, or those using darkfield or phase contrast methods. Fluorescent methods offer the greatest depth of view, however they require the cells to be stained or tagged, which as already discussed can have an impact on cell behaviour.

An alternative method of 3D cell tracking, that can obtain similar results to defocussed fluorescent set ups but does not require fluorescent cells, has been developed using a standard phase contrast microscope [167]. This method compares the diffraction patterns generated by cells to a reference library to give an approximation of z position. It has been shown to be effective at tracking a variety of bacterium and has been used to study the swimming and chemotactic behaviour of *V. alginolyticus* and *Caulobacter crescentus* [167–169].

Digital holography methods, specifically digital inline holographic microscopy (DIHM), can obtain results similar to above but without the need for a reference library. The DIHM process involves taking a video of a sample, where each frame is a hologram. These holograms are numerically re-focused in a way that enables the z position of cells to be found (see section 2.7 for a full explanation). DIHM is an excellent technique for cell tracking as it allows the imaging of large quantities of cells in three dimensions at high spatial and temporal resolution (limited only by the detector) [170]. DIHM does not require tagging or staining which eliminates concerns about the physiological impact of these chemicals on cells and their behaviour. It also allows for a large field of view and sample depth of view, enabling observation of both population and individual cell behaviour. In addition, it has a simple set up based on a standard laboratory microscope. This set up is robust and can be used in remote locations, such as for marine biology, and has potential applications in space exploration [171, 172]. DIHM gives spatial resolution close to the diffraction limit and can enable the study of both the morphology as well as the behaviour of cells [170].

The two main downsides to DIHM are that it can only image dilute samples and that the image processing is computationally demanding. However, for most applications these issues are not significant compared to the overall benefits of using this technique. DIHM has previously been used to study a wide range of micro-swimmers and their behaviours. This includes the study of algae and bacteria from glaciers [171], *E. coli*, run and tumbles [173], trapping at surfaces [103], and behaviour in shear flow [174], the chemotactic behaviour of *Leishmania* parisites [175], and the chemotactic efficiency of *Haloarchaea* [176]. In the future, DIHM image generation could be combined with advanced computational techniques such as machine learning and neural networks. This could enable much faster processing of images, potentially up to real time viewing. Overall, DIHM is the most appropriate available technique for studying *B. bacteriovorus* swimming behaviour.

2.7 Digital inline holographic microscopy

Digital inline holographic microscopy (DIHM) is a microscopy technique that works by utilising the wave nature of light and the resulting interference patterns generated by light-sample interactions. DIHM was used extensively in this project for the study of *B. bacteriovorus* motility and behaviour, see Fig. 2.8 for an outline of the workflow used. Details of this process including both the automated and manual aspects are in sections 2.7.4 - 2.7.7.2.

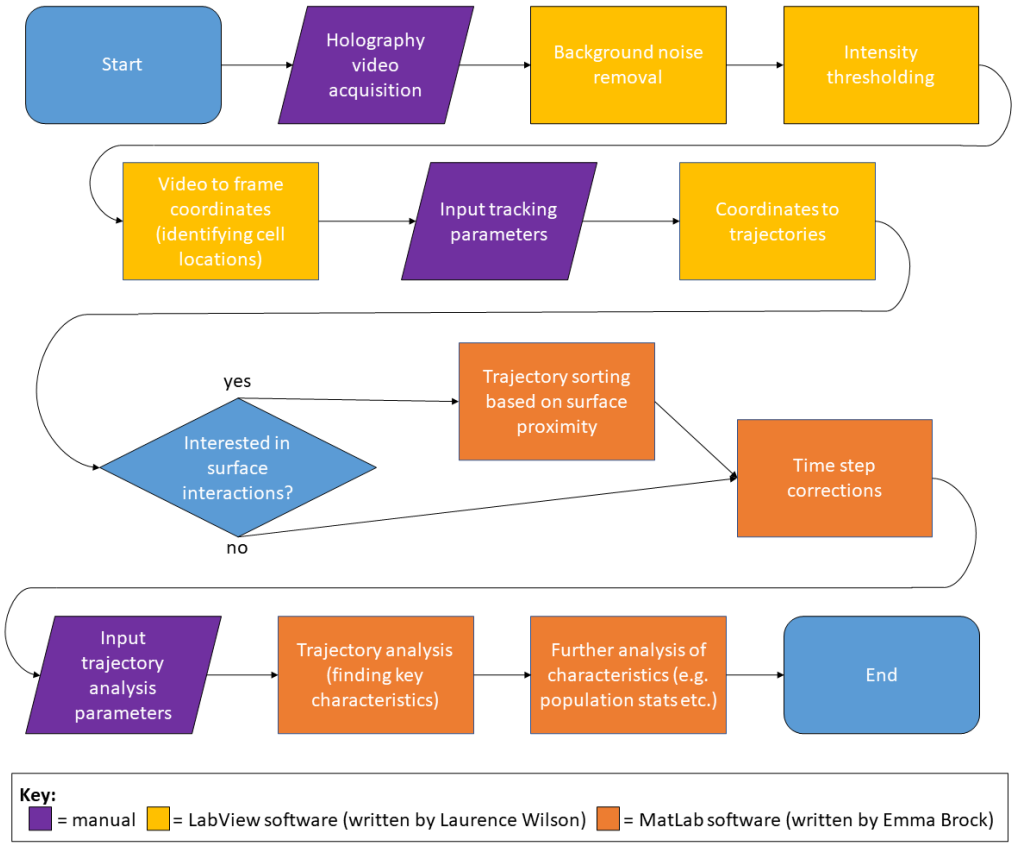

Figure 2.8: Workflow diagram showing the steps used for performing DIHM and analysis during this project. Key shows which parts of the process were performed manually or by bespoke software written in LabVIEW or MATLAB.

2.7.1 Introduction to holography

Holography was first discovered by physicist Dennis Gabor in the 1940s with the aim of improving the resolution of electron microscopy [177]. He went on to win the Nobel Prize in physics in 1971 for this "invention and development of the holographic method" [178]. The principles underlying his invention are widely applicable and, combined with the invention of lasers by Theodore Maiman in 1960 and the development of improved imaging sensors and computing in the 1990s, have been used in in a range of areas both within research and commercially [179]. Applications of holography have been as varied as forgery prevention and fabric development to bio-sensing technology and a wide array of applications in microscopy including DIHM. [180–182].

Holography does not form an image in the same way as typical microscopy or photography. Instead of simply recording the amplitude of light in a given position it also captures a complete record of the phase [183]. This method relies on the wave nature of light. Crucially, when two waves of the same amplitude and wavelength interact their relative phase dictates if they interfere constructively or destructively and therefore affects the resulting light, as illustrated in Fig. 2.9.

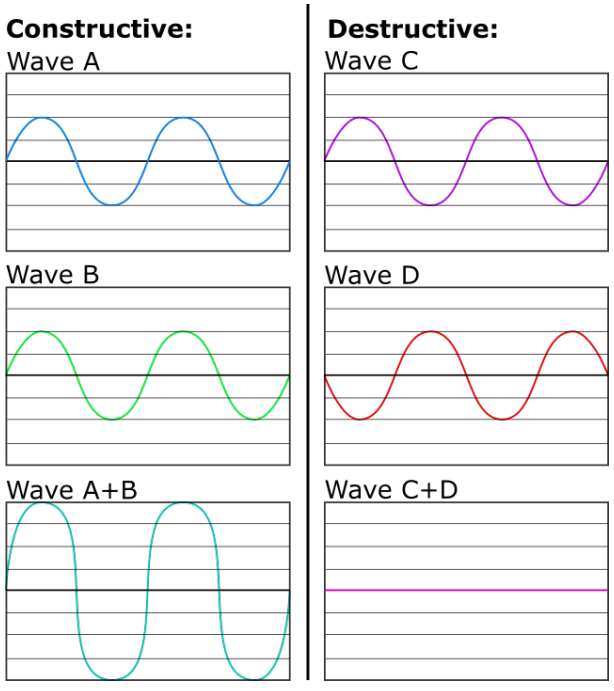

Figure 2.9: Diagram illustrating the interference of waves. *Left:* Constructive interference resulting in a wave with the same wavelength and frequency but double the amplitude of the original two waves. *Right:* Destructive interference resulting in no remaining wave - due to the two original waves having equal amplitude and wavelength but being half a wavelength out of phase.

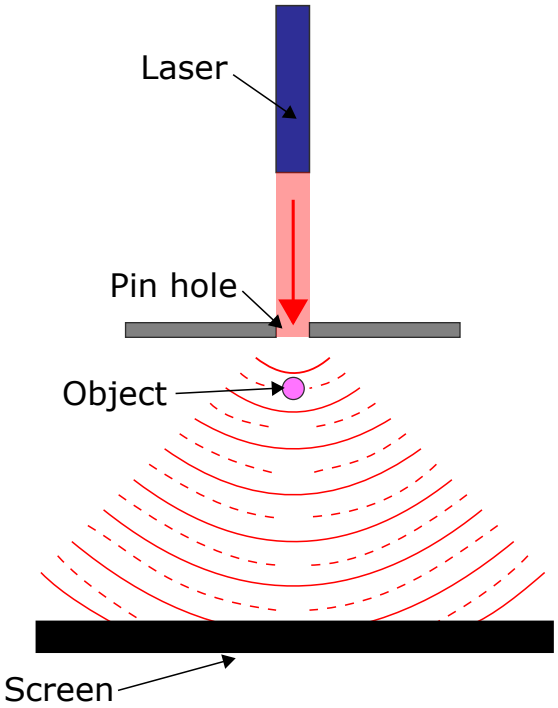

Figure 2.10: Schematic diagram of an inline holography set up where the solid red lines represent the reference beam and the dashed red lines represent the light scattered by the object. Figure adapted from [171].

It is important to note that the light source used is key to holography. The light must be monochromatic (all the same wavelength) and coherent (light waves in phase). In DIHM lasers or LEDs are used for illumination. LEDs have the advantages of being easier to set up and needing fewer health and safety considerations. However, lasers are significantly more coherent than LEDs. In this context this means that using lasers allowing imaging over much greater depth ranges - up to 5mm for lasers compared to only 200µm for LEDs [184]. In other applications, suc a measuring cell morphology the optical delimitation gained from using LEDs can beneficial [185]. However, in this study lasers were used to enable the longest possible cell trajectories to be captured.

There are a range of experimental set ups to choose from when producing holograms. These include both inline and off-axis options, which can have a variety of light beam positions, see [182] for examples. inline holography is the choice with the simplest optical path, where the reference and scattered light beams travel along nearly the same path. An example of inline holography can be seen in Fig. 2.10 where the pinhole ensures the light is spatially coherent (i.e. can be considered a point source of spherical wave fronts). The simplicity of inline holography makes it more straightforward to set up and also less impacted by vibrations than off-axis configurations. The main disadvantage of inline is

that it requires a large portion of the original light beam to pass through the sample meaning it is only suitable for imaging dilute, not dense, samples. It can also suffer from the twin image problem. The twin image problem is a natural by product of the hologram generation process. When an on-axis hologram is reconstructed a pair of images are generated at equal distances on either side of the object [186]. There will be the desired, real, image behind the object and then the virtual image in front of the object. This virtual image is formed due to the the conjugate object wavefront. Unfortunately, when either one of the images is in focus so is the other. This can degrade the signal to noise ratio and so the contrast of the desired image [186]. The DIHM technique used for this research project had an inline set-up whereby a single-mode optical fibre is used instead of a pin hole and the sample placed far enough away that the wave fronts are locally planar in the microscope field of view. The twin image problem is mitigated in this project by slightly defocusing the microscope before image collection.

Inline holography has two light paths to consider - the scattered beam (light that has been scattered by objects in the sample being imaged) and the unscattered or reference beam (the light that has passed straight through the sample without interacting). When the scattered beam and the reference beam interact they constructively and destructively interfere generating diffraction patterns. The nature of these diffraction patterns is dependent on the size, shape and location of the object that has scattered the light. The shape of the object will be represented in its diffraction pattern - in the case of a point source or small spherical object the diffraction pattern generated appears as a series of circular concentric rings as can be seen in Fig. 2.11. For an extended object such as a long rod the diffraction pattern will take this extended shape, and repeat in outlines from the central shape. The larger the object the larger the diffraction pattern it will produce (including the central shape becoming larger). The diffraction rings may become more distinct as larger objects will typically scatter more light. For objects of the same size and shape the further it is from the focal plane the larger the diffraction pattern will become - the central shape will become larger and pattern will become less defined (lower contrast). For DIHM these diffraction patterns are magnified by an objective lens and captured digitally with a camera. The recorded diffraction patterns constitute the digital hologram and contain all the information needed to reproduce the 3D image.

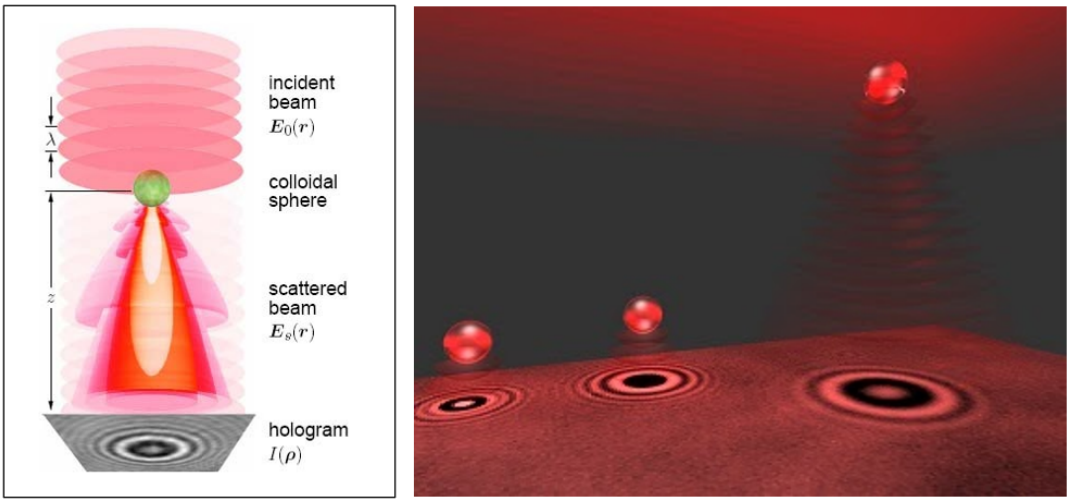

Figure 2.11: *Left:* Diagram demonstrating inline holography: A particle scatters a portion of an initially collimated laser beam. The scattered beam, here represented by 5 iso-amplitude surfaces, interferes with the unscattered portion of the beam in the focal plane of the microscope objective, thereby forming an inline hologram. Taken from [187]. *Right:* Diagram illustrating the hologram generated by multiple particles in a sample volume [188]

There are two main methods for decoding digital holograms: numerical refocusing and direct fitting [184]. Direct fitting methods based on Mie scattering theory are very accurate, however they require a pre-known model of the scatterer which significantly limits their application [189]. In addition, direct fitting methods are very computationally expensive and therefore time consuming. Numerical refocusing methods offer an alternative which can be applied to a wide range of weakly scattering objects (such as bacterial cells) without prior knowledge of their scattering properties [184]. This project utilises a fast and adaptable method called the Rayleigh-Sommerfeld back propagation method which is further described in section 2.7.5.2 below [189].

2.7.2 DIHM set up

One of the key advantages of DIHM is the simplicity and ease of set up. A standard inverted laboratory microscope (Nikon Eclipse Ti) was used for all experiments in this project. The condenser lens was removed and replaced with a laser fibre as can be seen in Fig. 2.12 A and B. The laser fibre was placed in a bespoke holder designed to fit the condenser lens apparatus and keep the source as stable as possible see Fig. 2.12 D. The holder was positioned approximately 5cm from the sample stage to give a planar illumination onto the sample.

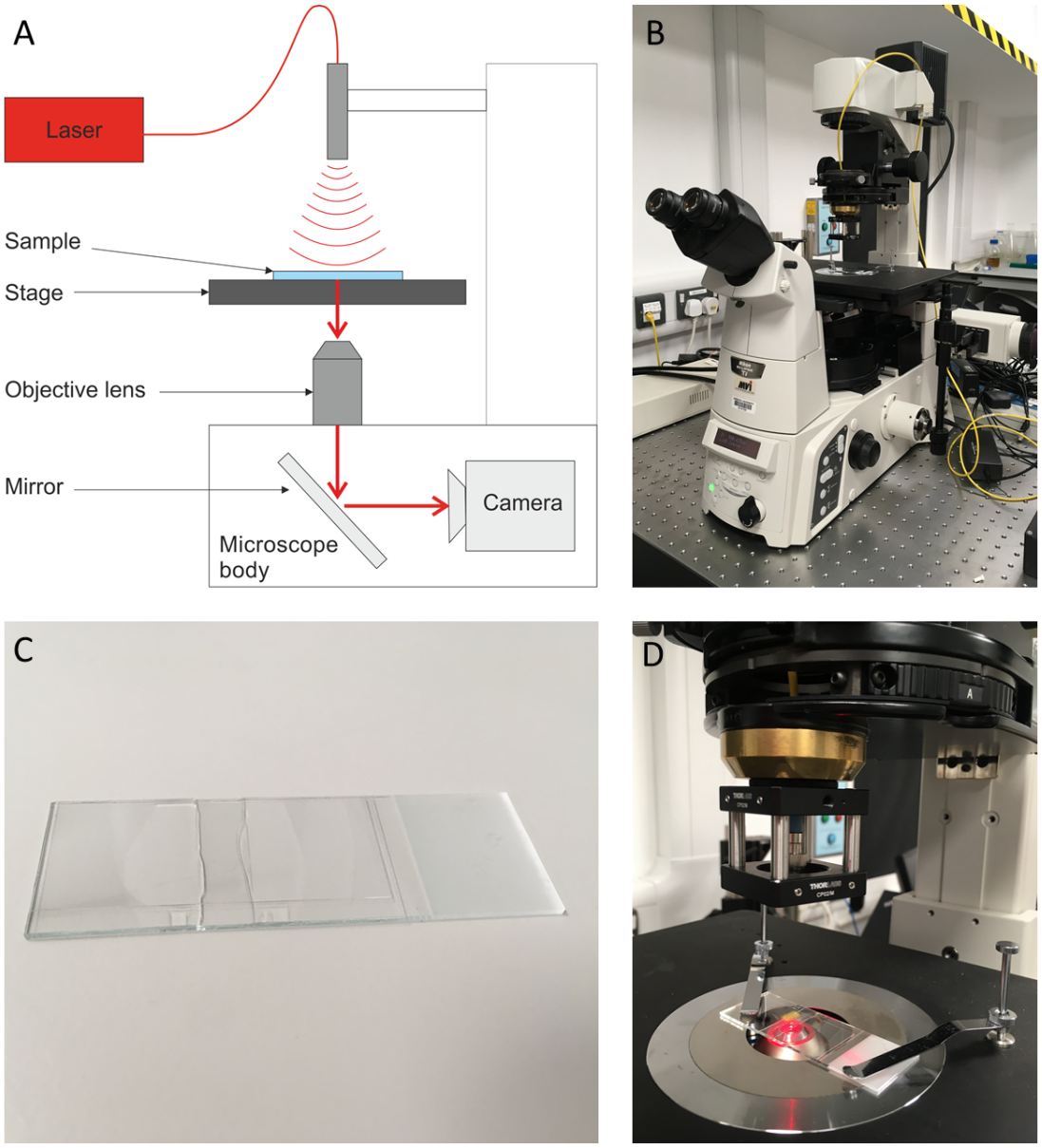

Figure 2.12: A) Schematic diagram of DIHM setup, B) Photograph of microscope set up used for this project, C) Photograph of sample chamber used for holography, and D) Close up photograph of laser holder and positioning.

In this set up the laser diode is interchangeable. During this project a fibre coupled laser diode of wavelength 642nm (red) was used. The laser was switched on approximately 20 minutes before imaging to allow the temperature to stabilise. This minimised fluctuations in light intensity which could impact cell localisation. A 40x magnification, 0.75 numerical aperture, air objective was used throughout the project as this gave the largest field of view whilst still be able to resolve the cells being studied.

2.7.3 Sample preparation

All the imaging done for this project used handmade sample chambers. These were made from microscopy slides, coverslips and optically neutral glue - glue that dries to have the same refractive index as glass. As can be seen in Fig. 2.12 C, two coverslips are glued to the microscope slide at the desired chamber width. A large coverslip is glued across the top to create the chamber - the chambers were typically 50-80µl in volume and around 200µm in depth. This thin shape helps to prevent fluid flow in the sample chamber which would impact on motility results. The optical glue is set using a UV lamp for around 15 minutes this causes it to cure and harden, after which the chambers can be used or stored for later. Once filled the chamber can be sealed using petroleum jelly or nail polish. Unless otherwise stated the sample chambers in this project were left open. This was due to the cells being grown aerobically and therefore needing a supply of oxygen. It also to minimised any impact on cell behaviour by chemicals in the sealant.

Sample preparation is generally relatively minimal for DIHM. Cells are typically washed into an imaging buffer and diluted to allow clear resolution of individual cells. The imaging buffer used for this project did not contain nutrients - it only contained calcium salts and a buffer to help maintain a stable pH of 7.6. The protocol used for *B. bacteriovorus* varied depending on the experiment, a full description can be found in section 2.8.

2.7.4 DIHM image recording

Once the sample was on the microscope a few short reference videos were collected and a quick background correction performed to allow optimisation of the microscope focus. This correction involves taking the median intensity value of each pixel over time, to create a median intensity pixel map. Then each frame in the reference video is divided by this map. This process is also used to minimise background noise during image processing - see section 2.7.5.1. The focus was

placed just outside of the sample chamber, generally just above. This meant that all the cells were on one side of the focal plane resulting in simpler and quicker video processing.

All videos were recorded using a Mikrotron EoSens CL MC-1362 monochrome CMOS camera at a frame rate of 100Hz. Previous studies of *Bdellovibrio bacteriovorus* cells have shown them to be fast swimmers, therefore the higher the frame rate used the more likely the full detail of re-orientation events would be captured. An imaging window of 1024x1024 pixels was used which, when using a 40x magnification, translates to a field of view of about 358x358μm^2 (for comparison *Bdellovibrio bacteriovorus* cells are 0.8-1.2μm in length). Using the largest possible window size results in longer trajectory capture and therefore a higher likelihood of imaging turning events and cell interactions. For the same reason videos were recorded for typically around 20-30 seconds, videos any longer than this would result in prohibitively large file sizes (greater than 2GB).

2.7.5 DIHM image analysis

The most time-consuming and complicated part of conducting DIHM is the image analysis. There are a number of key stages to this image analysis, including background filtering, cell location and track reconstruction. For this project this was done using LabVIEW software developed by Laurence Wilson [184, 190]. Once the cell swimming trajectories are obtained they can be further analysed to find key parameters such as swimming speeds, run times and re-orientation angles. For this project this was performed by MATLAB software written by Emma Brock. Additional analysis steps can be added for more complex cases, for example; to allow for removal of cells trajectories at the sample chamber surfaces and identification of cell types e.g. predator or prey (also done by MATLAB code written by Emma Brock). The key parameters obtained enable understanding of the motility and behaviours of cells such as predator-prey interactions.

2.7.5.1 Background noise reduction

The first step to the image analysis process is background noise reduction. Background noise can come from a variety of sources including noise intrinsic to the camera itself and any surface aberrations on the sample slide. The most important source of camera noise in DIHM is photon shot noise, this results from the natural variability of incident photon flux [170]. Camera noise sources can also include read noise, from fluctuations in the signal amplification in the camera sensor, and pattern noise, caused by slight discrepancies between individual pixel sensitivities on the camera chip [191]. Noise on the sample slide may come from dust, dirt or from stationary cells.

For each video collected, a median background image is generated by taking the median value of each pixel across the total time of the video. Each frame in the video is then divided by this, median background image. This process minimises intensity contributions from small fluctuations in pixel values - effectively smoothing the baseline background. This increases the signal to noise ratio enabling larger moving features to be seen - such as swimming cells. An example background reduced frame can be seen in Fig. 2.13.

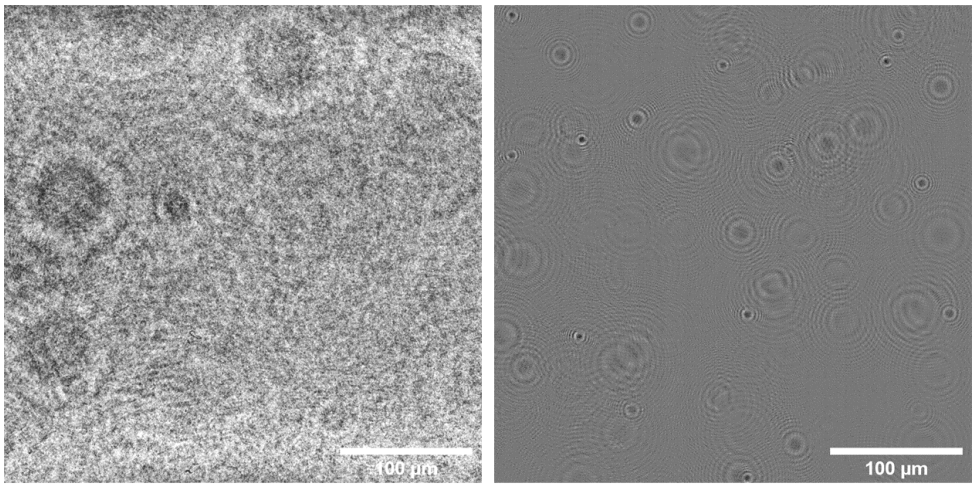

Figure 2.13: Example of background noise reduction from a DIHM video of *E. coli* cells. *Left:* Example frame from a raw DIHM hologram. *Right:* The same frame with the background noise reduced and contrast enhanced - the diffraction patterns from the cells can now be clearly seen. Scale bars represent 100µm.

2.7.5.2 Cell localisation

In order to identify the position of cells in the video, each frame is treated separately acting as it's own complete hologram. The methods used in this project rely on the Guoy phase shift and Rayleigh-Gans scattering theory, and so, can only be applied to weakly scattering objects that satisfy these conditions:

$$|m-1| \leq 1, \quad kd|m-1| \leq 1, \tag{2.4}$$

and

$$m = \frac{n_p}{n_m}, \tag{2.5}$$

where m is the relative refractive index (between n_p, the refractive index of the particle and, n_m the refractive index of the surrounding medium), λ is the wavelength of the illumination light and k is the wavenumber ($k = 2\pi n_m/\lambda$). Bacterial cells typically have a refractive index very close to the medium they are in so are well suited to this regime [189].

Each hologram generated in each frame of the video is numerically refocused using the Rayleigh-Sommerfeld back propagation method which is explained fully in [189] and [192]. In short, it is possible to use the Rayleigh-Sommerfeld propagator j to find the electric field at a distance z' from the plane of the hologram:

$$j(x',y',z') = \frac{1}{2\pi}\frac{\partial}{\partial z'}\frac{exp(ikr')}{r'}, \tag{2.6}$$

where

$$r' = \sqrt{(x'^2 + y'^2 + z'^2)}, \tag{2.7}$$

and the prime shows that the coordinates do not sit in the 'real' physical volume but rather within the mathematical reconstructed volume. The optical field can then be reconstructed at any distance from the plane of the hologram using the convolution below:

$$E_s(x',y',z') = E_0(x,y,0) \otimes j(x',y'z'). \tag{2.8}$$

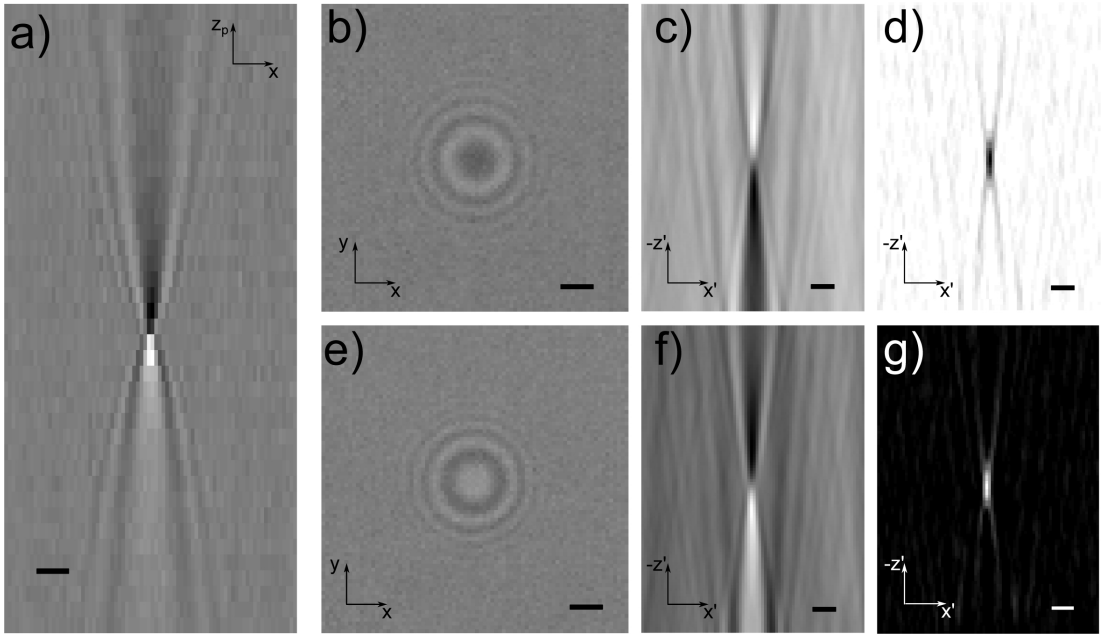

Figure 2.14: Figure showing examples from a hologram generated by a single spherical particle, including reconstruction. a) Vertical slice through the centre of the image stack, note how the contrast switches from light above the to dark below the particle position. b) Diffraction pattern produced by the particle at approximately 9 μm below the focal plane c) Vertical slice through the reconstructed optical field generated from b). d) The intensity gradient stack generated from b). e), f), and g) are the equivalent of b), c) and d) except the particle is located approximately 9µm above the focal plane. All scale bars represent 2µm. Taken from [189]

Effectively this method is generating a stack of images for each hologram similar to what would be seen if the focal plane was scanned vertically (in the z-direction) through the sample volume. The number and size of the vertical steps can be set by the user, in the case of this project 140-150, 2µm steps were used per hologram. The stack of images are then further analysed to find the position of the cells in the volume. This is done by using a version of a Sobel filter to generate an intensity gradient in the z direction [189]. Cells are found at point of highest intensity gradient as can be seen in figure 2.14. This method is very effective at locating cells in the z direction to a sub-pixel accuracy as long as the intensity gradient varies slowly in comparison to the step size.

As well as locating the cells in the z direction, they are also located in the x and y plane. This is done by projecting the maximum intensity of the intensity gradient in each frame. This results in an image of a dark background with bright spots - the spots are the cell locations. For each video an example frame is taken and a user will manually set an intensity threshold over which a pixel is considered to a cell or part of a cell. Any pixels below this threshold are then

set to a zero value. A built in LabVIEW function (count objects) will identify the remaining bright objects in the image, locate their central pixel and count them. One of the quick checks used to establish the thresholds during this project, was to estimate how many cells were in a a frame and check that the return number of cell localisations was similar to this value (typically around 100). If this value was much smaller or larger than expected it was a good indication that the threshold parameters needed to be changed. The intensity threshold is manually set for each video before full analysis.

The final result of the cell localisation processes is a text file for every frame in each video that contains a list of cell coordinates in x, y and z. These cell coordinates can be used to find swimming trajectories.

2.7.5.3 Trajectory reconstruction

The trajectory reconstruction works by looking through the cell coordinates in consecutive frames within the video. For each cell coordinate it looks in the following frame for the closest cell located within a user defined search sphere radius. When there is no longer a cell within the search sphere the track is ended. There are a number of additional functions including setting a minimum trajectory length and a trajectory splitting procedure.

In the case of trajectory splitting (often caused by two cells bumping into each other or closely crossing paths), the code will end the first trajectory at a split and identify the following two trajectories separately. Trajectories that are less than the minimum length will be automatically deleted - most often when cells are located at the edges of the sample chamber and pass in or out of the field of view.

Finally the code classifies the trajectories as cells that are swimming or diffusing using their mean squared displacement. Mean squared displacement, or MSD, is a measure of the movement of an object from it's starting position over time. It can be used as way to estimate if an object or in this case a bacterial cell is simply diffusing or if it is actively swimming through a medium.

The simplest way to think about this is as a comparison of the behaviour between a diffusing and a swimming object. If we first consider a particle in a starting position which we will call the origin. Considering a particle diffusing in 1D measuring it's position at regular intervals will result in a cluster of positions close to the origin, decreasing in regularity as they move away from that point. When plotting count against position this results in a Gaussian bell curve

centred around the origin. The width of this curve is dependent on two things: the diffusivity of the particle (ξ) and the time over which the positions were measured (τ). We can say that for a diffusing particle the MSD ($\langle x^2 \rangle_{diff}$) is:

$$\langle x^2 \rangle_{diff} = 2\xi\tau. \tag{2.9}$$

In contrast the MSD of a swimming particle is very much dependent on it's velocity:

$$\langle x^2 \rangle_{swim} = v^2\tau^2. \tag{2.10}$$

In this project the MSD for the cell on each trajectory was found in each dimension. The log of this MSD was plotted against τ to give a graph. From equations 2.9 and 2.10 it is possible to see that the gradient of the graph for a purely diffusing particle will be one and the gradient for a purely swimming particle will be two. Therefore we can apply a threshold to the gradient of these graphs to approximate which cells are swimming or not. Unfortunately, the reality of very small bacterial cells swimming in liquid is that they will be affected by the medium in which they swim resulting in a Brownian rotational motion component to their swimming trajectories. This will have a knock on effect on their MSD. Therefore the gradient threshold is lowered and an additional filter is applied. This effectively thresholds the intercept of the log MSD graph. The intercept of the graph is dependent on the speed of the particle - the higher the intercept the faster the movement. Both the threshold criteria must be met in order for a cell trajectory to be classified as swimming. Essentially this ensures that the mean squared displacement after a certain amount of time is high enough to qualify the cell as showing swimming behaviour.

2.7.5.4 Noise reduction in trajectories

Once the trajectories have been identified and classified, a cubic spline smoothing technique is used to smooth the trajectory data. This gives a curve which highlights key features in the trajectory and minimises the impact of noise on the results including cell properties such as swimming speed and re-orientation pattern. An example spline smoothed trajectory can be seen in figure 2.15. The noise reduction is achieved by minimising equation 2.11 below, in each dimension:

$$x_s(t) = b \sum_{n-1}^{i-0} w_i(y_i - f(x_i))^2 + (1-b) \int_{x_0}^{x_n-1} \gamma(x)(f''(x))^2)dx, \tag{2.11}$$

where $x_s(t)$ is the cublic spline fit of the trajectory in x, b is the balance parameter, w_i is the ith element of weight, y_i is the ith element of Y, x_i is the ith element of X, $f''(x)$ is the second order derivative of the cubic spline function f(x) and $\gamma(x)$ is the piece-wise constant function:

$$\gamma(x) = \gamma_i, x_i \leq x < x_{i+1}, \quad for \quad i = 0, 1, ..., n-2. \tag{2.12}$$

The user can input a value of b, between 0-1. This value determines the influence of each part of the equation. Therefore it determines what type of fit is produced. The first half of the equation finds the magnitude of the sum of the differences between the function fitted and the raw data points - otherwise known as the residuals. If the value of b is high this part of the equation dominates. The second part of the equation is related to the curvature of the fit. The function will try to minimise the curvature (create a straighter line of fit). If the b value is low this term will dominate. At the extremes; if b=0 then the cubic spline fit is simply a linear fit and if b=1 then the raw un-smoothed data is returned. As a note: w_i is set to 1 for this work as this data is fairly consistently noisy. Equation 2.12 is also applied in y and z to give the resulting smoothing seen in Fig. 2.15.

For this project the balance parameter was chosen by applying a range of values to a set of trajectories where re-orientation events had been manually identified. These trajectories, at different levels of smoothing, were then analysed to find the re-orientation events using the methods described in section 2.7.6.4. Trajectories that were considered to be under-smoothed showed over identification of reorientation events - noise was identified as reorientation. Trajectories that were considered to be over-smoothed failed to have reorientation events identified as the angle change dropped below the threshold. A balance parameter of 0.9999 was chosen. This smoothed the trajectories as little as possible whilst still enabling reorientation events to be identified. Please note this value was chosen in combination with the minimum angle change threshold described in section 2.7.6.4.

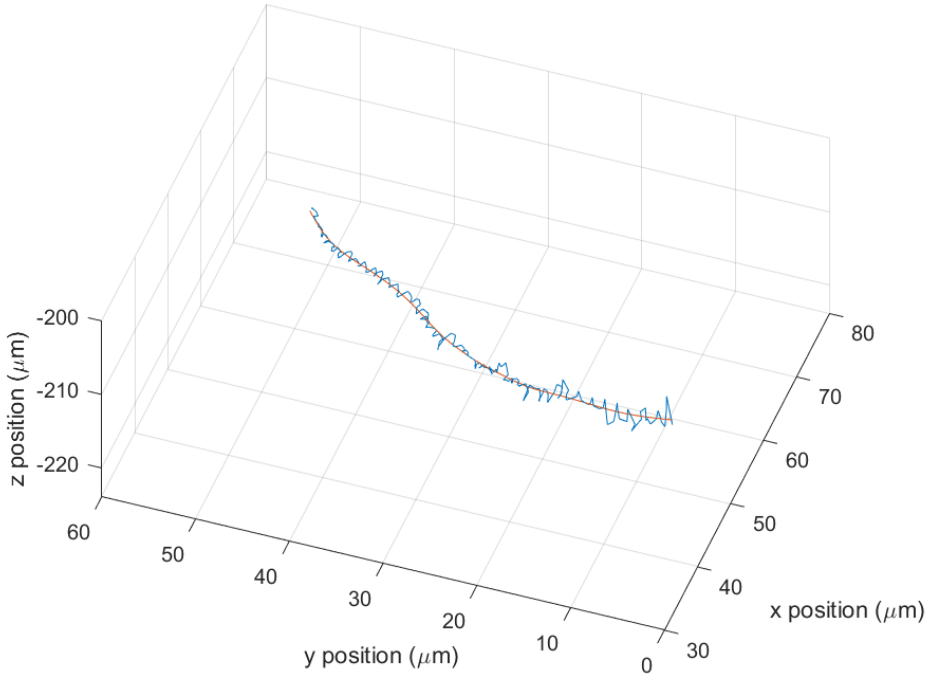

Figure 2.15: Plot of a segment of an *E. coli* swimming trajectory where the blue line is the raw data and the red is the spline smoothed version.

2.7.6 Cell trajectory analysis

I have written bespoke code in MATLAB to analyse the cell trajectories obtained from my holograms. Each cell swimming trajectory is individually analysed for the key parameters including cell swimming speed, run timesand re-orientation angles.

2.7.6.1 Trajectory interpolation

The first step of the trajectory analysis is to check and correct for any discontinuities in the time values of the trajectories. These happen rarely and can result from the trajectory reconstruction in section 2.7.5.3 (i.e. when cells are within the designation distance and time search but not in consecutive time points). Trajectories have their time data systematically checked to find any skips in the time values. If a skip is identified the missing time steps are inputted and the coordinate data is linearly interpolated to fill the missing points. The main reason for doing this is to simplify and speed up the data analysis in the following steps.

2.7.6.2 Surface proximity sorting

An optional processing step, before swimming characteristics are found, is to sort trajectories by their surface proximity. Plots are made of all the trajectories in a video and the approximate z position of the top and bottom surfaces of the sample chamber are noted. These are inputted into a MATLAB code which runs through each trajectory and checks the z coordinates. If a trajectory passes with a specified distance of a surface it is cut at that point. Any trajectory segments greater than 0.5 seconds (50 time points) long are then saved as individual trajectories characterised by whether they are in bulk or near surfaces. This time value was chosen to give long enough that the trajectories could feasibly contain a measurable reorientation event.

2.7.6.3 Swimming speeds

The next step in analysis is finding the swimming speeds. The mean swimming speed is calculated by summing the magnitude of the vectors between consecutive coordinates in a trajectory. This is divided by the total time for the track to give the mean speed per trajectory, as can be seen in equations 2.13 - 2.15.

$$p_i = (x_i, y_i, z_i), \tag{2.13}$$

$$d_i = |p_{i-1} - p_i| = \sqrt{((x_{i+1} - x_i)^2 + (y_{i+1} - y_i)^2 + (z_{i+1} - z_i)^2)}, \tag{2.14}$$

$$s = \frac{\sum_{i=1}^{n-1} d_i}{t_n - t_1}, \tag{2.15}$$

where p is the position of the cell at a given time, d is the distance between consecutive positions, s is the mean speed of the trajectory, n is the number of coordinates in the trajectory, and t is the time value at a given coordinate.

The maximum trajectory speeds are taken from the maximum instantaneous velocity vector from each trajectory. The instantaneous velocity vectors are calculated as in equation 2.16 and 2.17 below:

$$T = \frac{1}{f}, \tag{2.16}$$

$$v_i = \frac{(x_{i+1} - x_i, y_{i+1} - y_i, z_{i+1} - z_i)}{T}, \tag{2.17}$$

where T is the time between coordinates, f is the frequency at which the video was recorded (typically around 100Hz) and v is the instantaneous velocity vector.

2.7.6.4 Run times and re-orientation angles

The re-orientation events and corresponding run times(time between each event) are extracted from the data using a multi-step process. First the angle changes between consecutive vectors in the trajectory are calculated using equations 2.18 and 2.19 below:

$$q_i = p_{i+1} - p_i = (x_{i+1} - x_i, y_{i+1} - y_i, z_{i+1} - z_i), \tag{2.18}$$

$$\phi_i = \cos^{-1}\left(\frac{q_i \cdot q_{i+1}}{|q_i| \cdot |q_{i+1}|}\right), \tag{2.19}$$

where q is the vector between consecutive points and ϕ is the angle change between consecutive vectors.

A rolling mean angle value (taken over three values) is plotted against time for each trajectory. Turning events are identified by finding the peaks in this

graph that sit above a minimum threshold (in this study 10°), see figure 2.16 for an example. For this study the threshold value was chosen by comparing different threshold values to each other, on a set of trajectories where the peaks had been manually identified. It should be noted that this, like many of the other parameters used in the analysis, was a balancing act between capturing as many events as possible without falsely identifying noise as features. There is therefore a chance that a small number of low angle peaks maybe be missed. However, with large data sets the influence of this error becomes less significant. In general, the timestamp of the peaks that are above the threshold is recorded to give the position in time of the apex of the re-orientation events within the trajectory. Peaks that are too close to the beginning or end of the trajectory to be distinguished are discounted, as are any trajectories that only contain one peak. The amount of time between each re-orientation event is calculated from the peak positions. These times are recorded as the run times.

The last key parameter to be calculated is the turning angle of each re-orientation event. The turning angle of each re-orientation event is found using the same peak positions as for the run time calculations. These peak positions are taken as the apex of turning events.

In order to find the reorientation angle associated with a reorientation event a distance is chosen away from the apex of the turn (on both sides). Vectors are then drawn between the apex of the turn and these points and the angle between these two vectors is taken as the reorientation angle. This distance is set by studying a variety of trajectories and approximating a distance along the trajectory that will allow for angle calculation without being so far from the apex that any proceeding/subsequent turns are accidentally included. The code takes into account the average swimming speed of the trajectory and allocates a number of points either side of the apex that corresponds to approximately the chosen distance. It also checks that this is definitely less than the distance to the adjoining re-orientations. If the number of points is too great then the code automatically reduces this to be two points less than the distance to the closest turns. Once these checks have been made, the code then finds the vectors between these points and the apex of the turn. Finally it calculates the angle between these two vectors and records this as the turning angle for that event.

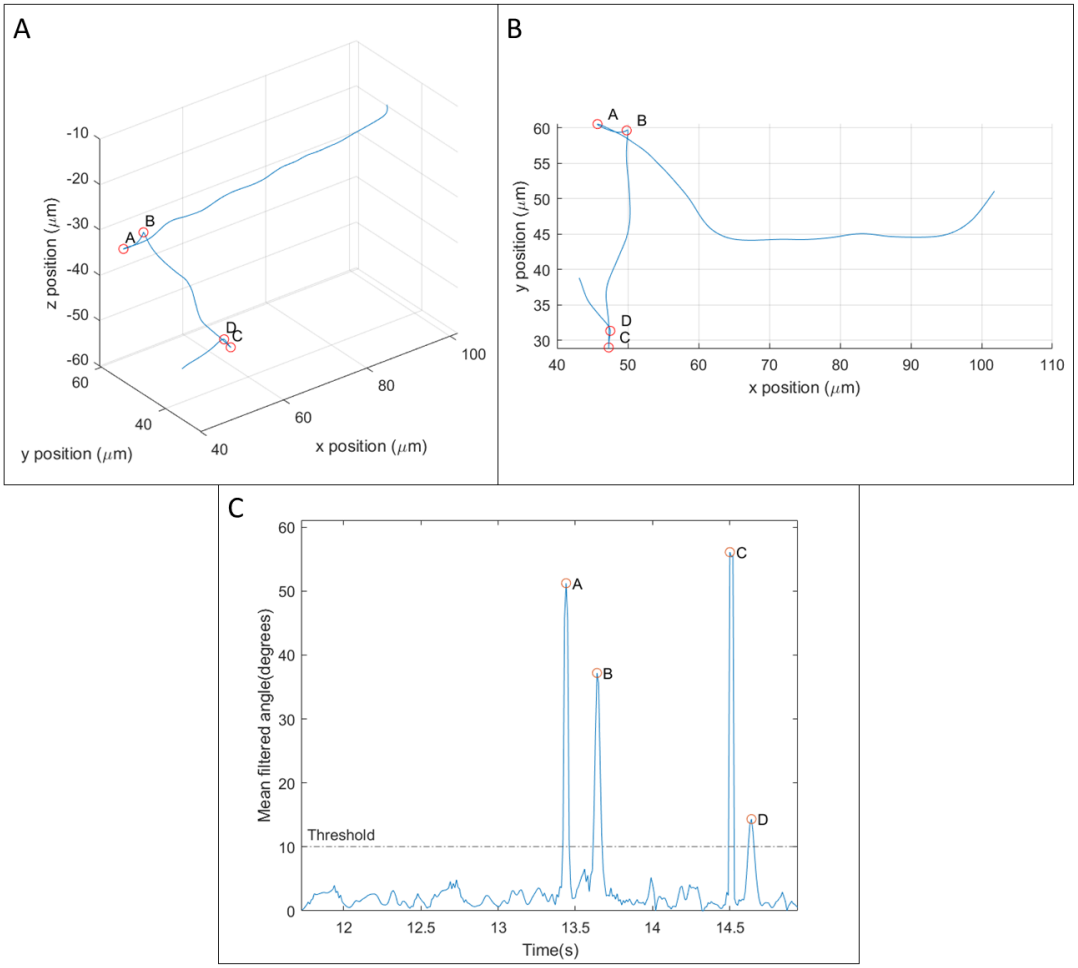

Figure 2.16: Figure illustrating re-orientation event identification in a *Bdellovibrio bacteriovorus* swimming trajectory. A) Three dimensional plot of the swimming trajectory where the re-orientation events are labelled as identified (see C)), B) The same trajectory as A) plotted in x and y to more clearly show the turning events, C) A graph of the mean filtered consecutive angle changes between vectors in the trajectory plotted against time, the dashed line shows the minimum threshold for re-orientations events with the identified events labelled (please note the time does not start at 0 and is taken from the original video recording).

2.7.6.5 Imaging frame rate

In order to ensure that the imaging frame rate did not impact upon the measured swimming characteristics, a set of exponential phase *E.coli* trajectories was down sampled from the a frame rate of 100 Hz to 50, 25 and 12.5 Hz. This data set is fully analysed and discussed in section 3.3.

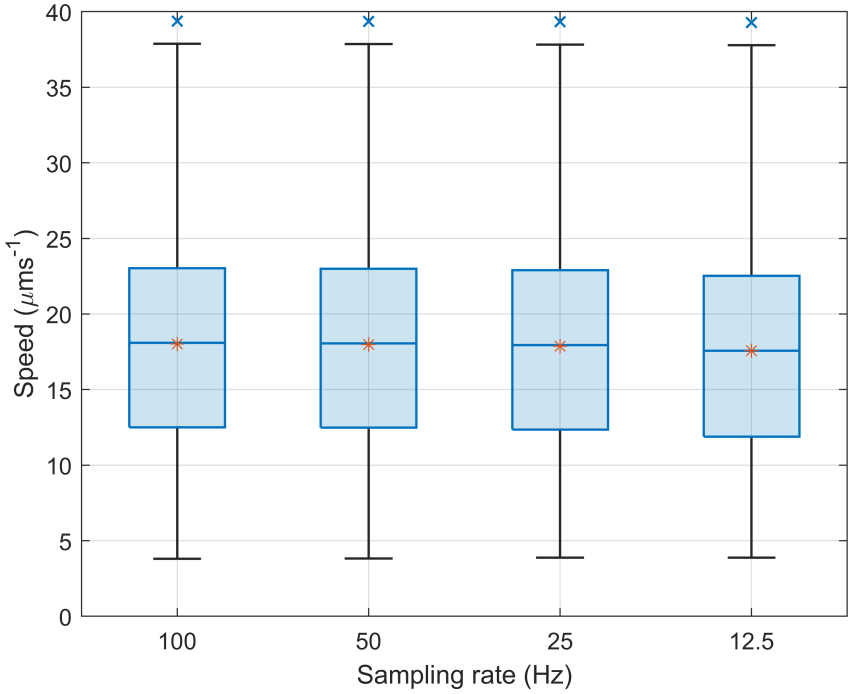

Figure 2.17: Boxplot showing the measured swimming speeds of exponential phase *E.coli* cells at different frame rates. The box shows the interquartile range (IQR), with the centre line shows the median value and the orange star the mean. Outliers are indicated by the blue x. The number of tracks analysed is 1364 in all cases.

As can be clearly seen from Fig. 2.17, down sampling the data did not have a significant impact upon the measured swimming speed, indicating that imaging at 100 HZ was not causing an increase in measured speed. However, at lower sampling rates the reorientation events were often not detected. The overall number of detected turns decreasing from 13180 at 100 Hz to only 7962 at 12.5 Hz. This is most likely due to turning events occurring too quickly for the apex of the turn to be captured and therefore the overall angle change dropping below the detection threshold. This will give misleading run time and reorientation angle values. As can been in Fig. 2.18, the average re-orientation angle dropped significantly with sampling rate from 76°at 100 Hz to 52°at 12.5 Hz. This data indicates that using a high frame rate is critical to capturing the full detail of motility behaviour including reorientation events.

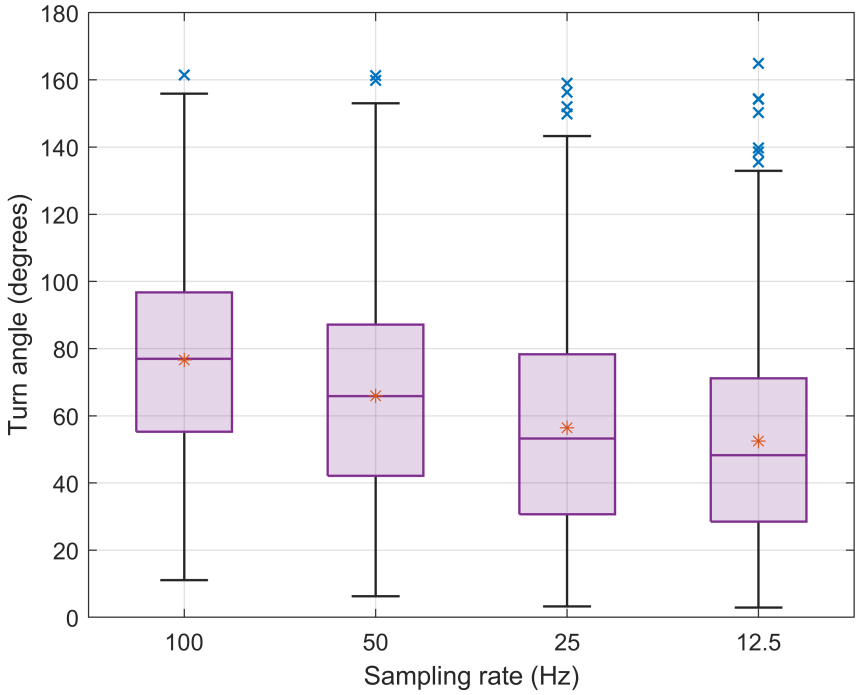

Figure 2.18: Boxplot showing the measured reorientation of exponential phase *E.coli* cells at different frame rates. The box shows the interquartile range (IQR), with the centre line shows the median value and the orange star the mean. Outliers are indicated by the blue x. The number of tracks analysed is 1364 in all cases.

2.7.7 Tracking errors in DIHM

There are sources of error throughout the process of imaging and tracking with DIHM. Some of these have been discussed in the sections above, including contributions from the noise in the camera in section 2.7.5.4. In addition to camera noise, there are other possible sources of error in the image capturing process. Firstly, dirt or dust on the surface of sample chamber could be incorrectly identified as a cell. However, these imperfections are generally removed by the background noise suppression described in section 2.7.5.1. If not, as these objects do not move they will be filtered by the LabVIEW code as non motile and so will not be recognised in swimming trajectories. Secondly dust can occasionally pass through the air between the laser optical fibre and the sample chamber. This will appear in the video as a very large fast moving object. This happened rarely, and any videos containing this were discarded before analysis. Also, any physical vibrations of the optical elements would impact the hologram quality. Therefore the microscope was placed on an air isolated optical bench. Lastly, flow in the sample chamber could cause errors in the motility results. Specifically, flow in the sample chamber could make cells appear to be swimming faster than they are. In order to reduce the

likelihood of flow, samples were put onto the stage and the laser turned on for 10 mins before data was collected. This enabled any slight temperature changes due to the laser to stabilise, minimising convection. In addition, the narrow chambers with very small openings (200 nm high), minimise the chance of evaporation and any resulting fluid flow.

As well as sources of error in the image capturing there are also sources of error in the cell localisation. These can result from the z step size or intensity threshold values being set incorrectly. The setting of these parameters is discussed in section 2.7.5.2. In particular the intensity threshold used to find the x and y position of cells is crucial. If this threshold is set too low it can enable any remaining noise in the video to be identified as a cells. Even if set at appropriate value this may happen occasionally however, caused by, for example stationary dust. The impact of this is again mitigated by the stationary nature of this noise.

In terms of analysing the trajectories for characteristic values there are a set of manually applied parameters that have to be balanced to enable the identification of features. This includes the balance parameter from the spline smoothing and the minimum angle threshold in the re-orientation detection. These two work in tandem on ensure the main features can be picked out from trajectories. The minimum amount of smoothing possible is used to enable accurate speed measurements to be made. The speed consistency across down sampling seen in Fig. 2.17 adds confidence that the measured speed value is accurate. In general it can be hard to tell the difference between very low angle changes and noise in a trajectory caused by Brownian motion. The addition of the rolling mean angle value in the reorientation detection code (discussed in section 2.7.6.4), helps to flatten the impact of noise that occurs on a shorter time scale than turning events. However, it is still possible that a small number of lower angle turns could be missed by the identification analysis.

As with any biological project, there is intrinsic variability within populations of bacteria including those which might be at different stages of their growth cycle. This can lead to variability in motility characteristics within a cell culture. In order to minimise the impact of any outliers on the measured values of a data set, it is important to image a large number of cells. In this project over 24,000 individual trajectories were captured and analysed. In addition, to this at least three separate cell cultures were used to make up the data set for each experiment. If there were any significant outlying results belonging to one culture this may indicate some issues with growth such as an infection, and this data

may be dismissed. During this project there were no outlying cultures.

As well as undertaking biological replicates, completing technical replicates can increase confidence in results. During this project multiple imaging runs were completed on different days. In addition, at least three videos were taken of every sample. Similarly to imaging many cultures, strange images or outlying results could be an indication of issues with the instrumentation. No outlying technical replicates were identified during this project.

Ultimately there will always be an aspect of estimation in the motility characteristics obtained from DIHM. This is mostly due to the nature of the analysis process. However, during this project significant efforts were made to reduce the impact of noise and choose the most appropriate parameters during analysis. This, combined with the very large number of cells imaged, minimised the contribution of error in results obtained here.

2.7.7.1 Histograms for population level data

Once the key motility characteristics have been calculated they are plotted and studied to look for patterns that may tell us more about the swimming behaviour of the cells. The MATLAB analysis code generates histograms including of the average swimming speeds per trajectory, run-lengths and plots of run-length against turning angle etc. Unless otherwise stated the number of bins and their width was determined using the Freedman-Dicanois rule (see appendix A). Histograms were fitted using built in MATLAB distribution fitting functions (fitdist), including kernel density fittings. In the case of the run times histograms the x axes were clipped to not show bins with two or less runs, enabling better visualisation of the main distributions. Further specifics of these plots can be found in the results chapter.

2.7.7.2 Statistical significance testing

When looking for differences or changes in behaviour the mean and standard error were considered first. However, statistical testing was also applied as there were cases where the distributions of data were very similar and the differences subtle and not immediately clear. This consisted of using the Kruskal-Wallis test. This particular method was chosen as unlike other popular significance testing methods such a the Mann-Whitney U-test it does not assume an underlying Gaussian distribution to the data - the importance of which will become apparent in the results chapter.

2.8 Cell culturing procedure and sample preparation

2.8.1 *B. bacteriovorus* culturing procedure and sample preparation

Throughout this project *B. bacteriovorus* were cultured using a procedure based on the published protocol by Carey Lambert [193], with a step by step guide, including media recipes, in appendix B. *E. coli HCB1*, a highly motile strain used by Howard Berg in classic studies of bacterial motility, was used throughout all experiments as the prey bacterium [162]. *E.coli* strains have a variety of different swimming abilities - this strain was chosen as it has well studied characteristics and as a highly motile strain is an interesting challenge for the predatory cells.

The prey cells were grown using an *E. coli* glycerol stock stored at -80°C to inoculate 20ml of YT media in a 125ml conical flask. They were incubated overnight (approximately 16h) at 29°C and 150rpm shaking. The cells were then removed from the incubator the following morning for use in experiments. Unless otherwise stated, these are the prey cells referred to throughout this thesis. I found that it was essential to *B.bacteriovorus* growth that newly cultured prey cells were used every time. Therefore these were prepared fresh each day.

The process of culturing *B. bacteriovorus* started by making double layer, overlay, YPSC agar plates. The bottom layer of the plate contained only YPSC media and was thicker than the top layer (1% agar). The top layer of the agar plates was much softer (0.6% agar) and contained live stationary phase *E. coli* prey cells. This required the agar to be cooled to just above setting temperature (60°C) and the live prey cells added before pouring. This softer agar allowed predation to occur. Frozen -80°C glycerol stocks of *B. bacteriovorus* were dotted onto the centre of these plates. They were then incubated upright, at 29°C, for one night, then upside down, also at 29°C, for 5-7days or until clearing of the top layer was seen (this indicates predation). The amount of time for clearing and the extent of clearing was quite variable, as can be see in Fig. 2.19. However, once it appeared, plates could be used multiple times to create new liquid cultures. The upmost care had to be take to maintain sterile technique.

Once the plate had shown clearing the next stage of culturing could be carried out. This involved making a mini lysate of predating cells and prey in liquid. It was prepared in a 15ml test tube. This contained 2ml of Calcium/HEPES buffer,

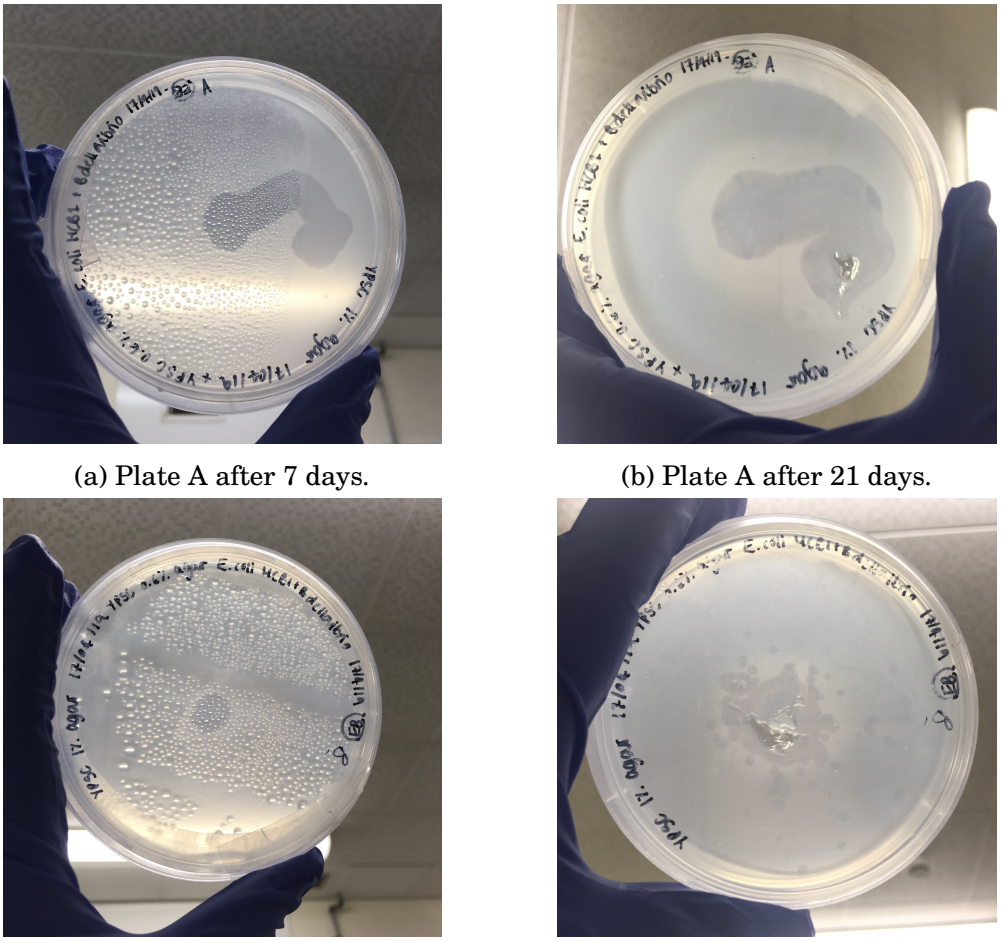

(a) Plate A after 7 days.

(b) Plate A after 21 days.

(c) Plate B after 7 days.

(d) Plate B after 21 days.

Figure 2.19: Photographs of *B. bacteriovorus* overlay agar plates - 1% agar, YPSC under-layer, and 0.6% agar, YPSC over-layer, impregnated with live *E.coli* prey cells. *B. bacteriovorus* spotted on showing as a clearing of the top agar layer.

150µl of prey cells and cleared agar picked from the overlay plate. This mixture was incubated at 29°C and 150rpm shaking for 1-2days until highly motile *B. bacteriovorus* could be seen using darkfield microscopy.

Finally a main lysate was prepared for use in experiments. This contained 50ml of Calcium/HEPES buffer, 3ml of prey cells and 1ml of mini lysate, prepared in a 250ml conical flask. This was incubated at 29°C with 200rpm shaking for 24h. This main lysate was sub-cultured every 24h using fresh prey cells and replacing the mini lysate inoculation with the previous main lysate (1ml each time). I found that *B.bacteriovorus* was most successful when this feeding and sub-culturing process was performed at strictly the same time every day, with fresh prey cells that had also been grown in at a consistent time.

All *B. bacteriovorus* cells were imaged between 18-24h of co-culture in the Calcium/HEPES buffer they were grown in. This buffer has no nutrients - only calcium salts and pH buffer (to maintain a pH of 7.6). Samples of 3ml were removed from the main lysate for imaging. The 3ml samples were filtered using a 0.45μm syringe filter to remove any remaining prey cells and debris. The filtered cells were initially imaged using a darkfield microscope to check cell activity and density. Next they were diluted to an appropriate density for holography using sterile Calcium/HEPES buffer - typically between 50-100 times dilution. The diluted sample was pipetted into the sample chambers (made as specified in section 2.7) ready for imaging.

2.8.2 *E. coli* culturing procedure and sample preparation

In order to more easily determine between predator and prey cells in mixed sample experiments, the baseline motility characteristics of *E. coli* cells were studied alone. This section describes the procedure used to prepare the cells for these 'prey only' experiments.

In order to make a good comparison to the prey cells used in predation experiments the *E. coli HCB1* were grown in the same way as for the *B.bacteriovorus* method - as specified in section 2.8.1. For the stationary phase prey cells, they were then imaged immediately or stored in the fridge for short periods before imaging at room temperature. For the exponential phase cells, 100μl of the overnight culture was then taken and added to 10ml of YT. These cells were incubated at 29°C, 150rpm shaking for approximately 4h, or until an optical density (OD_{600}) of approximately 0.25 or greater was achieved.

In both the stationary and exponential phase cases, the cells were washed before they were imaged - to remove any debris and reduce the background scattering from the medium. This washing was performed by centrifuging 1ml of cells for 3min at 800rpm, then removing the supernatant and re-suspending them in Calcium/HEPES buffer. This process was repeated 3 times. The cells were then diluted between 10-100 times with more Calcium/HEPES depending on the original density and checked under darkfield to confirm an appropriate quantity of motile cells. This cell suspension was then pipetted into a sample chamber for imaging.

CHAPTER 3

RESULTS: *B. bacteriovorus* SWIMMING BEHAVIOUR

3.1 Introduction

This chapter presents the results for this research project including the characteristics of prey *E. coli* swimming behaviour both in exponential and stationary growth phases, the baseline motility characteristics of *B. bacteriovorus* alone and some hypotheses about their behaviour and a comparison of *B. bacteriovorus* swimming behaviour near surfaces to that in the bulk. Finally, a study of *B. bacteriovorus* swimming behaviour in the presence of prey cells is presented in which I look for evidence of prey hunting behaviour.

All trajectories analysed in this section are from cells which have been determined to be actively swimming (not dead or diffusing cells), using the methods described in section 2.7.5.3.

3.2 *E. coli* prey motility

In order to more easily determine between predator and prey cells in future experiments, the baseline motility characteristics of *E. coli* prey cells were studied alone. Both exponential and stationary phase cells were studied as *B. bacteriovorus* encounters a variety of prey conditions in its natural environments and whilst in laboratory conditions they are typically fed with stationary phase cells, exponential phase cells are generally faster swimming and more motile and therefore present a more interesting predation challenge.

3.2.1 *E. coli* example swimming trajectories

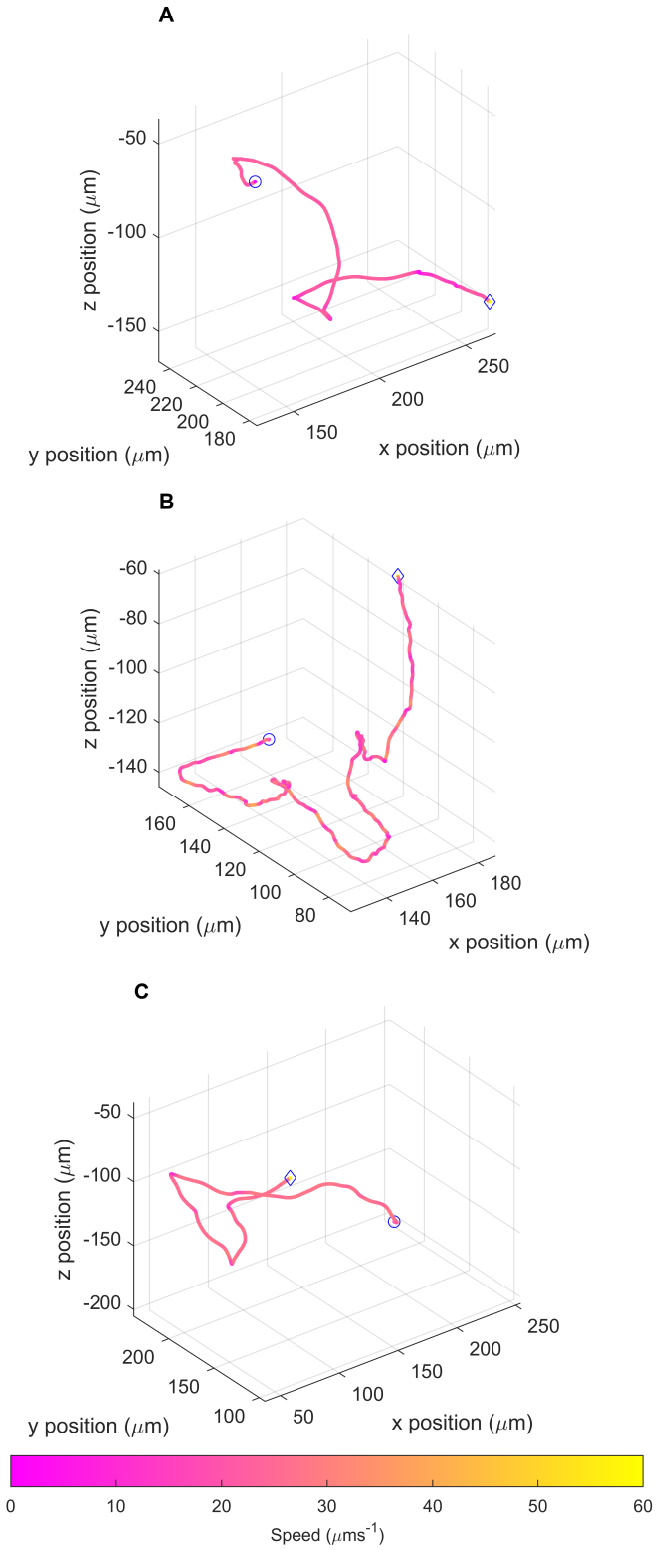

Figure 3.1: Example 3D swimming trajectories of exponential phase *E. coli HCB1*. The colour indicates the speed along the trajectory, shown by the . The circle indicates the start point of each trajectory and the diamond the end point.

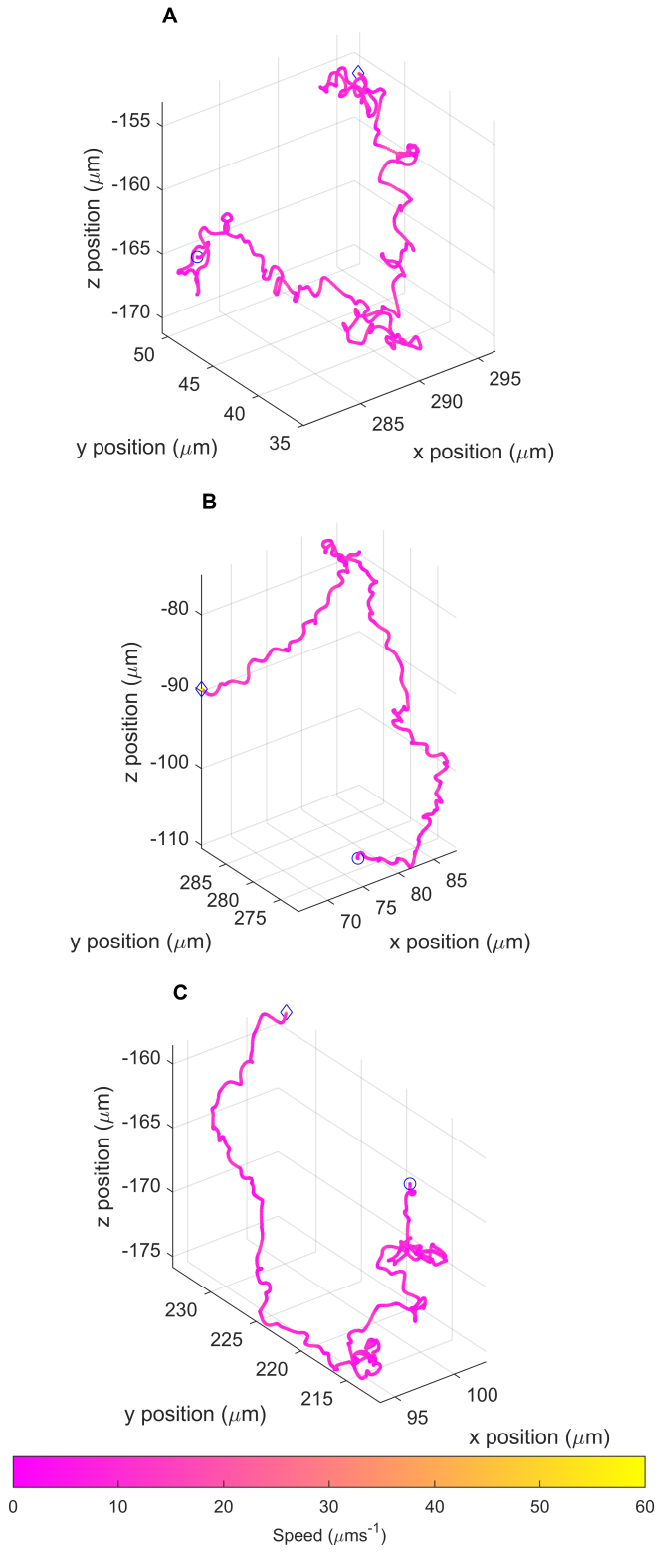

Figure 3.2: Example 3D swimming trajectories of stationary phase *E. coli HCB1*. The colour indicates the speed along the trajectory, shown by the colour bar. The circle indicates the start point of each trajectory and the diamond the end point.

Figs. 3.1 and 3.2 show some examples of the *E. coli* swimming trajectories gathered during this project. As can be seen in these figure the cells performed a random walk with longer sections (runs) interspersed with changes of direction (re-orientation events). The exponential phase cell trajectories, in Fig. 3.2 are typical of *E. coli* cells, showing the run and tumble type behaviour first described by Howard Berg and later studied extensively by various groups [98, 173, 194–197].

The stationary phase cell trajectories, in Fig. 3.1, show a lower persistence than the exponential cells that may result from a decrease in swimming speed and average run time. This and further differences or similarities in key characteristics, including swimming speed, have been quantified and discussed in sections 3.2.2-3.2.6 below.

3.2.2 *E. coli* swimming speeds

Fig. 3.3 shows histograms comparing the mean swimming speeds of exponential phase (A/yellow) and stationary phase (B/red) *E. coli* cells. The exponential phase cells swim at 18.0 μms^{-1} with a standard deviation of 6.9 μms^{-1} and standard error of 0.2 μms^{-1}. The distribution has a skew of 0.20 and a kurtosis of 2.52. In comparison the stationary phase cells swim at 9.9 μms^{-1}, with a standard deviation of 3.5 μms^{-1} and a standard error of 0.2 μms^{-1}. This distribution has a skew of 0.011 and a kurtosis of 2.42. This indicates both distributions are fairly symmetrical and have few outliers. Stationary phase cells show a drop in speed of 8.1 μms^{-1}, to just over half the speed of the exponential cells. The Kruskal-Wallis test gives these data sets a p value of 1.0×10^{-65} which confirms that the difference between them is significant.

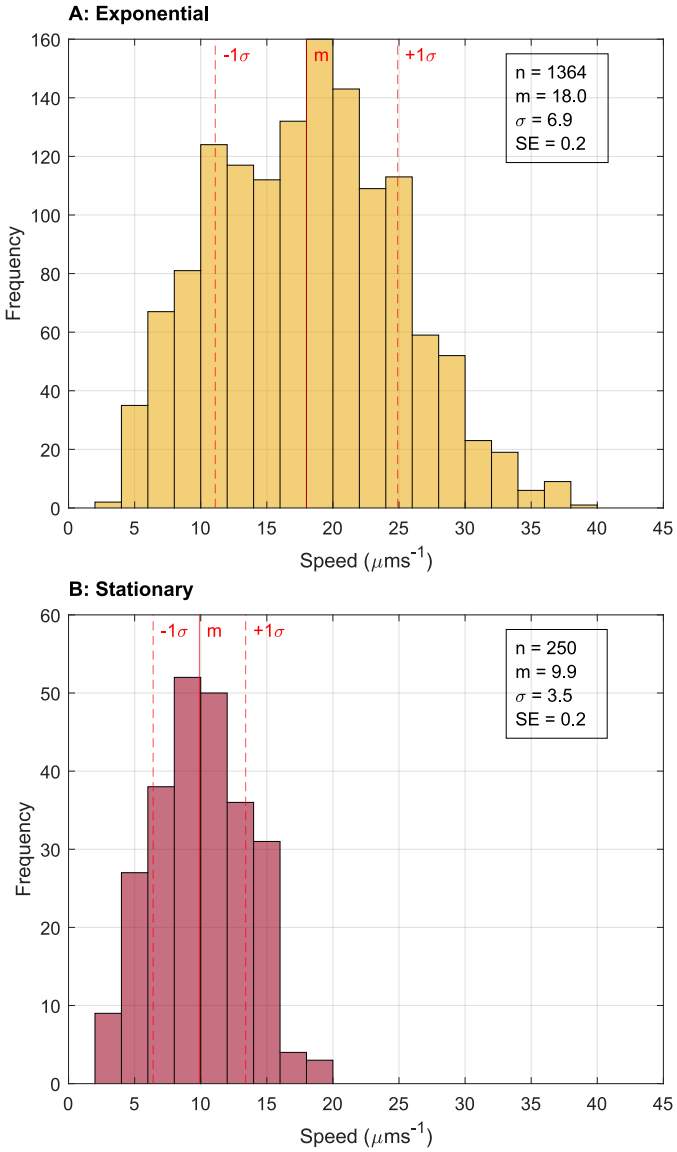

Figure 3.3: Histograms showing the mean swimming speed for *E. coli HCB1*. *A:* Exponential phase cells (yellow). *B:* Stationary phase cells (red). In both cases n is the number of trajectories, m is the mean (also indicted by the solid red line), σ is the standard deviation (also indicated by the dashed red lines) and SE is the standard error.

3.2.3 *E. coli* run times

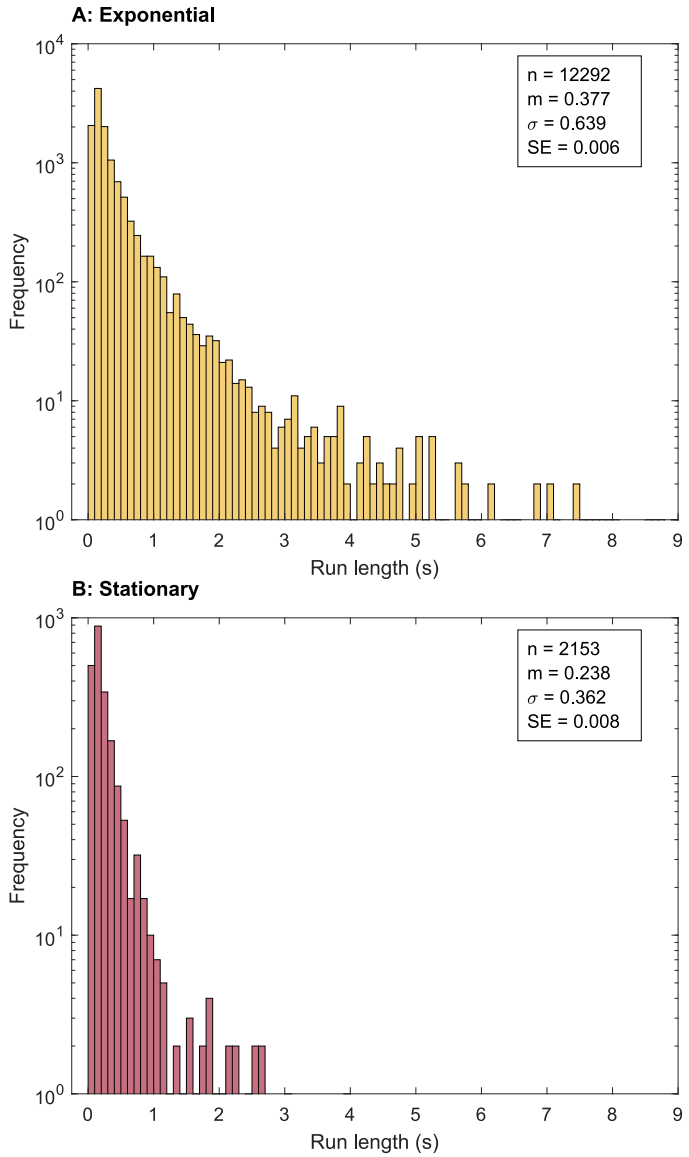

Figure 3.4: Histograms showing the run times for *E. coli HCB1*. *A:* Exponential phase cells (yellow). *B:* Stationary phase cells (red). In both cases n is the number of trajectories, m is the mean, σ is the standard deviation and SE is the standard error.

Fig. 3.4 shows histograms comparing the run times of exponential phase (A/yellow) and stationary phase (B/red) *E. coli* cells. The exponential phase cells have a mean run time of 0.377 s, with a standard deviation of 0.639 s and a standard error of 0.006 s. The stationary phase cells have a mean run time of 0.238 s with a standard deviation 0.362 s and a standard 0.008 s. There is a drop in the average run time of 0.139 s, showing that the stationary phase cells re-orient more frequently as can be seen qualitatively in Fig. 3.2. The Kruskal-Wallis test gives these data sets a p value of 2.2×10^{-38} which confirms that the difference between them is significant.

3.2.4 *E. coli* re-orientation angles

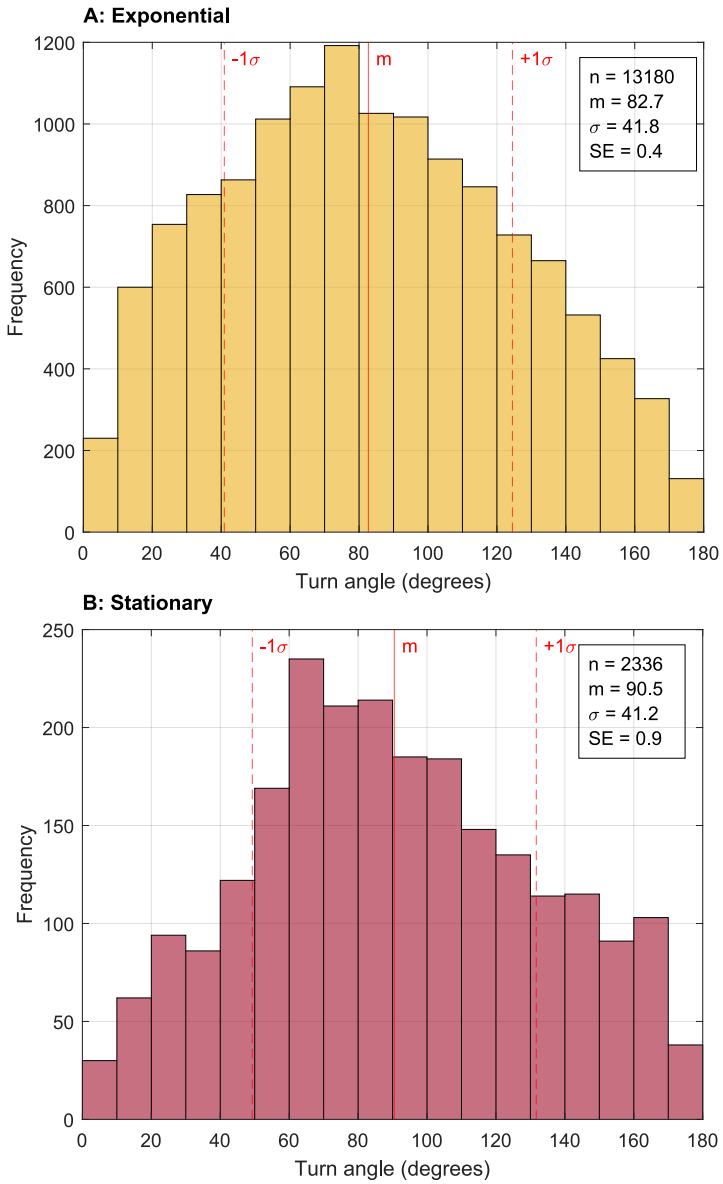

Figure 3.5: Histograms showing the re-orientation angles for *E. coli HCB1*. *A:* Exponential phase cells (yellow). *B:* Stationary phase cells (red). In both cases n is the number of trajectories, m is the mean and σ is the standard deviation.

Fig. 3.5 shows histograms comparing the re-orientation angles of exponential phase (A/yellow) and stationary phase (B/red) *E. coli* cells. The exponential phase cells have a mean re-orientation angle of 82.7 °, a standard deviation of 41.8 °, and a standard error of 0.4 °. The stationary phase cells have a mean re-orientation angle of 90.5 °, a standard deviation of 41.2 °, and a standard error of 0.9 °. Interestingly, the stationary phase cells have a greater turning angle by 7.8 °. The Kruskal-Wallis test gives these data sets a p value of 3.4×10^{-10} which confirms that the difference between them is significant.

3.2.5 *E. coli* trajectory characteristic patterns

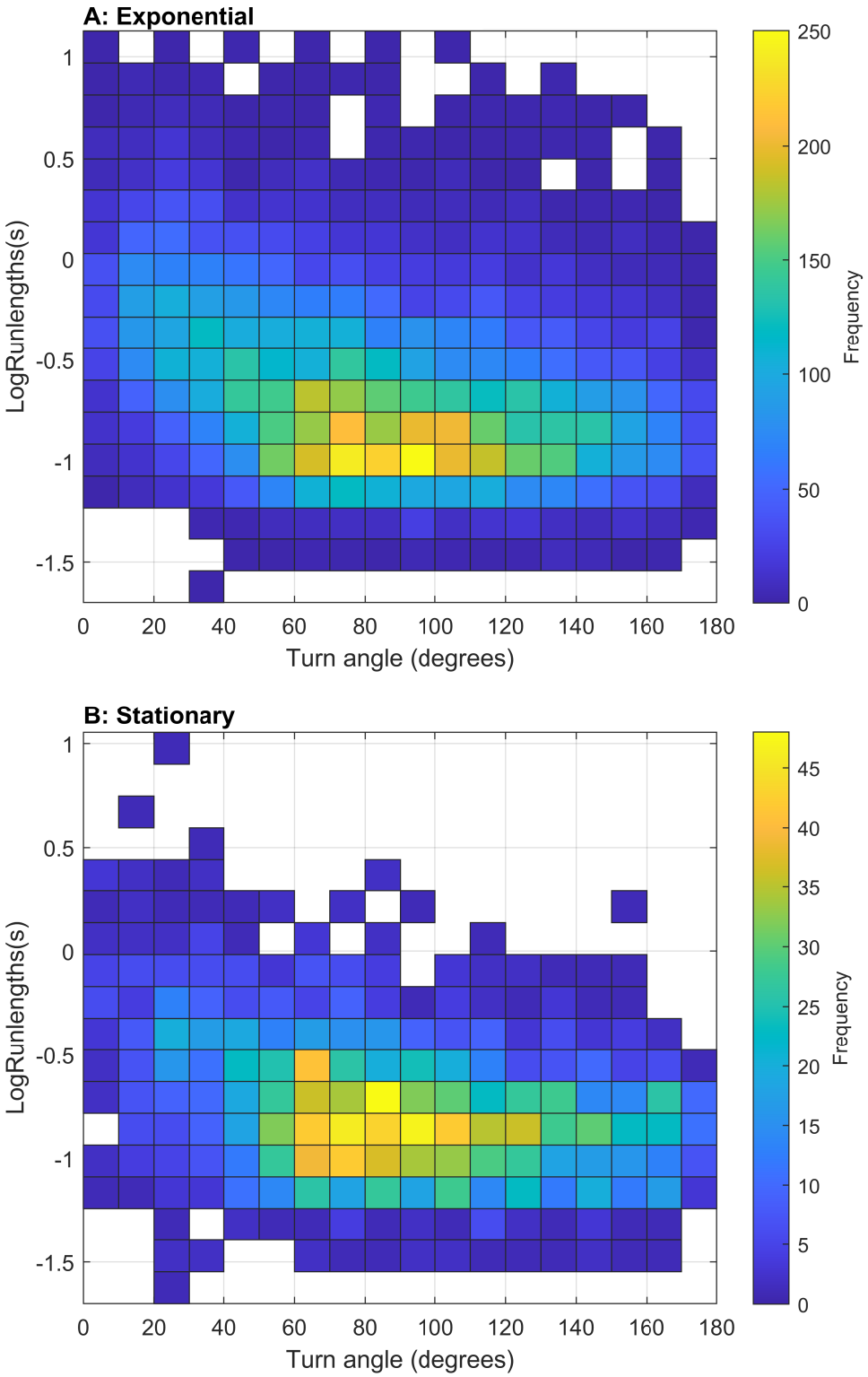

Figure 3.6: Bi-variate histograms of *E. coli* re-orientation angles against run times. *A:* Exponential phase cells. *B:* Stationary phase cells. The colour bar indicates the frequency when 1 count = 1 re-orientation event.

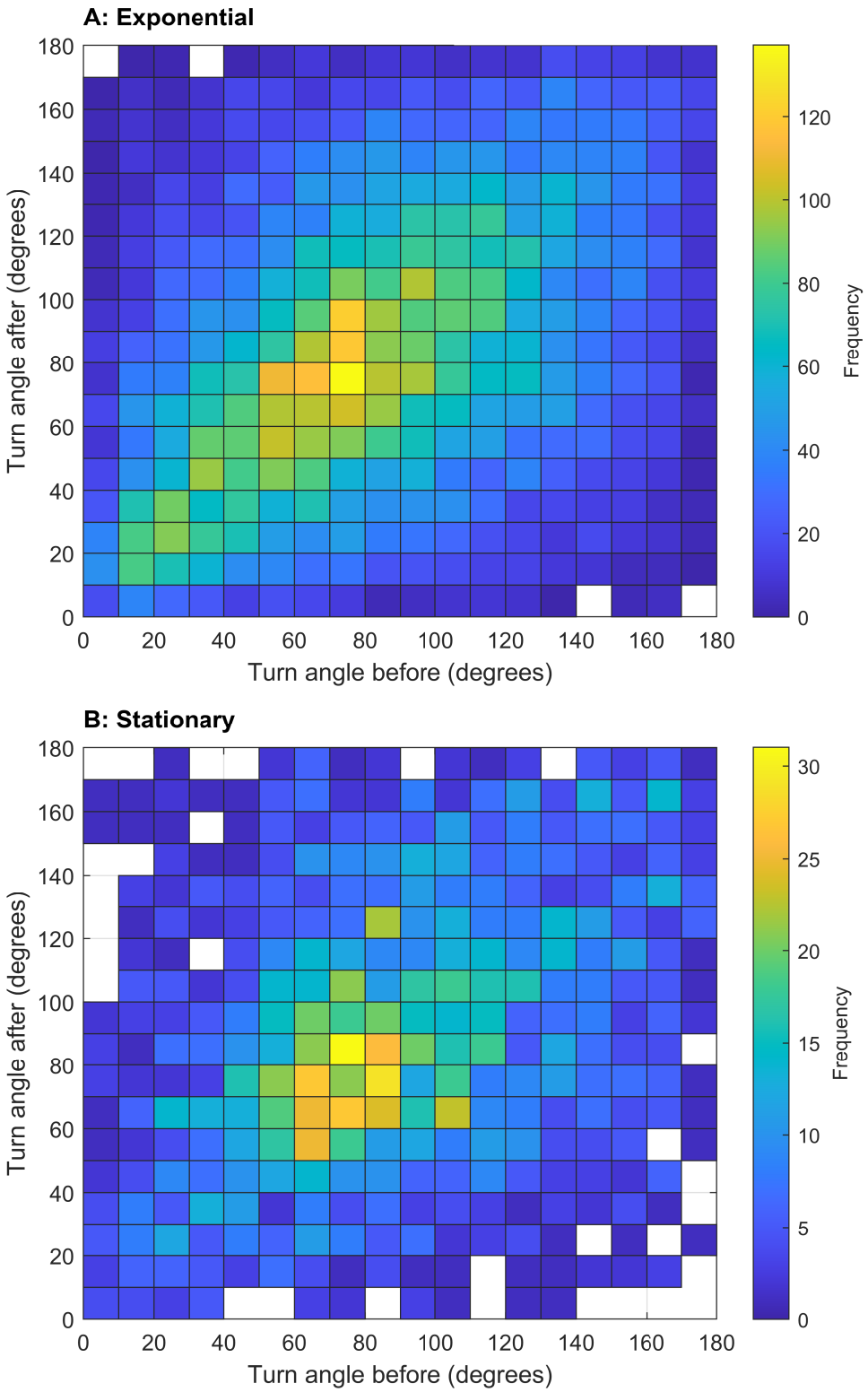

Figure 3.7: Bi-variate histograms of *E. coli* re-orientation angles before and after a run. *A:* Exponential phase cells. *B:* Stationary phase cells. The colour bar indicates the frequency when 1 count = 1 run.

Fig.s 3.6 and 3.7 displays bi-variate histograms showing the relationship between run times and re-orientation angles, and the pattern of re-orientation angles found in *E. coli* cells. The two sets of histograms show similar patterns that indicate a consistent swimming style.

Fig. 3.6A and B both show a single cluster of events with a shape that slopes upwards towards the lower angle end of the plot. It appears that below approximately 40 ° re-orientation angles are more likely to be associated with longer runs than higher angle changes. This pattern can be seen in both the exponential and stationary phase cells. These plots also have a similar covariance: A of -6.19 degree-seconds and B of -3.68 degree-seconds. This confirms that the cells behave similarly in the exponential and stationary phase.

Both plots in Fig. 3.7 have a high frequency band moving from bottom left to top right of the plot. The covariance values of 677 degree-degrees, for Fig. 3.7A, and 591 degree-degrees, for Fig. 3.7B, show there is a positive correlation between turning angles before and after a run. This indicates that each re-orientation event is likely to be followed by another of similar angle change.

3.2.6 Discussion: *E. coli* motility characteristics

The data in sections 3.2.1-3.2.5 show the characteristic behaviour of *E. coli* cells demonstrating the run and tumble style of swimming which has been previously documented by Howard Berg and others [98, 103, 124, 173, 195]. This run and tumble style swimming is consistent between both the exponential and stationary phase cells, as indicated by the similarities of the shape and covariance of the plots in Figs. 3.6 and 3.7. However, despite this consistent style there are clear differences in all of the key characteristics.

The swimming speed of the exponential phase cells, 18.0±6.9 μms^{-1} (± indicates standard deviation) is within the range of other studies of *E. coli* swimming in three dimensions: approximately 10-26 μms^{-1} [98, 103, 124, 173, 198]. The variations in these speeds is most likely a result of the natural physiological variations between the strains of *E. coli* studied. These differences could be due to environmental pressures driving factors such as changes in cell body size, flagellum length and structure, biochemical machinery that determines their swimming response to stimuli and other related biological functions.

The exponential phase *E. coli* run times found in this study are shorter than previous studies at 0.377±0.639 s compared to 0.86 ±1.18 s found by Berg and Brown [98] and 0.93 ±1.32 s by Molaei et al [103]. The variation between the different cell strains used may account for the shorter run times in this study. The long tailed distribution seen in the run times appears very similar to that for wild type *E. coli* cells found by Huo et al. [124]. They found that wild type cells had a large variation in their run duration including few very long runs consistent with a Lévy walk model of behaviour. As discussed in section 1.3.4, Lévy walk is a pattern of behaviour which enables efficient searching of an environment for sparsely located nutrients. It is possible that the wild type cells in this study also utilise a Lévy walk to improve their nutrient locating efficiency. This distribution is also what gives rise to the shape of the run length histogram, including the peak in the data (and therefore the first histogram bin not having the greatest frequency value).

The mean turn angle found for the exponential phase *E. coli* cells is 82.7±41.8° making it greater than those found by both Berg and Brown at 68.0 ±36.0 ° and Molaei et al. at 71.3 ±44.0 ° [98, 103]. As previously mentioned, this is most likely due to variation between cell strains. A previous study by Kong et al. found through modelling that, *E.coli* reorientation angle is dependent upon both the number and the position of the flagella, both of which can vary with cell strain [199]. They also found that reorientation is approximately linearly correlated to the tumbling time of the cell. It is hard to say if there is a optimum turning angle for *E.coli* swimming behaviour. Any optimum value would be dependent on the the environmental conditions including the viscosity and homogeneity of the medium through which the cells are moving. It would also be linked to the run times of the cells. For instance if cells were to have a high average reorientation angle combined with a low average run time this would result in low persistence trajectories. In contrast a low average reorientation angle and high average run length would result in high persistence trajectories. In reality there is distribution in both which results in some intermediary persistence. In the context of nutrient searching efficiency, most studies have focused on run times rather than reorientation angles (see section 1.3.4 for details).

Stationary phase *E. coli* motility hasn't been studied in this depth before. This is perhaps because the fraction of motile cells drops substantially when moving from exponential to stationary phase. The stationary phase *E. coli* cells show a significant drop in the swimming speed compared to exponential phase cells of approximately 8.1 μms^{-1}. Considering the biological context of stationary

phase cells this change is logical. The stationary phase of the bacterial life-cycle is generally considered to be the stage at which cells have stopped growing but still remain metabolically active [200]. It can be brought about by a number of stressors in the cells environment such as changes in pH or temperature but is most often associated with a lack of nutrients [201]. There are a variety of ways that cells behave in stationary phase including entering forms of dormancy [202]. However, in all of these cases and when considering the significant proportion of the cells energy budget which is taken up by the flagellar motor, it is logical that swimming would be decreased to conserve energy for other essential mechanisms within the cells. Indeed a previous study has shown a drop in both the number of flagella and the amount of flagellum that is found in stationary phase cultures compared to exponential phase, as well as drop in overall swimming speed [203].

The stationary phase *E. coli* cells also showed a significant change in mean run time - dropping by approximately 0.139 s. In addition, they show a significant increase in mean turning angle by 7.8 °. Both of these changes are interesting and require further study to understand fully. However, it is known that the run times of *E. coli* are mediated by the chemotaxis chemical pathway within the cell whilst in the exponential phase of cell growth. It may be possible that when moving into the stationary phase this pathway is disrupted in some way which could impact both the run times and turning angles of the cell. Past studies have show that cells lose flagella in the stationary phase, which would impact their swimming significantly. In particular, cells may be in some type of intermediary stage of flagellum shedding or re-absorption which would change their overall motility characteristics. As previously mentioned, it is important to recognise that different strains of *E. coli* and differences in culturing media and techniques which contribute to the environment of the cells can have a non-negligible impact on motility. This may account for some of differences between the results seen here and in previous studies.

The *E. coli* prey cell behaviour described in this section can be considered somewhat of a baseline - it serves as a useful comparison to the following sections on *B. bacteriovorus* behaviour which as can be seen below shows a distinctly different pattern of swimming. It has also been used to to enable bacteria type identification from trajectory data as described in section 3.6.2.

3.3 *B. bacteriovorus* motility

3.3.1 *B. bacteriovorus* example trajectories

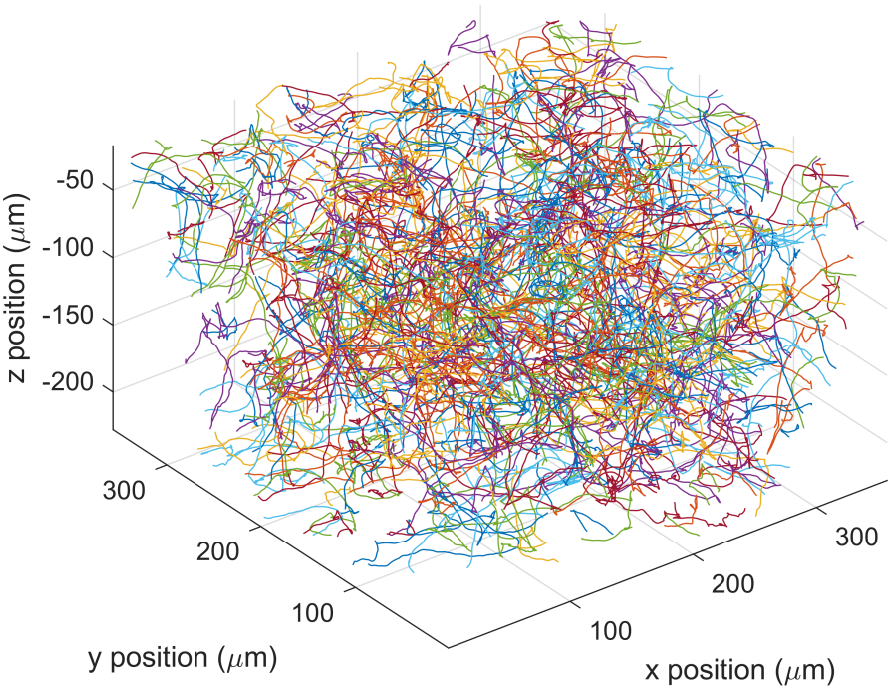

Figure 3.8: Three dimensional plot of *B. bacteriovorus* swimming trajectories taken from a single video, showing a cross-section of the entire sample chamber. Each coloured plot represents a single trajectory.

The plot in Fig. 3.8 contains 607 three dimensional *B. bacteriovorus* swimming trajectories - this is approximately 3% of the total 20408 *B. bacteriovorus* swimming trajectories imaged and analysed during this project (samples containing only *B. bacteriovorus*).

Fig. 3.9 shows as series of plots of single *B. bacteriovorus* swimming trajectories. Here the colour indicates the speed along the trajectory. As can be seen in the example trajectories the cells swim in a random walk of long persistent runs punctuated by re-orientation events. The plots show that the speed of the cells varies along the trajectory, reducing most significantly around re-orientation events.

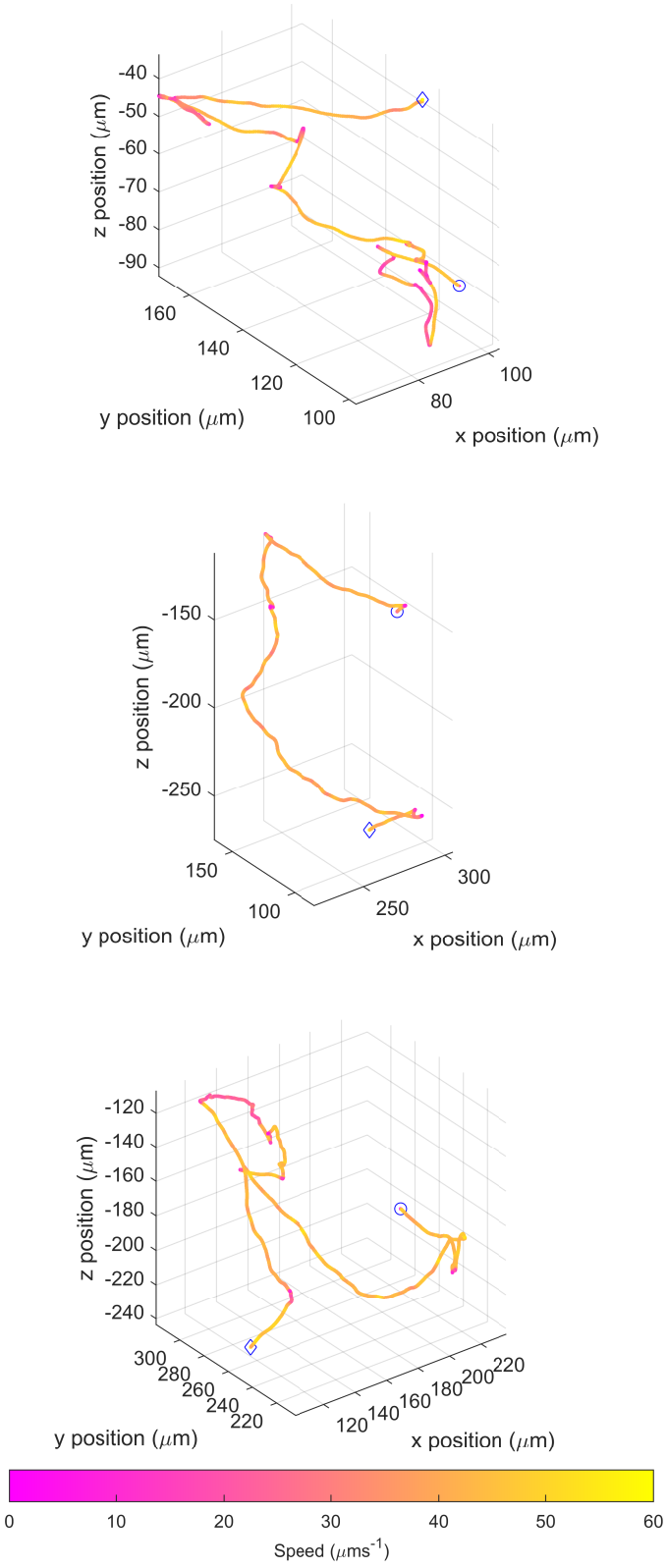

Figure 3.9: Example 3D swimming trajectories of *B. bacteriovorus*. The colour indicates the speed along the trajectory, shown by the colour bar. The circle indicates the start point of each trajectory and the diamond the end point

3.3.2 *B. bacteriovorus* swimming speeds

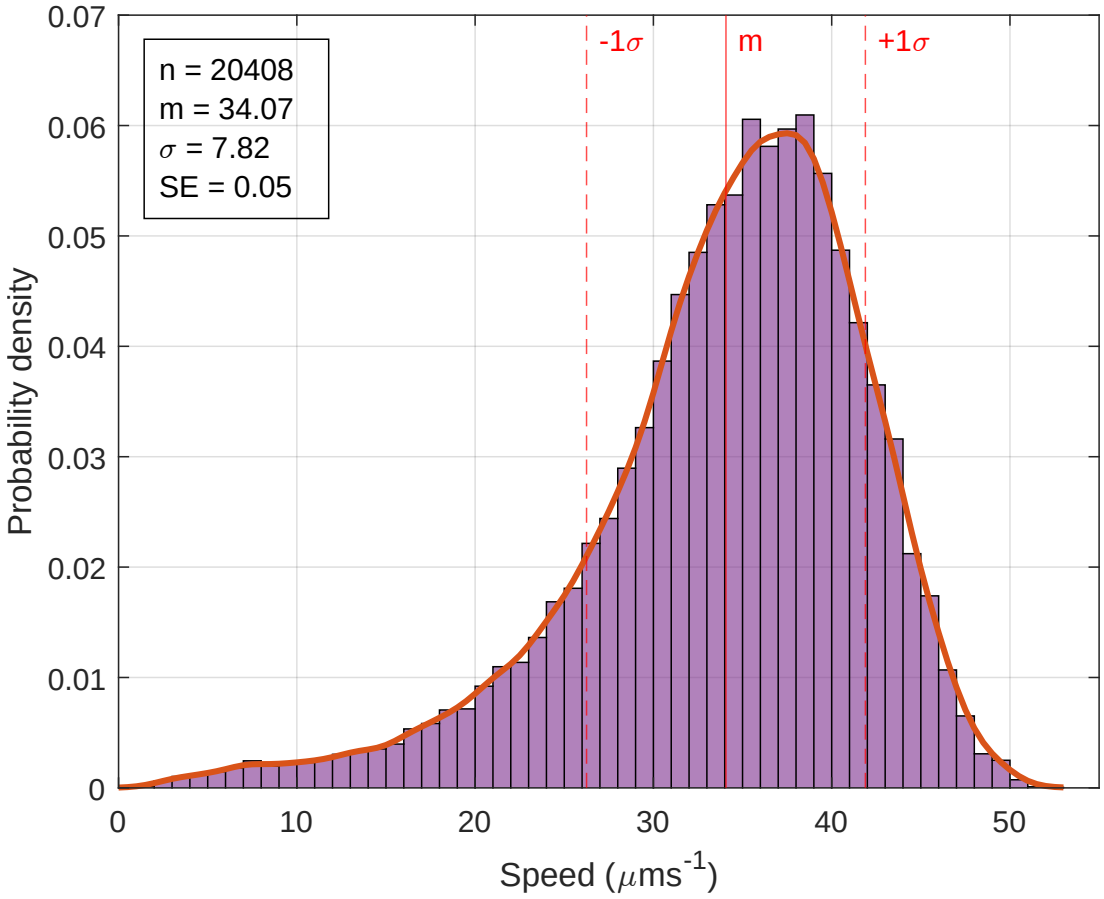

Figure 3.10: Histogram showing the distribution of mean swimming speeds of *B. bacteriovorus* trajectories. The key includes some overview statistics : n is the number of trajectories, m is the overall mean speed (also shown by the solid red line), σ is the standard deviation (also shown by the dashed red lines), and SE is the standard error. The histogram has been fitted with a kernel density estimation curve.

Fig. 3.10 shows a histogram of the average swimming speeds of *B. bacteriovorus* trajectories. Each value in the histogram represents the mean instantaneous velocity vector of a trajectory with n being the number of trajectories. The overall mean swimming speed is 34.1 μms^{-1} with a standard deviation of 7.8 μms^{-1} and a standard error of 0.05 μms^{-1}. The histogram has been fitted using a kernel density estimation (KDE), non-parametric model shown by the red line. The distribution has a skew of -0.99 and a kurtosis of 4.4, this indicates that the distribution has a heavy left handed skew and relatively few outliers. It *B.bacteriovorus* is significantly more left skewed than the *E.coli* distributions in Fig. 3.3. The breadth of the distribution reflects the intrinsic variation within the population of cells, showing a long left handed tail towards slower speeds.

3.3.3 *B. bacteriovorus* run times

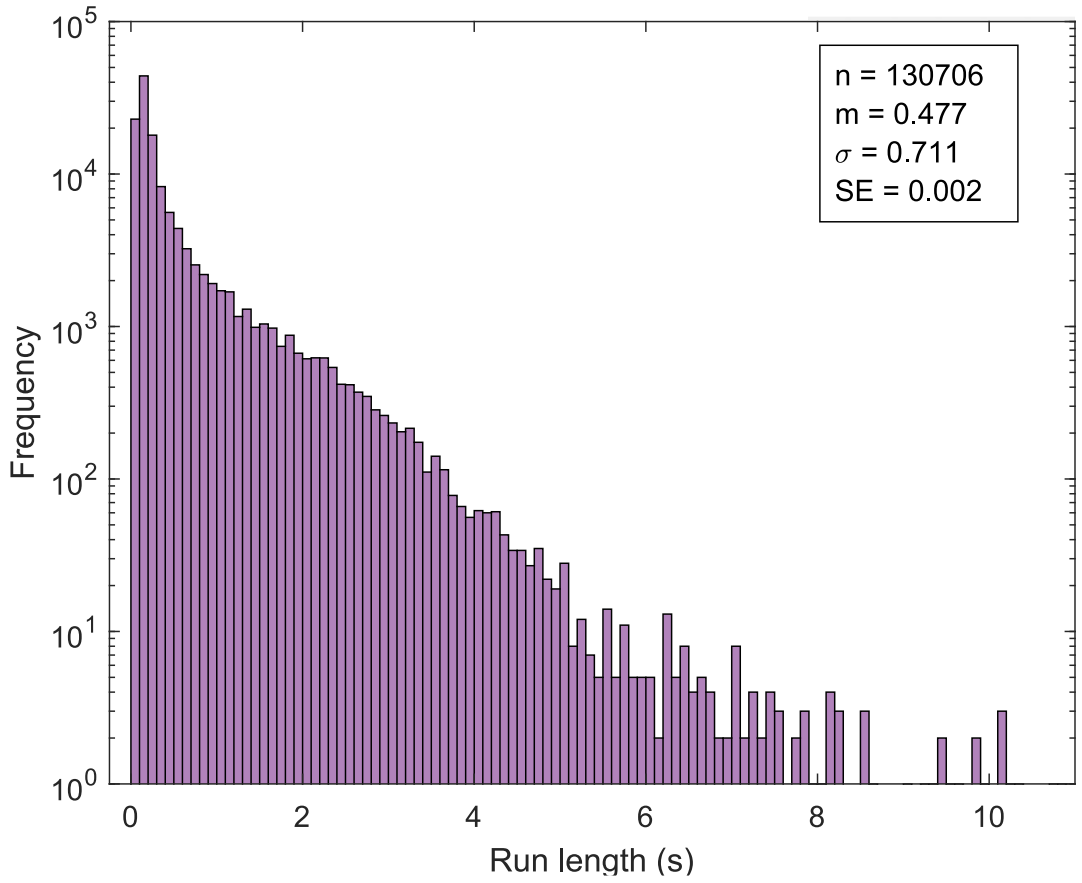

Figure 3.11: Histogram showing the distribution of run times for *B. bacteriovorus* swimming trajectories. Where n is the number of runs, m is the mean run time, σ is the standard deviation and SE is the standard deviation. Note the x axis has been clipped at 11 s to better display the distribution (excludes bins containing 2 or less runs).

The histogram in Fig. 3.11 shows the distribution of run times (amounts of time between re-orientation events) for *B. bacteriovorus*. The histogram is taken from analysis of 130706 runs which have an average length of 0.477 s, with a standard deviation of 0.71 s and a standard error of 0.002 s. Qualitatively, the distribution appears to be an approximation of a bi-exponential decay, suggests there are possibly two subsets of runs occurring.

3.3.4 *B. bacteriovorus* re-orientation angles

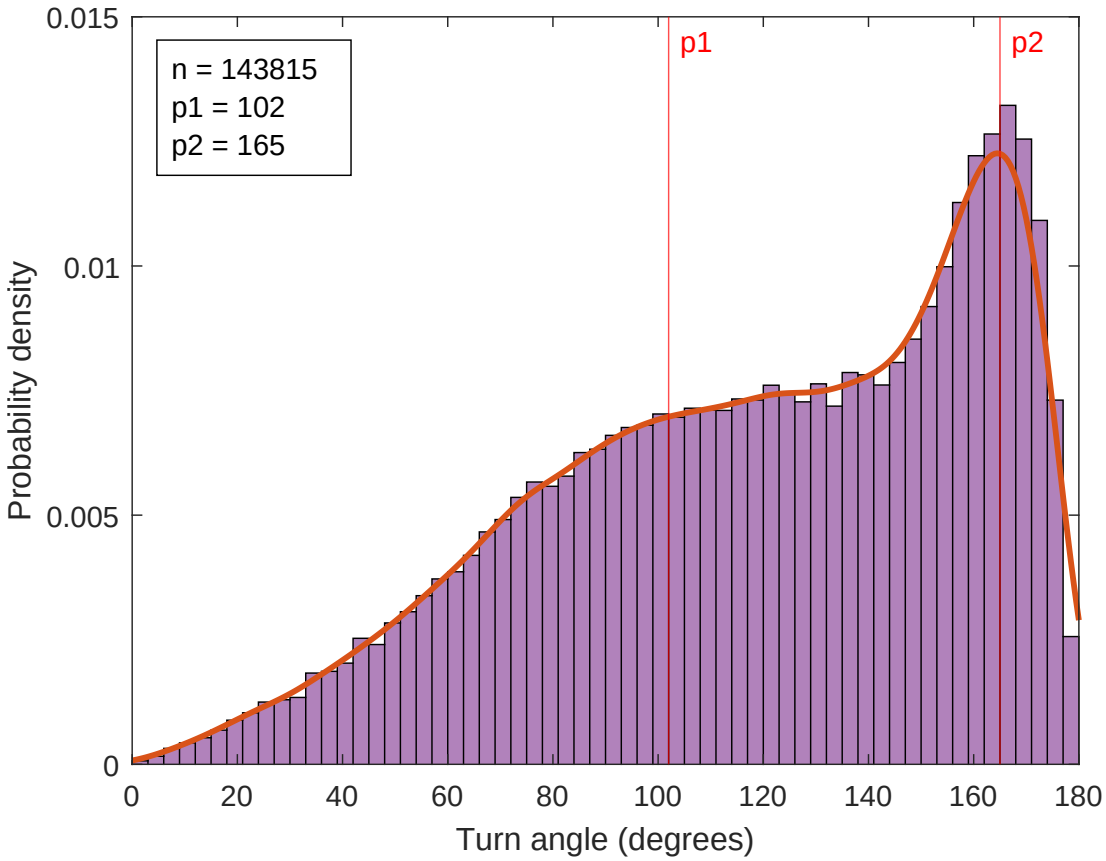

Figure 3.12: Histogram showing the distribution of re-orientation angles for *B.bacteriovorus*. Where n is the number of re-orientation events, $p1$ is the approximate location of the lower angle peak and $p2$ is the approximate location of the higher angle peak.

The histogram in Fig. 3.12 shows the distribution of re-orientation angles for *B. bacteriovorus*. This is one of the more interesting characteristics studied here as the complexity of the histogram most clearly suggests a complexity in the swimming motion of *B. bacteriovorus*. The histogram has been fitted using a KDE shown by the red line. There is a bimodal distribution with a broader, shallower peak centred around approximately 102 ° and a narrower, taller peak centred around approximately 165 °.

3.3.5 *B. bacteriovorus* trajectory characteristic patterns

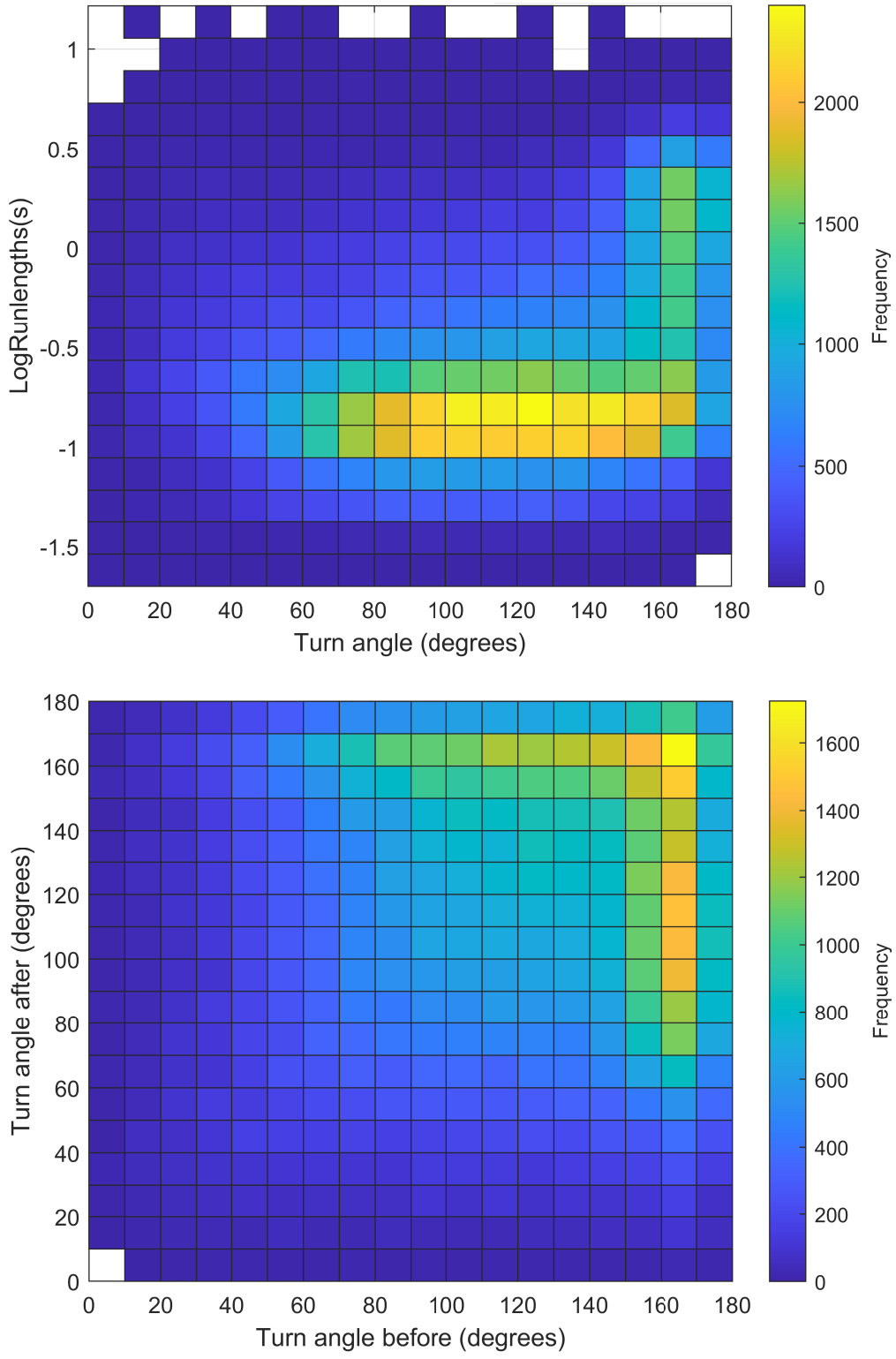

Figure 3.13: Bi-variate histograms of *B. bacteriovorus* swimming characteristics. *Top:* Re-orientation angles vs. the proceeding run times. *Bottom:* Re-orientation angles before vs. after a run. In both cases the colour indicates frequency as denoted by the colour bars on the right of the plots.

The top plot in Fig. 3.13 shows a bivariate histogram of re-orientation angles against the log of previous run times for *B. bacteriovorus*, where colour indicates frequency. The log of the run times was used to more easily visually distinguish the pattern. There two clearly defined clusters, showing a relationship between the two characteristics; with longer run duration being most likely to be followed by sharper turns with larger turning angles. Shorter run duration is typically followed by smaller turning angles. However, these have a much greater range of possible angles. It also appears that there are a greater number of runs with a short duration than a long duration. This plot has a covariance of 6.98 degree-seconds. Compared to *E.coli*, which had an average covariance of -4.94 degree-seconds, both have no significant correlation of turn angle to run length. However, the patterns seen are quite different with *E.coli* only showing one cluster compared to *B.bacteriovorus* showing two.

The bottom plot of Fig. 3.13 shows a bivariate histogram of re-orientation angle before and after runs. There is an upside down L shaped cluster in the top right hand corner of the plot. This shape of clustering suggests that there is a pattern or order to the two subsets of turns. It shows that high-angle turns can be followed by another high angle turn or by a lower-angle turn. However, low-angle turns are much less likely to be followed by another low-angle turn. The covariance of this plot is 17.5 degree-degrees. In contrast, the *E.coli* data showed an average covariance of 634 degree-degrees. This shows that *B.bacteriovorus* has a significantly different motility pattern to *E.coli*.

3.3.6 Discussion: *B. bacteriovorus* motility characteristics

The *B. bacteriovorus* motility characteristics presented here confirm previous studies showing *B. bacteriovorus* to be a highly motile and fast swimming bacteria relative to its size. The three dimensional nature of this study has illustrated in new detail the complexity of their swimming behaviour discussed in detail below. The swimming speed of *B. bacteriovorus* was found to be 34.1 ±7.8 μms^{-1} (where the ± indicates the standard deviation). This result is in line with most speeds found for previous studies of a range of *B. bacteriovorus* strains; typically approximately 30-60 μms^{-1}, although one study has seen speeds of up to 160 μms^{-1} μms^{-1} [137, 137, 141, 142, 204]. Fig.3.10 shows that the speeds have a relatively broad distribution with a long tail to the lower end - with a skew of -0.99. Interestingly *E.coli* has a relatively symmetrical distribution with a slight right handed skew of 0.20 and 0.011 for exponential and stationary phase cell respectively. This will be partially due to natural variations within the *B.bacteriovorus*

cell population but, in part, may also be due to the use of an a-synchronous culture resulting in a mixture of cells at different stages of the attack phase being present. Previous studies of *B. bacteriovorus* have shown that there is significant variation in the size and shape of attack phase cells, with new progeny cells nearly doubling in length between initial bdelloplast lysis and maturation [73]. Past studies of *E. coli* have shown that longer cells swim significantly slower then shorter cells. Cells approximately five times as long as wild type cells swam at approximately half the speed [205]. It therefore stands to reason that *B. bacteriovorus* swimming may be affected similarly. The reason for the slight right hand skewness of *E.coli* is unclear. However, it may be due to different flagellation of the cells. E.coli has a tuft of flagellum, whereas *B.bacteriovorus* only has one flagellum. Due to this there is more possibility for variation in *E.coli* than *B.bacteriovorus*, including difference in number and length of flagellum per cell. This could cause a broader distribution of swimming speeds in *E.coli*, which may go some way to explaining the differences in distribution shape.

The combined results of the run time and re-orientation angle characteristics show a fascinating bi-phasic re-orientation style with a clear link between the run times proceeding a turn and the resulting angle change. There is a pattern of behaviour mostly clearly illustrated by the plots in Fig. 3.13 which show two clear sub sets of re-orientation events and that a high angle turn can be followed by another high angle turn or a lower angle turn, but a lower angle turn will not be followed by a lower angle turn. I hypothesise from these results that *B. bacteriovorus* are performing a relatively newly discovered type of swimming pattern known as run-reverse-flick.

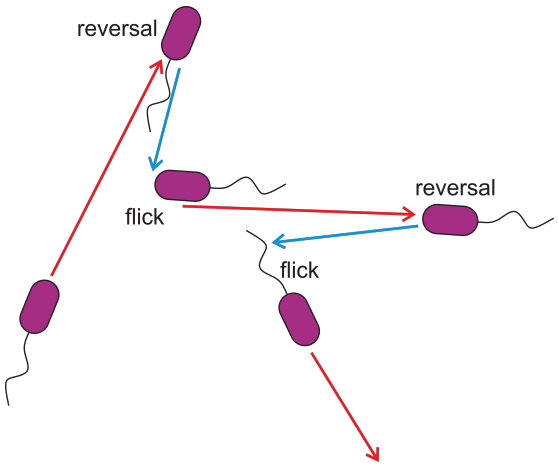

Figure 3.14: Schematic diagram of run-reverse-flick pattern of swimming. Where the red arrow represents the run, the blue arrow the reversal and the reorientation are labelled. Note that the cell body to flagella position is an approximation.

Run-reverse-flick behaviour was first observed by Xie et al. in both *Vibrio alginolyticus* and *Pseudoalteromonas haloplanktis* cells [206]. They demonstrated that the cells had an interesting bi-modally distributed set of re-orientation angles (remarkably similar to those seen in the *B. bacteriovorus* data in this study). The key attributes of this swimming type are to have a high angle turn (known as a reversal) followed by a lower angle turn (known as a flick) which together randomly re-orientate the cell - acting as the functional equivalent of a tumble in the more well known *E. coli* run and tumble type swimming. The amount of time between a reversal and flick (of the same event) is variable but is generally less than that between each overall reorientation. From this data it is has not been possible to identify which turns are reversals and which are flicks due to the breadth of the peaks in the reorientation angle distribution. This means it is not possible to identify which runs are associated with each part of the pattern. In the future, it may be possible to do this by visualising the cell body and flagellum simultaneously. The run-reverse-flick pattern of behaviour is illustrated in Fig.3.14 and examples of *B. bacteriovorus* displaying this behaviour can be seen in Fig.3.15.

Due to wide variation seen in bacterial swimming patterns it is logical to presume that the run-reverse-flick pattern evolved due to it providing a competitive edge to the cells using it. It may also be that it is simply the most efficient way to swim for single polar flagellated cells. Xie et al. postulated that this motility behaviour improves the fitness of the bacterium by making chemotaxis more efficient in environments where the distribution of nutrients is spatially anisotropic. Spatially anisotropic environments are environments where the properties vary depending on direction. This can include situations where there is fluid flow such as in marine habitats. Further study of this bacterial behaviour by the Xie group confirmed this advantage, and showed that chemo-sensing and migration was present in both the forward and backwards parts of the *V. alginolyticus* swimming cycle. This made it particularly well suited to responding to transitory signals. They therefore suggested that it would be likely that other species would be found to perform similar behaviour especially in marine habitats [207]. Indeed, since then, it has been shown that a number of different species including *Shewenella putrefaciens*, *Vibrio cholerae*, *Vibrio coralliilyticus*, and mixed seawater populations of bacterium perform run-reverse-flick re-orientations [91, 112, 208]. I believe that *B. bacteriovorus* can now be added to this group.

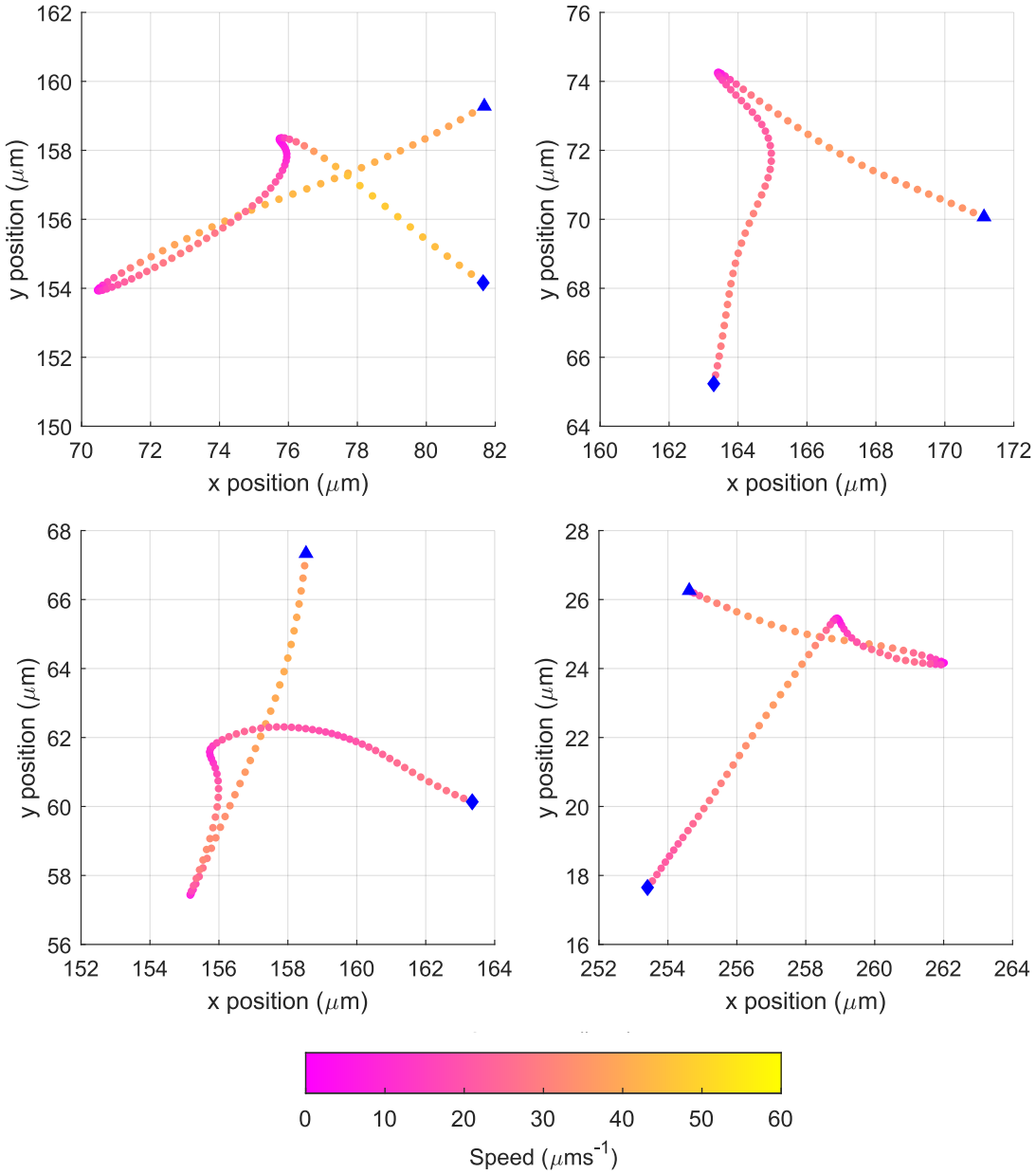

Figure 3.15: Example plots of *B. bacteriovorus* re-orientation events showing a two step turning mechanism consisting of a high angle reversal followed by a lower angle flick. In all plots the triangle denotes the start of the trajectory segment and the diamond the end. The colour indicates the swimming speed as shown by the bar at the bottom of the figure.

An in depth study of flicking behaviour by Kwangmin et al. suggested that it was caused by a buckling instability in the hook section of bacterial flagellum [91]. Their data showed that flick occurred exclusively when the cells where swimming forwards (with the flagellum behind the cell body in the direction of motion). Therefore they hypothesised that the compression forces put on the hook during forward swimming causes it to buckle resulting in the rapid change of direction known as a flick. They further supported this theory by showing that the probability of flicks occurring was appreciably decreased with swimming speed. The slower the cells swam, the less compression on the hook and therefore the less likely a flick was to occur. A similar pattern was also seen by Grognot et al. [208]. This combined with the wide distribution of swimming speed seen in *B. bacteriovorus* may explain why there was a marked number of repeated reversals in the data in Fig. 3.13.

However, there is some ambiguity to the theory presented by Kwangmin et al. They suggest that flicks only occur during forward runs, which implies that it is not possible to see consecutive turning events containing a flick ie. the pattern would go run-reverse-flick, run reverse, run-reverse-flick, run reverse etc. This is not the pattern seen in the *B. bacteriovorus* data. When individual trajectories are studied it is not uncommon to see consecutive run-reverse-flick events. More studies will need to be done to understand the mechanics of their motion.

The previously mentioned advantage run-reverse-flick gives cells for performing chemotaxis towards spatially anisotropic sources of nutrients that give off transitory signals is acutely relevant to the problem of *B. bacteriovorus* sensing and moving towards prey cells in their environment. This is especially so when you consider the range of environments *B. bacteriovorus* has been found in and the wide spectrum of motile prey cell types they successfully predate. As well as allowing them to sense and find moving prey, run-reverse-flick could confer them a significant advantage over cells with less efficient motility behaviour. This would perhaps allow *B. bacteriovorus* to out run, or out manoeuvre, prey that may be trying to escape or exist in a dense community of prey cells, e.g a biofilm.

3.4 Temporal consistency of *B. bacteriovorus* motility characteristics

For this section *B. bacteriovorus* was studied over a time series in an attempt to understand if length of co-culturing time affects behaviour. The main lysate was sampled once an hour every hour between 19-24 h of co-culturing time. This time window was selected as it contained the most commonly used sampling windows for previous *B. bacteriovorus* experiments, typically from 20-21 h, with additional samples before and after. The samples were prepared as specified in section 2.8.1.

3.4.1 *B. bacteriovorus* swimming speeds: time series

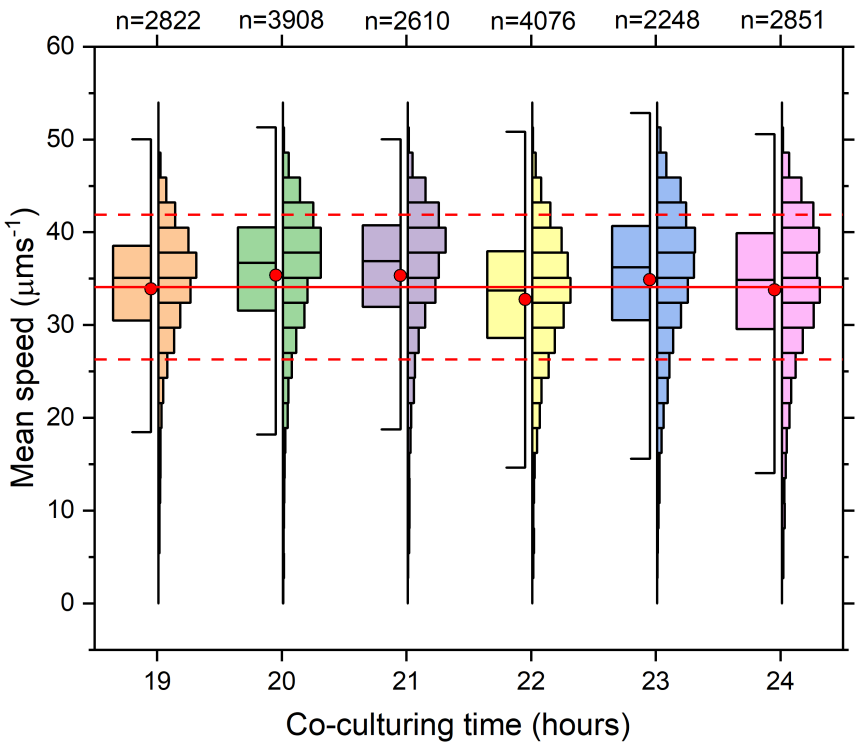

Figure 3.16: Plot showing the mean swimming speeds of *B. bacteriovorus* at a series of co-culturing times (19-24 h). The box plots on the left of each time point have a range of the 25-75 percentile with the central line indicating the median value and the red dot the mean value. The right hand side of each time point is a histogram of the data (bin width dictated by the lowest number of bins for all data sets as worked out using the Freedman Diaconis rule). The overall mean of all combined data is shown by the solid red horizontal line, with the dashed red horizontal lines showing the standard deviation. The top x axis indicates the number of trajectories in each data set.

The plot in Fig. 3.16 show a time series for the mean swimming speeds of *B. bacteriovorus* between 19-24 h of co-culturing. The solid red horizontal line represents the overall mean speed and the dashed lines the standard deviation. At every time point the mean and median values (the red dots and centre line of the box plots) are very close to the overall mean and well within the standard deviation. There is no trend to the mean speed suggesting that *B. bacteriovorus* swimming speed is stable and consistent over this time window of co-culturing.

3.4.2 *B. bacteriovorus* run times: time series

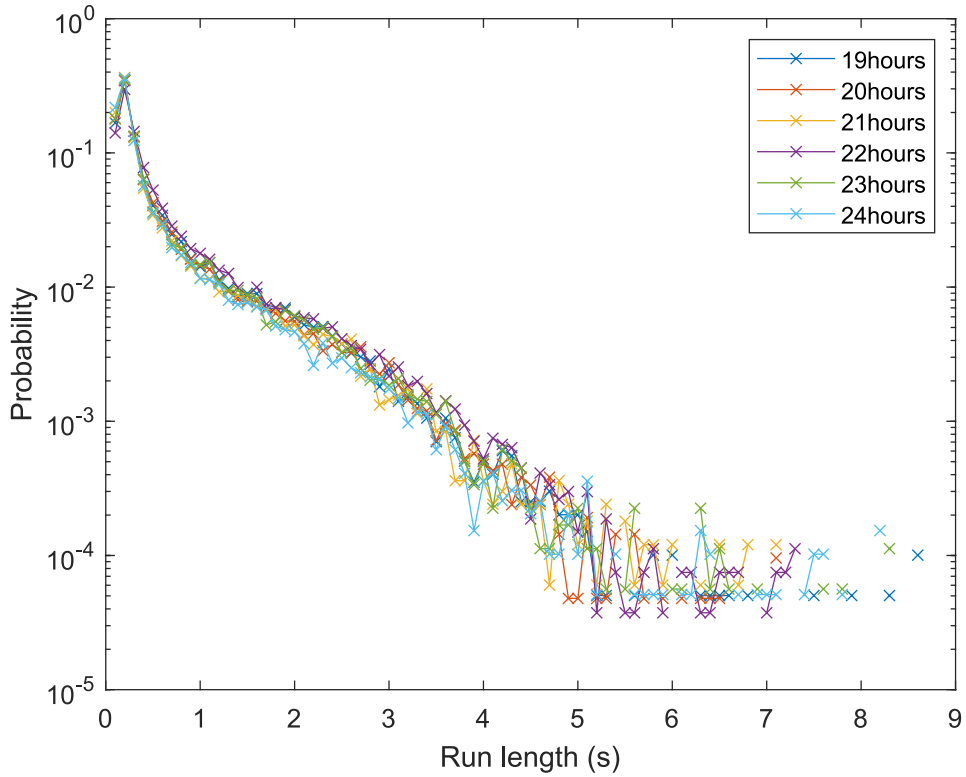

Figure 3.17: Plot showing a comparison of the distribution of run times for *B. bacteriovorus* over a time window of 19-24 h. The time is shown in the index. Each point on the plot for each hour represents the top of the histogram bar for that data set. The probability is found by dividing the sample number in each bin by the total number of samples for that data set. Please note that this plot is clipped at 9s on the x axis to more clearly show the key data.

The plot in Fig. 3.17 shows the comparison of the distribution of run times over the time window of 19-24 h. Similarly to their mean swimming speed *B. bacteriovorus* do not show any significant change or trend in run times over the time of 19-24 h co-culturing.

3.4.3 *B. bacteriovorus* re-orientation angles: time series

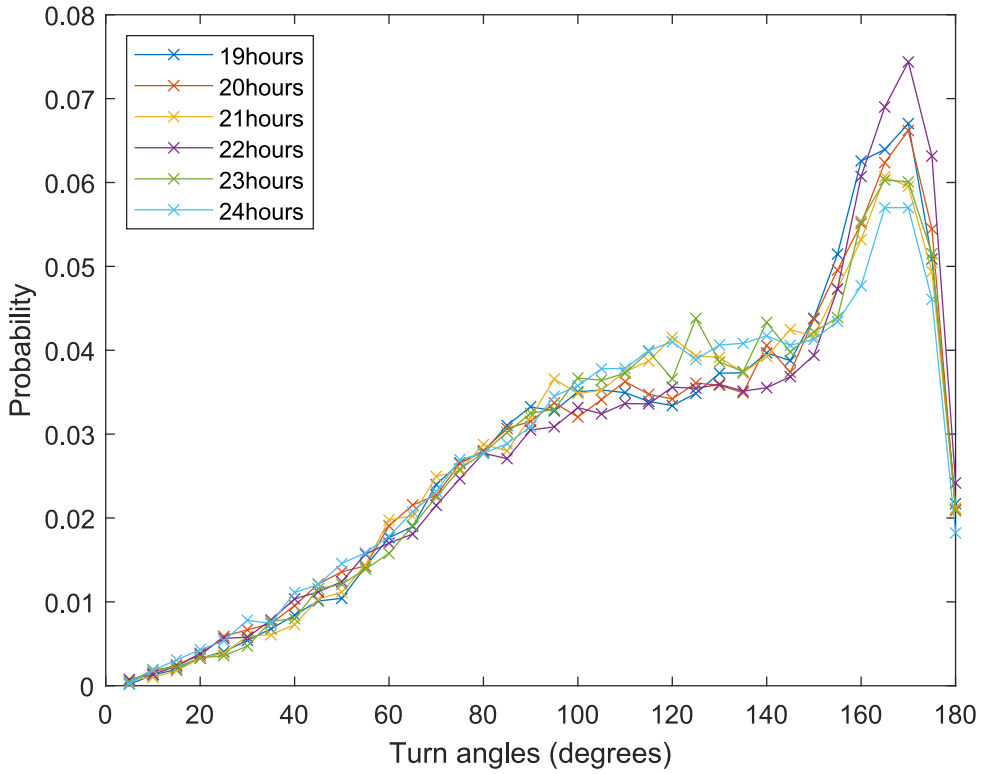

Figure 3.18: Plot showing comparison of *B. bacteriovorus* turning angles over 19-24 h of co-culturing. Each line represents one hour of the data set as shown in the legend. Each point on each plot represents the top of the histogram bar for that data. The probability is found by dividing the sample number in each bin by the total number of samples for that data set.

Fig. 3.18 shows a comparison of the distribution of re-orientation angles for the hours between 19-24 h of co-culturing. There is some variation in the distributions, particularly in the high angle peak at around 160 ° with 22 h having the greatest peak at this value. However there is very little variation in the lower angle peak and no clear trend in the behaviour.

3.4.4 Discussion: *B. bacteriovorus* motility characteristics temporal consistency

The results presented in this section show that *B. bacteriovorus* swimming behaviour is consistent within the co-culturing time window of 19-24 h. This result makes sense from the perspective that this is a mixed life-cycle stage (asynchronous) population with an excess prey cell resource. Throughout the chosen time window there were sufficient prey cells for the population to remain viable and therefore motility was maintained.

In contrast, a previous study by Sathyamoorthy et al., studying synchronous populations of starved *B. bacteriovorus*, found that both HD100 and 109J strains showed a significant drop in the proportion of swimming cells over time as well as variations in swimming speed [209]. HD100 showed an initial increase in swimming speed up to approximately 2.5 h and then a steady decrease over time until a total population arrest at approximately 8 h. It is an interesting observation in the context of the results in section 3.2.2-3.2.6 as it shows parallels in behaviour to stationary phase *E. coli* cells, that also reduce or arrest swimming when nutrients are lacking. Interestingly, the arrested *B.bacteriovours* cells re-activated swimming behaviour when given live prey cells, prey cell culture supernatant or certain amino acids. This re-activation happened in as quickly as 60 s [209]. This is clear evidence that *B. bacteriovorus* are able to detect live prey within their environments and react to prey by modifying their behaviour. I would expect that if I repeated my experiment (with the asynchronous culture) but continued to sample the co-culture beyond 24h the fraction of motile cells would begin to decrease as would the average swimming speed due to the prey source becoming depleted from predation.

It is useful to know that swimming remains consistent whilst prey cells are plentiful as it removes concerns about experiments needing to be performed within very limited time windows. It also suggests that when applied in systems beyond the lab *B. bacteriovorus* are likely to remain effective predators whilst there remains an abundance of prey cells. This has relevance when thinking about the application of *B. bacteriovorus* medically, as *B. bacteriovorus* should continue being motile and therefore (hopefully) predating effectively until the prey source (the source of infection) has been cleared (not considering the immune response of the host).

3.5 *B. bacteriovorus* motility at surfaces

This section compares *B. bacteriovorus* swimming behaviour within 10 μm of the top and bottom surfaces of the sample chamber compared to the bulk fluid of the chamber. The trajectories were selected as explained in section 2.7.6.2. As explained in section 1.3.5, previous studies have suggested predator-surface and prey-surface interactions may be an essential component in *B. bacteriovorus* locating prey in their environment [108, 147].

3.5.1 *B. bacteriovorus* swimming speeds: surfaces vs. bulk

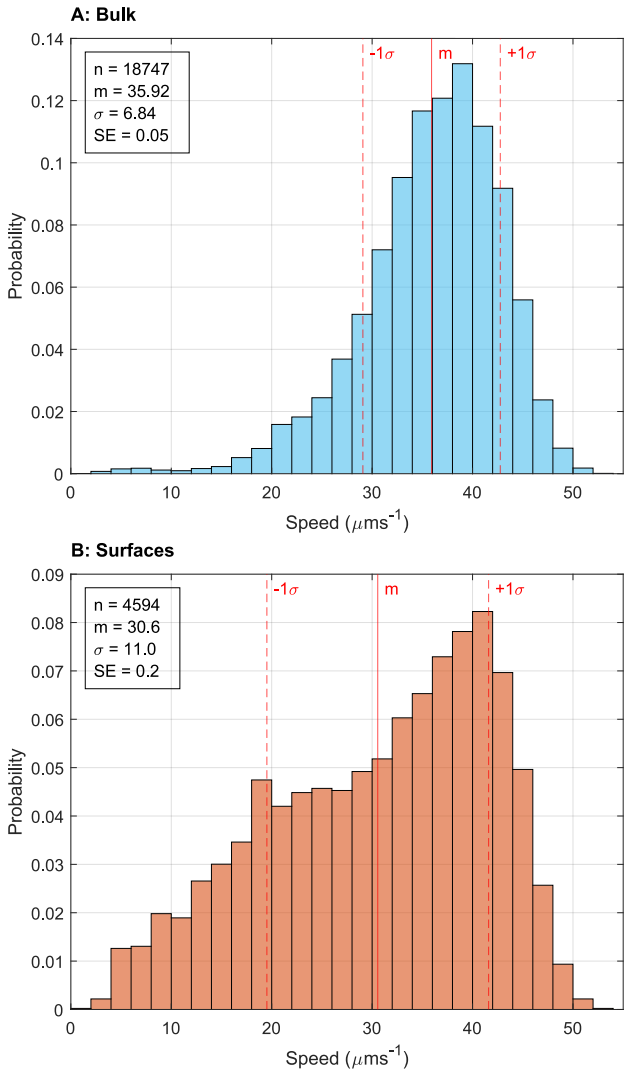

Figure 3.19: Histograms showing the mean swimming speeds of *B. bacteriovorus* swimming trajectories in bulk liquid compared to within 10 μm of sample chamber surfaces. In both cases, n is the number of trajectories, m is the overall mean speed (also shown by solid red line), and σ is the standard deviation (also shown by dashed red lines) and SE is the standard error. *A:* Bulk, *B:* Surfaces.

The plots in Fig. 3.19 show the mean speeds for *B. bacteriovorus* trajectories in bulk fluid compared to trajectories within 10 μm of surfaces. The cells swimming in bulk have a mean speed of 35.9 μms^{-1} with a standard deviation of 6.8 μms^{-1} and a standard error of 0.050 μms^{-1}. In comparison the cells swimming near the surfaces have a mean speed of 30.6 μms^{-1}, a standard deviation of 11.0 μms^{-1} and a standard error of 0.16 μms^{-1}. They show that there is a drop in mean speed near to surfaces of approximately 5 μms^{-1}. The Kruskal-Wallis test gives these data sets a p value of 1.1×10^{-168} which confirms that the difference between them is significant.

3.5.2 *B. bacteriovorus* run times: surfaces vs. bulk

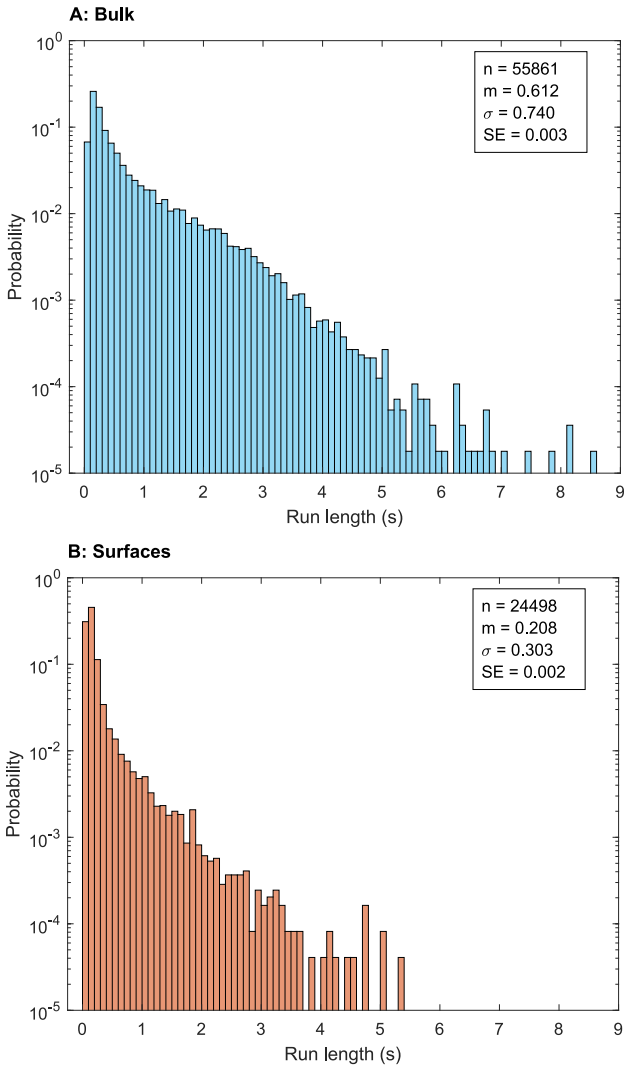

Figure 3.20: Histograms showing the run times of *B. bacteriovorus* swimming trajectories in main bulk liquid compared to within 10 μm of sample chamber surfaces. In both cases, where n is the number of trajectories, m is the overall mean speed,and σ is the standard deviation. *A:* Bulk, *B:* Surfaces.

The plots in Fig. 3.20 show the run times for *B. bacteriovorus* swimming bulk compared to next to surfaces. For cells swimming in bulk the mean run time is 0.61 s with a standard deviation of 0.74 s and a standard error of 0.0031 s. In contrast the cells swimming within 10 of surfaces show a much shorter mean run time of 0.21 s with a standard deviation of 0.30 s and a standard error of 0.0019 s. This drop in mean run time of 0.4 s tells us that the cells are turning more often when close to surfaces than in bulk. The Kruskal-Wallis test gives these data sets a p value of 0 which confirms that the difference between them is significant.

3.5.3 *B. bacteriovorus* re-orientation angles: surfaces vs. bulk

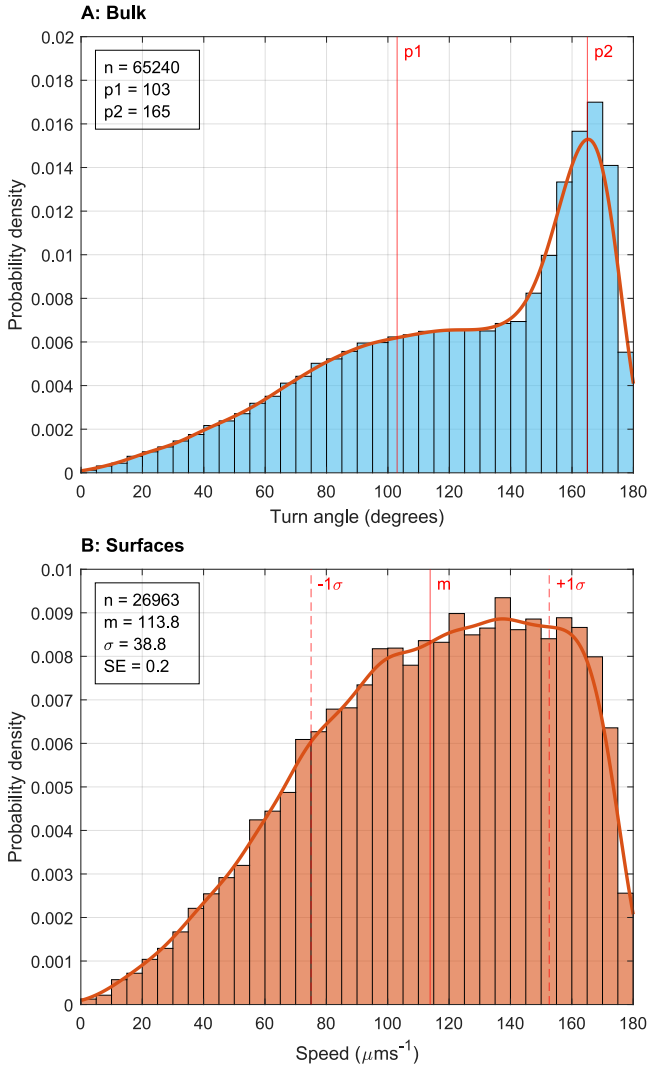

Figure 3.21: Histograms showing the reorientation angles of *B. bacteriovorus* swimming trajectories in main bulk liquid compared to within 10 μm of sample chamber surfaces. In both cases, where n is the number of trajectories, m is the overall mean speed and σ is the standard deviation.*A:* Bulk, *B:* Surfaces

The plots in Fig. 3.21 show the re-orientation angles of *B. bacteriovorus* swimming in bulk compared to swimming near surfaces. Both histograms have been fitted using a KDE shown by the red line. There is a significant change to the distribution of the re-orientation angles. The histogram goes from having a bi-modal distribution, with peaks at 103 ° and 165 °, when the cells are swimming in bulk, to a single-peaked distribution near to surfaces. This suggests a change from run-reverse-flick style of swimming to a more homogeneous motility pattern. The Kruskal-Wallis test gives these data sets a p value of 3.4×10^{-175} which confirms that the difference between them is significant.

3.5.4 *B. bacteriovorus* characteristic patterns: surfaces vs. bulk

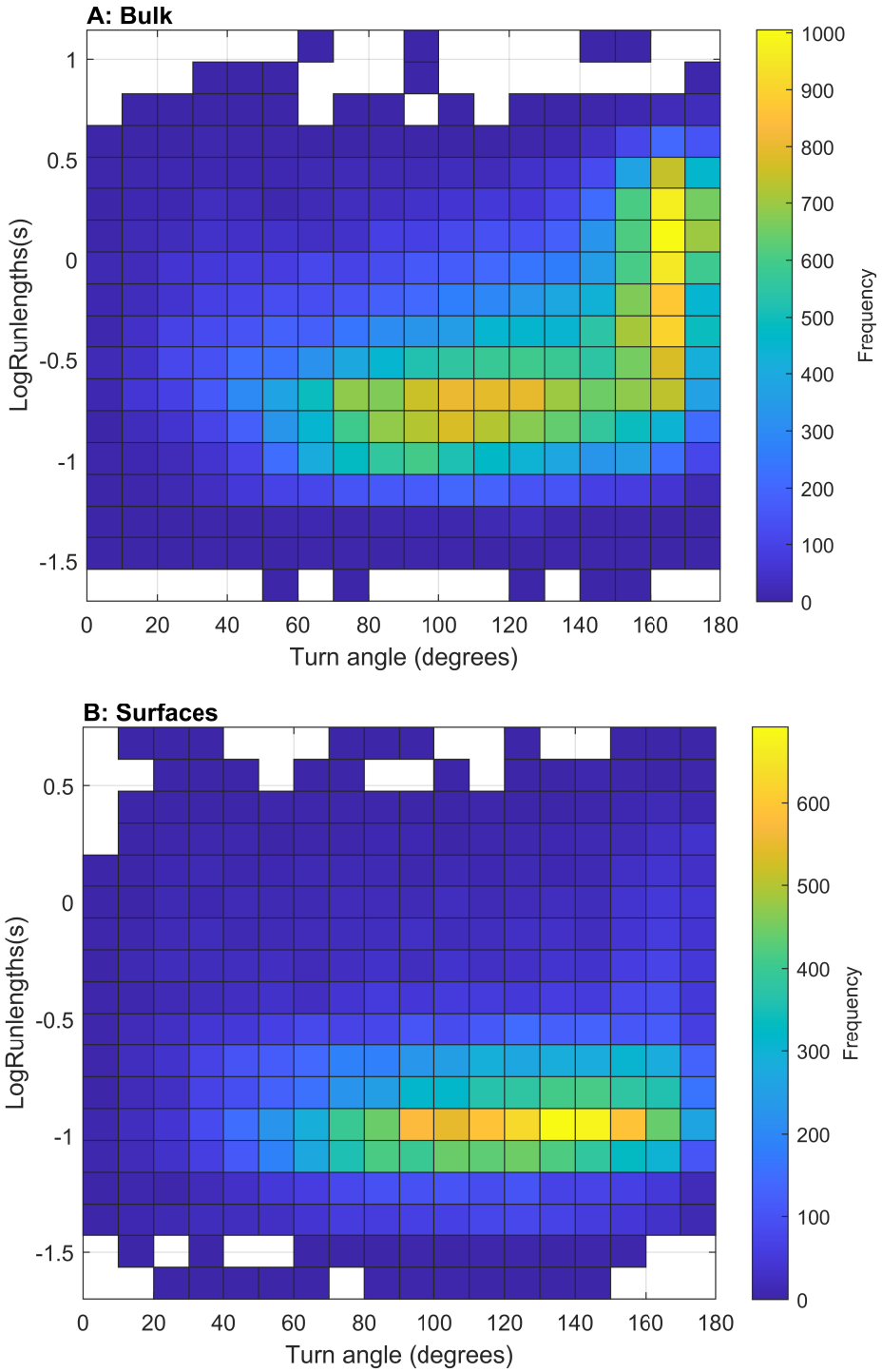

Figure 3.22: Histograms showing the reorientation angles of *B. bacteriovorus* swimming trajectories against the proceeding run times in main bulk liquid compared to within 10 μm of sample chamber surfaces. The colour indicates the frequency as shown by the colour bars on the right hand side of each plot.*A:* Bulk, *B:* Surfaces

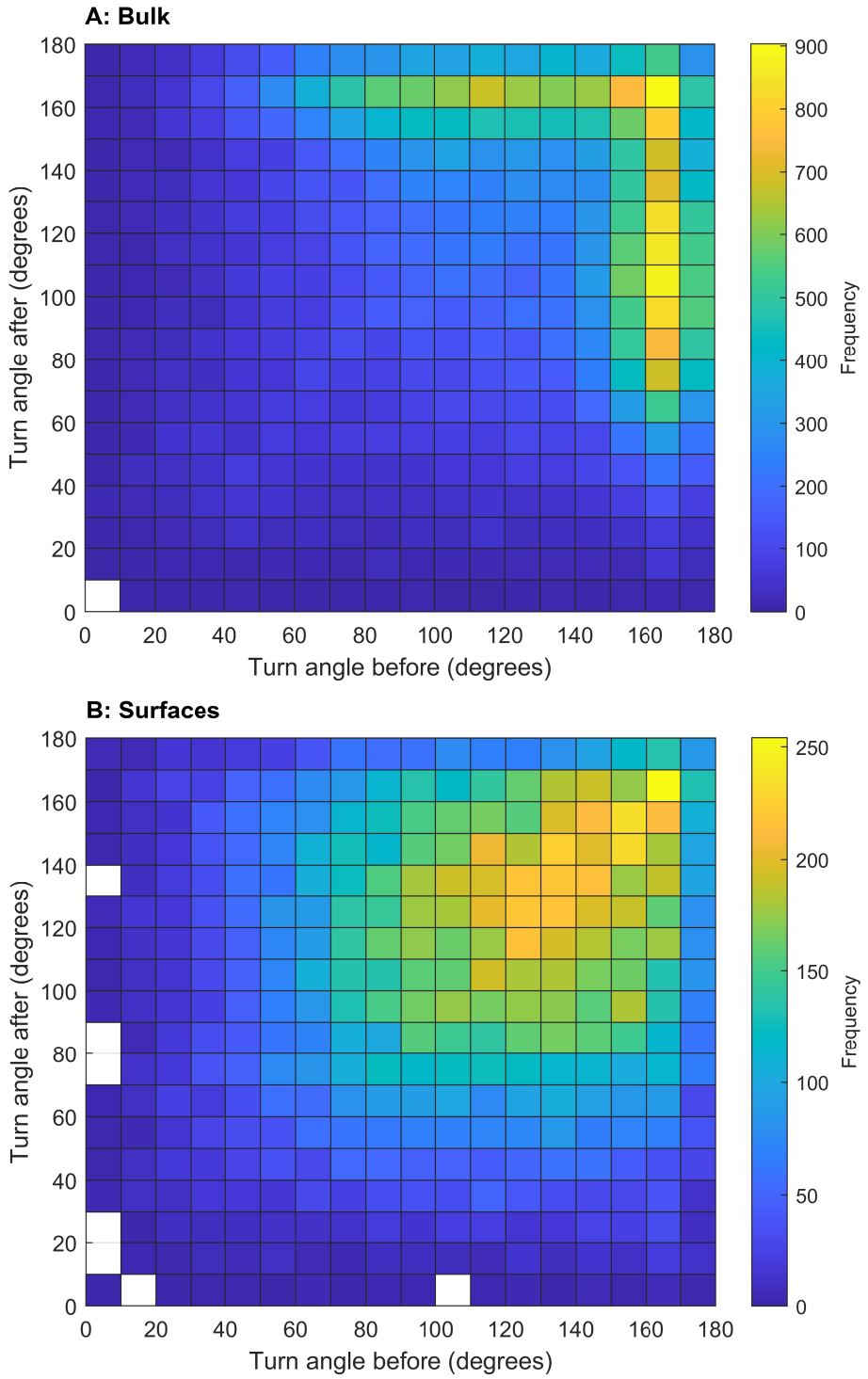

Figure 3.23: Bivariate histograms showing the reorientation angles before and after each run from *B. bacteriovorus* swimming trajectories in main bulk liquid compared to within 10 µm of sample chamber surfaces. The colour indicates the frequency as shown by the colour bars on the right hand side of each plot. *A:* Bulk, *B:* Surfaces

The plots in Figs. 3.22 and 3.23 agree with and add to the picture of a change in swimming style near surfaces. Fig. 3.22 clearly shows two clusters in A and only one in B. The two clusters in Fig. 3.22A (in bulk) match those more generally found in the *B.bacteriovorus* trajectories, where long runs are associated with high angle turns and shorter runs associated with lower angle turns. This suggests a run-reverse-flick style of swimming.

In contrast, in Fig. 3.22B, the cluster associated with long runs and high angle turns is gone. This suggests that at surfaces *B.bacteriovorus* is no longer performing run-reverse-flick. Fig. 3.23 also indicates a change of behaviour. Fig. 3.23A (in bulk) shows a pattern to the order of turning events that is not seen in Fig. 3.23B (near surfaces). Near to surfaces the pattern is more similar to *E.coli* motility, albeit with a higher average angle. The covariance of 3.23A is -118 degree-degrees, compared to 140 for 3.23B.These plots and values show that at surfaces *B.bacteriovorus* has homogeneous style of swimming where there is no longer a complex pattern or order to the changes in direction. At surfaces re-orientations are most likely to be followed and proceeded by events with a similar turn angle.

3.5.5 Discussion: *B. bacteriovorus* surfaces vs. bulk motility characteristics

The data in the sections 3.5.1-3.5.4 show a clear difference in motility behaviour of *B. bacteriovorus* in bulk fluid to within 10 μm of surfaces. There was a drop in swimming speed of approximately 5 μms^{-1} in addition to a change in the overall motility pattern - moving away from a bi-phasic, run-reverse-flick, motility style to a more homogeneous behaviour with a continuous distribution of re-orientation angle changes. The drop in swimming speed seen in these *B. bacteriovorus* results echoes some previous studies of both *E. coli* and *Pseudomonas aeruginosa* which also saw drops in swimming speed at surfaces [102, 105]. Interestingly the results shown here are in disagreement with a recent study which suggested that cells swim significantly faster at surfaces and in high viscosity environments due to a reduction in cell body wobbling [210].

The overall behaviour changes may be due to a number of factors including passive hydrodynamic interactions between the cells and the surfaces - coming from collisions with and debris on the sample chamber surfaces. There may also be changes in behaviour because of additional forces on the flagellum and cell body. This are due to enhanced viscosity near surfaces, within approximately 5 cell body radii of the surface. These viscosity changes can be described by Faxens law which is an alteration to Stokes' Laws and describes the friction on a spherical object in viscous fluid when it moves near to a surface [211]. For *B.bacteriovorus* with a cell length of up to 1.2 μm this would be from around 6 μm of the surface (within the 0- 10 μm studied here). It may also be possible for there to be active interactions happening with the cells sensing the surfaces. *B.bacteriovorus* do have pili on their surfaces which they use to sense, attach to and infiltrate prey cells [65, 67, 68]. It is therefore possible that these pili could be used to sense surfaces in general including those of a sample chamber. It is unclear from these results if the observed motility changes at surfaces are a result of passive or active behaviour.

Previously Jashnsaz et al. have suggested that *B.bacteriovous* use surface accumulation of both prey cells and themselves as a way to enhance predation efficiency [108]. This is an interesting theory however it does not take into account the wide variety of environments *B. bacteriovorus* is found in, including bulk fluids such as sea water. Although, it is worth noting that aggregation has been observed in Gram-negative bacteria in sea water perhaps representing a form of surface the cells may need to negotiate even in fluid environments [212]. Without further study it is hard to say if the modified behaviour seen in my results would confer any predation advantage, for example in terms of searching efficiency. However, in the context of medical application where surfaces are abundant and biofilms on surfaces are of significant interest these changes in behaviour are relevant. Further work needs to be done to fully understood this surface motility behaviour and it's possible impacts on predation efficiency.

3.6 *B. bacteriovorus* motility changes in the presence of live prey cells

3.6.1 Mixed predator-prey sample preparation

The sample preparation for the mixed samples was simple. Both predator and prey were prepared in exactly the same manner as for the previous experiments where they were imaged separately. The two sample types (both in Ca/HEPES buffer) were mixed gently in a plastic microcentrifuge tube and then diluted using more Ca/HEPES buffer to a suitable density for holography. This mix was left for 10min to allow the cells to begin to interact and then it was pipetted into a sample chamber ready for imaging.

3.6.2 Mixed predator-prey image analysis method

In order to find the best ways of distinguishing between cell types a few different methods were tried including looking at the intensity of cell locations in the holograms and using the characteristic parameters as indicators. The latter proved to be the most effective method. The Figs. in 3.24 and 3.25 show a comparison of the mean speeds and turning angles of the mixed predator-prey samples compared to the separate samples. The top two plots show both the mixed and separate data, where the coloured histogram bars present the mixed predator-prey data, the line plots with stars the prey alone and the line plots with circles the predators alone. The bottom two plots show the residuals of the mixed data minus the *E. coli* data in each case i.e. either exponential or stationary phase cells as indicated by the labels. There is greater cross over between the exponential phase *E. coli* cell behaviour and the *B. bacteriovorus* than the stationary phase *E. coli*. However, in both cases there are thresholds above which a trajectory is more likely to be *B. bacteriovorus* than *E. coli*. The residual plots in particular show clear threshold values. In order to make comparison simpler, an approximate mean between the two types of prey residual thresholds was taken to give an overall set of thresholds. These values were applied to the mixed data sets to give an estimate of a cell type for each trajectory - cells were counted as *B. bacteriovorus* if their mean speed was above 20 μms^{-1} and they contained at least one turning angle above 110°. The same filters were applied to the *B. bacteriovorus* data from section 3.3.2 to allow a comparison between *B. bacteriovorus* behaviour with and without prey and so look for any changes in motility characteristics that may be triggered by the presence of live prey cells.

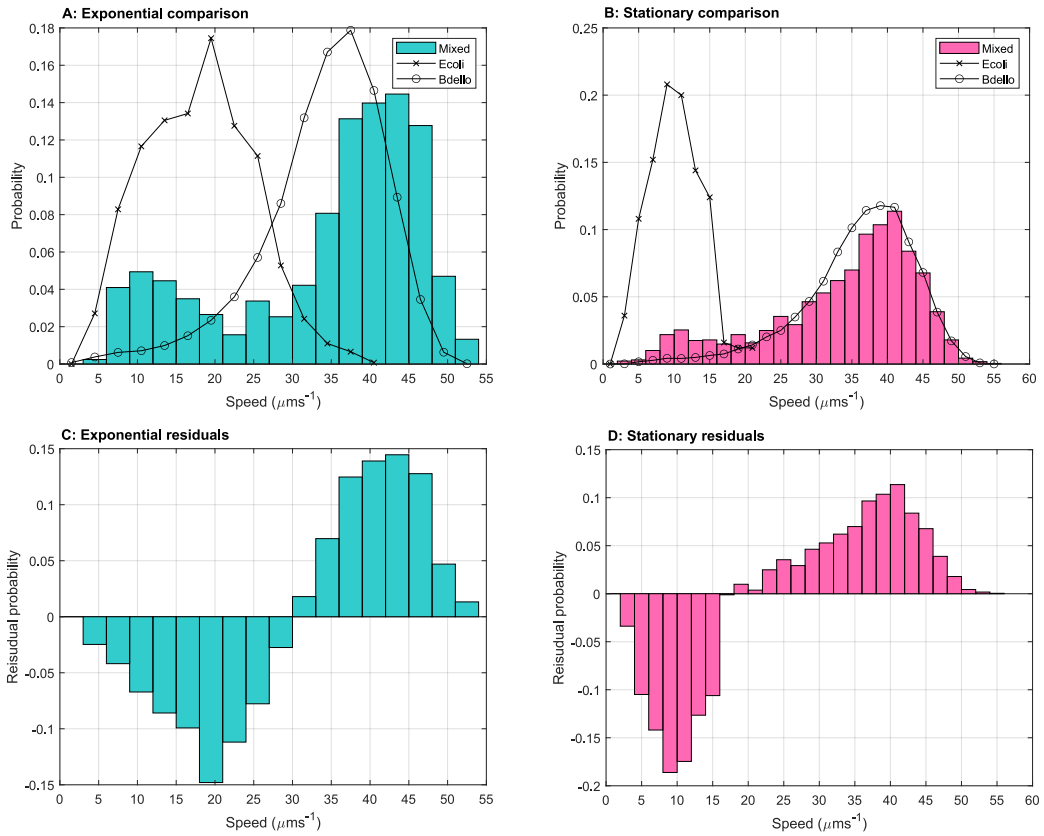

Figure 3.24: Mixed *B. bacteriovorus* and *E. coli* mixed samples mean swimming speeds comparison and residuals histograms. *Left:* (Cyan) *B. bacteriovorus* mixed with exponential phase *E. coli*. *Right:* (Pink) *B. bacteriovorus* mixed with stationary phase *E. coli*.*Top:* Histogram bars are the mixed data, the line plots are a plot of the histogram bar tops for *E. coli* alone (cross) and *B. bacteriovorus* alone (circles). *Bottom:* Residual histograms consisting of the probability of the mixed data minus the probability of the *E. coli* alone.

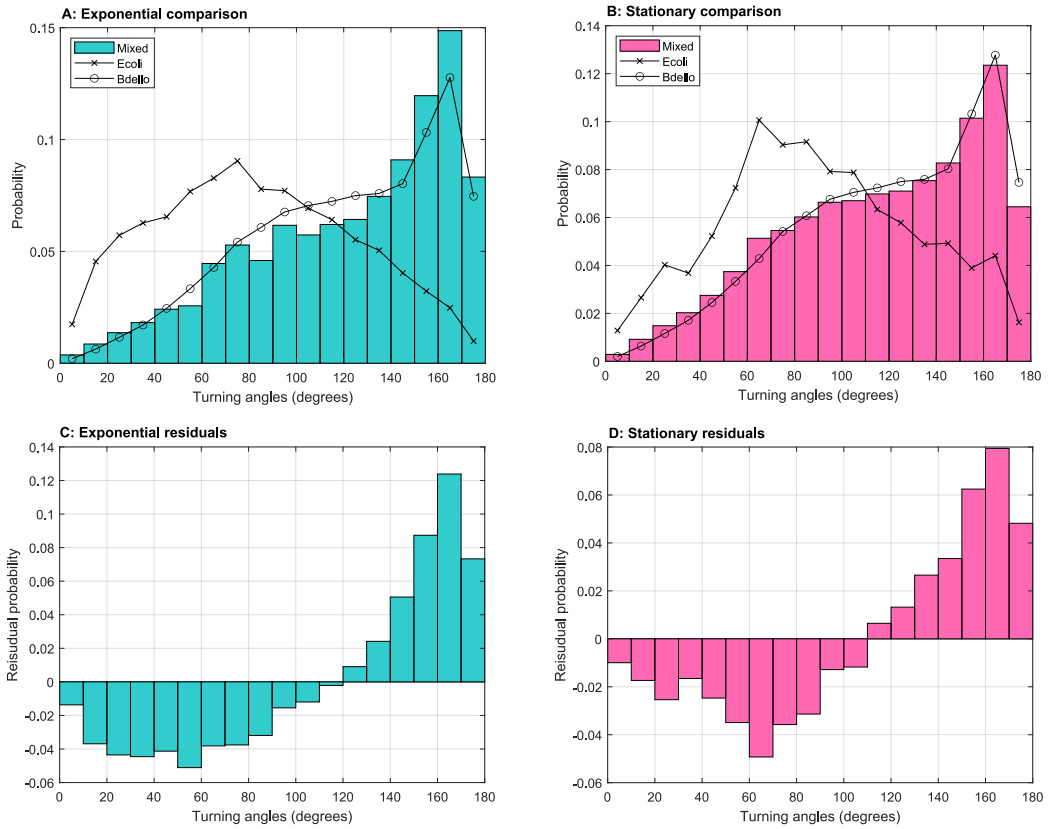

Figure 3.25: Mixed *B. bacteriovorus* and *E. coli* mixed samples turning angles comparison and residuals histograms. *Left:* (Cyan) *B. bacteriovorus* mixed with exponential phase *E. coli*. *Right:* (Pink) *B. bacteriovorus* mixed with stationary phase *E. coli*.*Top:* Histogram bars are the mixed data, the line plots are a plot of the histogram bar tops for *E. coli* alone (cross) and *B. bacteriovorus* alone (circles). *Bottom:* Residual histograms consisting of the probability of the mixed data minus the probability of the *E. coli* alone.

3.6.3 Mixed predator-prey swimming speeds

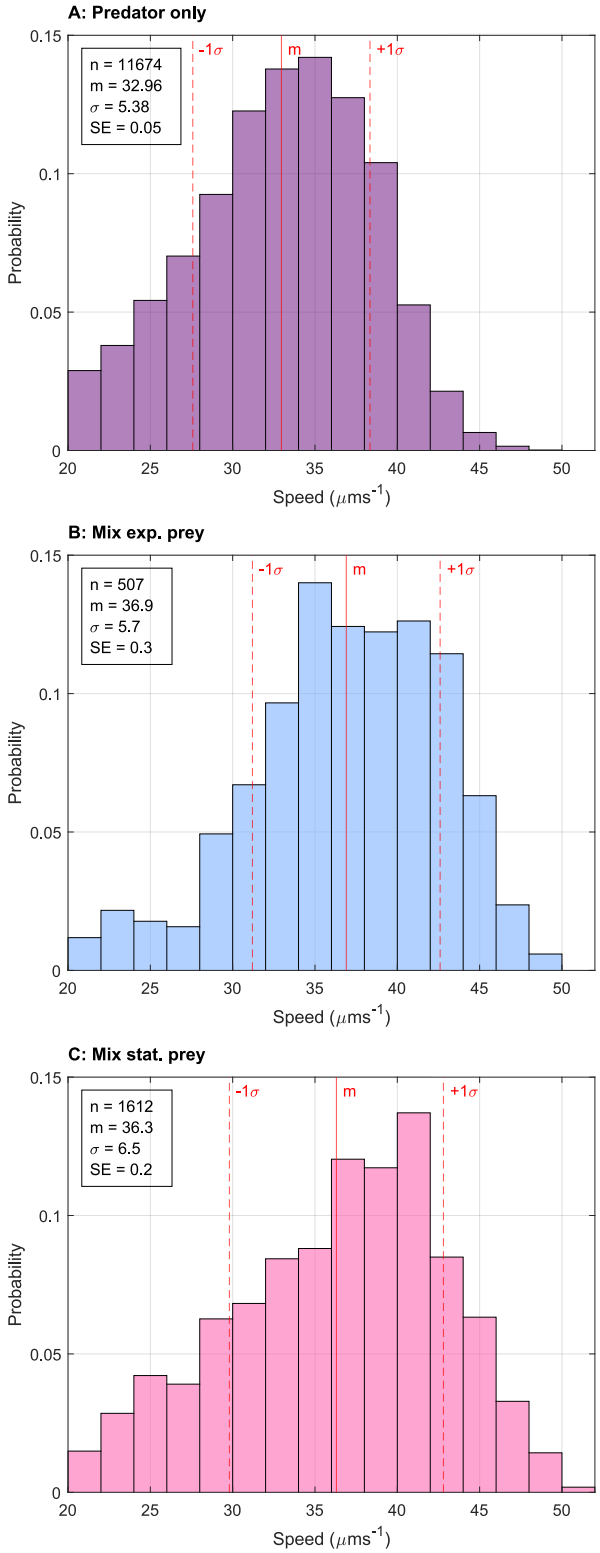

Figure 3.26: Histograms of *B. bacteriovorus* mean swimming speeds, alone and mixed with prey. *A: B. bacteriovorus* alone. *B:* Mixed with exponential *E. coli*. *C:* Mixed with stationary phase *E. coli*. In all cases n is the number of trajectories, m is the mean value (also represented by the solid red lines), and σ is the standard deviation (also represented by the dashed red lines) and SE is the standard error.

3.6.4 Mixed predator-prey run times

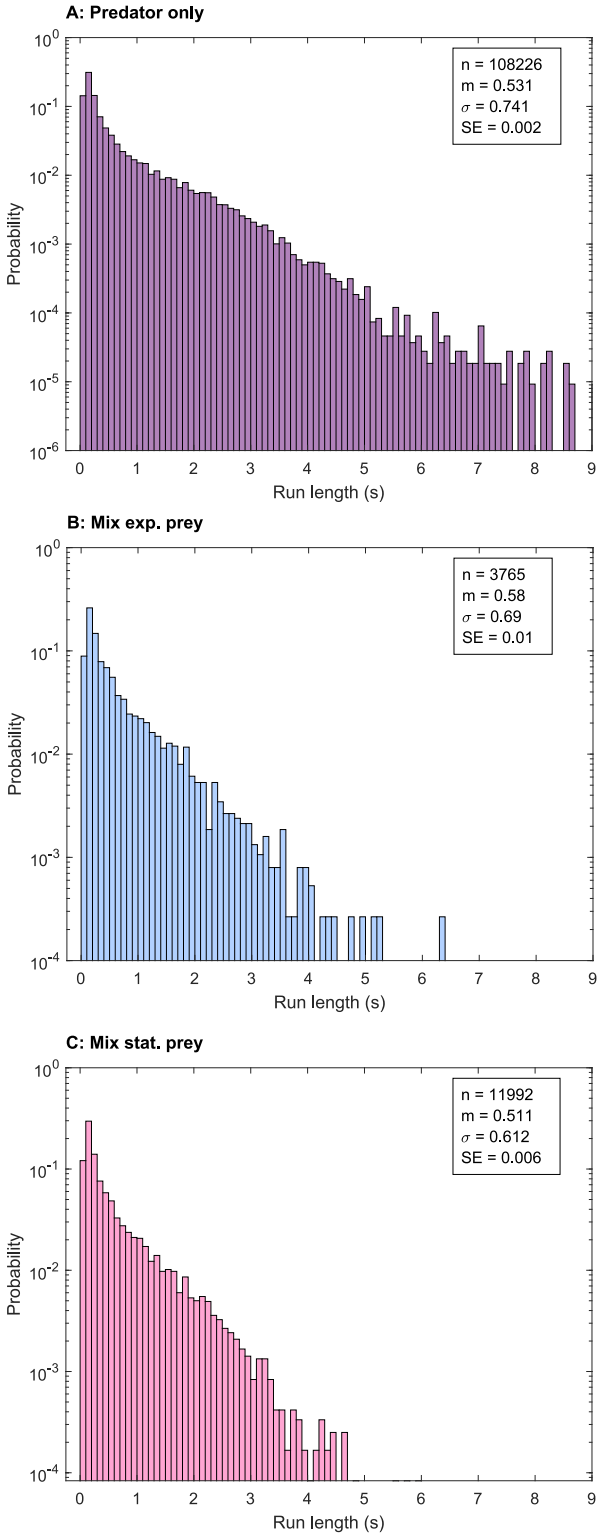

Figure 3.27: Histograms of *B. bacteriovorus* run times, alone and mixed with prey. *A: B. bacteriovorus* alone. *B:* Mixed with exponential *E. coli*. *C:* Mixed with stationary phase *E. coli*. In all cases n is the number of trajectories, m is the mean value, and σ is the standard deviation and SE is the standard error.

3.6.5 Mixed predator-prey re-orientation angles

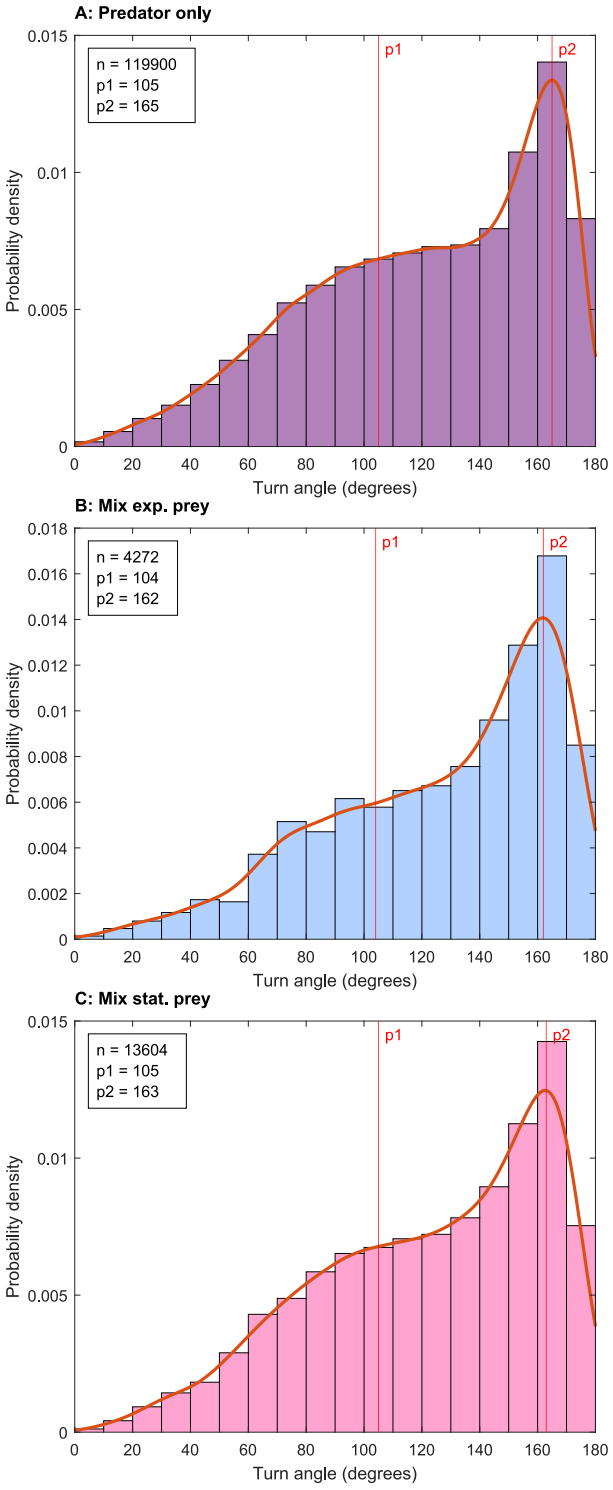

Figure 3.28: Histograms of *B. bacteriovorus* turning angles, alone and mixed with prey. *A: B. bacteriovorus* alone. *B:* Mixed with exponential *E. coli*. *C:* Mixed with stationary phase *E. coli*. In all cases n is the number of trajectories, $p1$ is the first fitted peak and $p2$ is the second fitted peak (as determined using a Gaussian mixed model approach where all values are approximate).

The *B. bacteriovorus* alone has a mean swimming speed of 33.0 μms^{-1}, with a standard deviation of 5.4 $\mu ms^{-1}$and a standard error of 0.050 μms^{-1}. The exponential phase *E. coli* mix has a mean speed of 36.9 μms^{-1}, with a standard deviation of 5.7 μms^{-1} and a standard error of 0.25 μms^{-1}. The stationary phase *E. coli* mix has a mean speed of 36.3 μms^{-1}, with a standard deviation of 6.5 μms^{-1} and a standard error of 0.16 μms^{-1}. In both mixed samples the means swimming speed increases by a small but significant amount of approximately 4 μms^{-1}.

The *B. bacteriovorus* alone has an average run time of 0.53 s, with a standard deviation of 0.74 s and a standard error of 0.0023 s. The exponential phase *E. coli* mix has an average run time of 0.58 s, with a standard deviation of 0.69 s and a standard error of 0.011 s. The stationary phase *E. coli* mix has an average run time of 0.51 s, with a standard deviation of 0.61 s and a standard error of 0.0056 s. As the exponential phase mix shows an increase by 0.06 s and the stationary phase mix a decrease by 0.2 s, these data sets suggest that *B. bacteriovorus* does not change it's run time distribution in the presence of live prey.

Similarly, the re-orientation angles of *B. bacteriovorus* do not appear to change with the presence of live prey cells. The approximate peak positions of the flick events are 105 °, 104 °, and 105 °, for the predator, mixed exponential and mixed stationary data, respectively. The approximate peak positions of reverse events are also very alike at 165 °, 162 °, 163 °, for the predator, mixed exponential and mixed stationary data, respectively.

3.6.6 Discussion: *B. bacteriovorus* changes in motility characteristics in the presence of live prey cells

The data in sections 3.6.3-3.6.5 show that *B. bacteriovorus* cells do not change swimming style in the presence of live prey. They continue to perform run-reverse-flick with re-orientation events at similar rates to *B. bacteriovorus* alone. However, they do increase their swimming speed.

The increase of swimming speed in the presence of prey cells is an interesting result. It is logical that this could be a mechanism to aid in predation efficiency. An increase in swimming speed in areas of high prey cell density will increase the rate at which *B. bacteriovorus* collide with prey cells - their collision frequency. In turn increasing overall predation rates. This behaviour would be a form of active hunting that does not depend on tracking individual prey. Interestingly, it is also a method that doesn't rely on any prior knowledge of the prey cell type and therefore would be effective on the wide range of prey cell strains (including varied morphology and behaviours) that *B. bacteriovorus* are able to predate.

To better understand the impact of increasing swimming speed on searching efficiency, the collision frequency of cells in a volume can be approximately calculated, using kinetic theory from physics. In order to do so, certain assumptions must be made. Firstly, the cells are assumed to be small, hard and spherical with a mass m. The cells only exert force on each other when they collide and these collisions are elastic in nature. When collisions do occur their duration is negligible and their are no forces of attraction between the cells. It also assumed that between collisions cells move in a straight line. This calculation also presumes that all the cells are moving with the same average velocity. For the purpose of this approximation, the cells are considered to an equal mix of predatory *B.bacteriovorus* and prey *E.coli* cells.

If a *B.bacteriovorus* cell is moving through an environment, it will collide with another cell if it comes within a distance D. Where D is equal to the radius of the *B.bacteriovorus* cell plus the radius of the *E.coli* cell. Approximating the radius of *B.bacteriovorus* to be 0.5 μm and the radius of *E.coli* to be 1 μm, and assuming an equal mix of predator and prey, $D \approx 1.5$. The path of a *B.bacteriovorus* cell can then be thought of a cylinder of space. If a cell passes into this space then a collision will occur. The *B.bacteriovorus* cell will move a distance Ω along this cylinder in a time t, where Ω is equal to the cells velocity, $\langle v \rangle$, times t ($\langle v \rangle t$). Therefore, the *B.bacteriovorus* path will have a volume equal to $\pi D^2 \langle v \rangle t$.

In order to work out the likelihood of collisions, the density of the cells is important. Considering all other cells to be stationary, if there is a number of cells per unit volume of n then the number of cells within the *B.bacteriovorus* path (and so the number of cell collisions in that path) will be $n\pi D^2\langle v\rangle t$.

The average distance a cell will travel without colliding with another cell is known as the mean free path, λ. This can be found by dividing the distance the cell travels down its path by the number of cell collisions in its path:

$$\lambda = \frac{\langle v\rangle t}{n\pi D^2\langle v\rangle t} = \frac{1}{n\pi D^2} \tag{3.1}$$

Taking into account that most of the cells will be swimming the mean free path changes. The average relative velocity between cells can be defined as $v_{relative} = \sqrt{2}\langle v\rangle$. Therefore the mean free path is:

$$\lambda = \frac{1}{\sqrt{2}n\pi D^2} \tag{3.2}$$

Collision frequency of the cells, Z, is the velocity of the cells divided by their mean free path:

$$Z = \frac{v}{\lambda} = v\sqrt{2}n\pi D^2 \tag{3.3}$$

For this approximation, the velocity of the cells can be taken as an average of exponential phase *E.coli* and the *B.bacteriovorus* mixed with exponential phase cells. This gives a velocity of 27.5 μms^{-1}. There will be an average D of 1.5 μm. The unit density can be approximated on the imaging set up as 5.5x10^{12} m^{-3} (from around 150 cells per imaging volume of 250 μm^3). This gives a collision frequency of approximately 0.0026 s^{-1} - or approximately 1 collision every 6 minutes. It is important to note that these samples were very dilute for the purposes of imaging.

There are obviously a number of assumptions in this calculation that do not reflect the full system complexity. This includes the fact the cells in a real system will interact and do not swim in straight lines between collisions. However despite this there are a number of key points demonstrated here. The collision frequency is linked to the size and density of cells. Therefore navigating to an area of high prey density is clearly a good way for predators to increase their predation efficiency. Also, as collision frequency scales with speed, the faster a given *B.bacteriovorus* cell swims the more likely it is to encounter a prey.

In addition to simply increasing collision frequency, it may be that there are other, more complex, reasons to swim faster in the presence of prey. For example, if prey bacteria have an ability to detect predators, or some form of defence or resistance, as has been suggested in [213]. It is also possible that prey use some kind of warning mechanism to communicate to other cells that predators are present. In all of the above situations faster predators are more likely to successfully attack. Therefore, implying swimming faster when prey are abundant makes *B. bacteriovorus* more effective predators, than if they were non-responsive.

However, an increase of speed alone does not explain previously observed *B. bacteriovorus* directional chemotactic behaviour towards certain chemicals and high densities of prey bacterium [108, 144–148]. A key limitation to this experimental setup is that the predator and prey cells were approximately uniformly mixed and therefore any directional chemotactic behaviour can not be seen. Future experiments (further discussed in section 4.2) using prey cells in a fixed, known, location could be used to determine if the re-orientation rate biases their random walk towards the prey cells - analogous to *E. coli* biased random walks.

CHAPTER 4

CONCLUSIONS

4.1 Results summary and conclusions

This chapter summarises the key results of this research project including the key characteristics (swimming speeds, run times and re-orientation angles) of *B. bacteriovorus* in various conditions, a brief discussion of these results and ideas for future work.

4.1.1 Summary tables of key *B. bacteriovorus* motility characteristics

***B. bacteriovorus* Swimming Speeds** ($\mu m s^{-1}$)			
Conditions	Speed	σ	SE
Standard	34.07	7.82	0.05
Bulk	35.92	6.84	0.05
Surfaces	30.6	11.0	0.2
Thresholded as mix	32.96	5.38	0.05
Mixed w. exp. prey	36.9	5.7	0.3
Mixed w. stat. prey	36.3	6.5	0.2

Table 4.1: Table showing a summary of the mean swimming speed results of *B. bacteriovorus*, including mean swimming speeds of *B. bacteriovorus* alone including all swimming trajectories (standard), in bulk, at surfaces, standard but with the same conditions applied as mixed with prey cells (thresholded as mix), mixed with exponential phase prey cells (mixed w. exp. prey), and mixed with stationary phase prey cells (mixed w. stat. prey). The standard deviation and standard error of each value are given.

***B. bacteriovorus* Run Times** (s)			
Conditions	Run time	σ	SE
Standard	0.477	0.711	0.002
Bulk	0.612	0.740	0.003
Surfaces	0.208	0.303	0.002
Thresholded as mix	0.531	0.741	0.002
Mixed w. exp. prey	0.58	0.69	0.01
Mixed w. stat. prey	0.511	0.612	0.006

Table 4.2: Table showing a summary of the run time results of *B. bacteriovorus*, including run times of *B. bacteriovorus* alone including all swimming trajectories (standard), in bulk, at surfaces, standard but with the same conditions applied as mixed with prey cells (thresholded as mix), mixed with exponential phase prey cells (mixed w. exp. prey), and mixed with stationary phase prey cells (mixed w. stat. prey). The standard deviation and standard error of each value are given.

***B. bacteriovorus* Turn Angles** (°)		
Conditions	Turn angle P1	Turn angle P2
Standard	102	165
Bulk	103	165
Surfaces	114	-
Thresholded as mix	105	165
Mixed w. exp. prey	104	162
Mixed w. stat. prey	105	163

Table 4.3: Table showing a summary of the re-orientation (turn) angle results of *B. bacteriovorus*, including turn angles of *B. bacteriovorus* alone including all swimming trajectories (standard), in bulk, at surfaces, standard but with the same conditions applied as mixed with prey cells (thresholded as mix), mixed with exponential phase prey cells (mixed w. exp. prey), and mixed with stationary phase prey cells (mixed w. stat. prey). P1 indicates the first peak in the turn angle distribution and P2 the second (as determined using a Gaussian mixed model approach where all values are approximate).

4.1.2 Conclusions

This project has studied *B. bacteriovorus* motility behaviour in three dimensions for the first time and in much greater detail than previous work. This has revealed previously unknown *B. bacteriovorus* characteristics including run times and reorientation angles they perform whilst swimming. These characteristics, combined with swimming speeds, indicate that *B. bacteriovorus* have an interesting and complex swimming style which, whilst consistent over time, can be altered both by proximity to surfaces and the presence of prey cells.

Before investigating *B.bacteriovorus* motility, prey *E.coli* cell motility was studied. Both exponential and stationary phase *E.coli* show the characteristic run and tumble swimming style previously found by Howard Berg and many others [98, 103, 124, 173, 195]. The swimming speed results obtained for exponential phase *E.coli* of 18.0±6.9 μms^{-1} is within the range of previous 3D studies - approximately 10-26 μms^{-1} [98, 103, 124, 173, 198]. The run times and reorientation angles of the exponential phase cells are 0.377±0.639 s and 82.7±41.8 ° respectively. These differ slightly from existing values but within the given errors [98, 103]. The differences could be due to a number of factors including the cell strains used and variations in culturing techniques and media.

Stationary phase *E.coli* motility has not been studied at this level of detail before. The key characteristics were quantified, finding the swimming speed to be 9.9±6.9 μms^{-1}, the run time to be 0.238±0.639 s, and the reorientation angle to be 90.5±41.2 °. These characteristics differ significantly from the exponential phase *E.coli*, with a decrease in both swimming speed and run time and an increase in turning angle. This results in slower, less persistent swimming trajectories than those of the exponential *E.coli* cells. A previous study by Amsler et al. has also found a decrease in overall swimming speed in stationary phase cells [203]. There are a number of possible reasons for this change in behaviour including stressors within the cell, differences in flagellum number and size, as well as alterations in the chemotaxis pathway [201–203].

Overall, the *E.coli* results showed the expected run and tumble motility mechanism, with characteristic values similar to those previously seen. These results served as a useful comparison to the *B.bacteriovorus* motility and enabled the identification of cell types in the mixed sample studies.

The central goal of this project was to study the motility characteristics of *B.bacteriovorus* in three dimensions, to aid in understanding of their life cycle and predation mechanisms. This was achieved, giving new insights into their behaviour in previously unseen detail. This study found that *B.bacteriovorus* have a swimming speed of 34.1 ±7.8 μms^{-1}. This value fits within the average range found by previous studies of approximately 30-60 μms^{-1} [137, 141, 142, 204]. *B.bacteriovorus* run time was found to be 0.477±0.711 s and have an interesting long tailed distribution, possibly in the manner of a Lévy walk. The *B.bacteriovorus* reorientation angle distribution is particularly interesting with two peaks at approximately 102 ° and 165 ° . When the run times are plotted against the turn angles it becomes apparent that there is a relationship between them. There are two clearly defined clusters; with longer run times being most likely to be followed by higher reorientation angles. Shorter runs are typically followed by smaller reorientation angles. However, these smaller angle changes have a broader distribution. In addition, it is possible to see that there is pattern to the order of these reorientation angles, with high angle turns most likely to be followed by low angle turns. It is rare for a low angle turn to be followed by another low angle turn.

From the characteristics and patterns in the results here, I hypothesise that *B. bacteriovorus* have a run-reverse-flick style of swimming with a biphasic reorientation pattern consisting of consecutive high angle reversals and low angle flicks. This pattern is maintained well over a time window of 18-24h, most likely due to an excess supply of prey *in vitro* enabling continuous predation.

The motility behaviour of *B.bacteriovorus* was also studied near to surfaces. It was found that when the cells are within 10μm of surfaces the run-reverse flick pattern disappears. The cells swim slower at around 30.6±11.0 μms^{-1}, a reduction of 5 μms^{-1} compared to swimming in bulk fluids. They also re-orient more often having a run time 0.21±0.30 s, which is a reduction 0.4 s compared to bulk. There is also a significantly altered swimming pattern consisting of a wide continuous distribution of reorientation angles. These reorientation angles do not have a complex pattern - they are most likely to be followed by another of a similar value. Past studies of other types of bacteria of both *E. coli* and *Pseudomonas aeruginosa* have also found reductions in swimming speed and changes of cell behaviour [102, 105]. These changes are most likely caused by hydrodynamic interactions of the cell body and the flagellum with the surfaces [211].

Lastly, the behaviour of *B.bacteriovorus* was studied when mixed with live *E.coli* prey cells. It was found that the run-reverse-flick motility pattern was preserved in this case and no significant changes were seen in turning angle or run length (see tables 4.2 and 4.3). However, their swimming speed increased when compared to *B.bacteriovorus* alone. *B.bacteriovorus* alone (with thresholds as applied to mixed samples) had a swimming speed of 32.96±5.38 μms^{-1}. In comparison, when mixed with *E.coli* prey cells this increased to 36.9±5.7 μms^{-1} and 36.3±6.5 μms^{-1} (for exponential and stationary phase prey respectively). This increase in swimming speed is likely a mechanism by which *B.bacteriovorus* boosts its predation efficiency. Increasing swimming speed will increase the likelihood to collide with prey cells present in the environment. Thereby, it increases the chance of successful predation. This method does not rely on prior knowledge of a prey cell type or active tracking of individual prey cells. It indicates that *B.bacteriovorus* is able to sense and respond to areas of high prey density which has previously been hinted at in past studies [108, 144–148].

The results obtained here add to existing knowledge of *B. bacteriovorus* motility, going some way to explain their complex swimming behaviour in fluid environments. I hope that this work can help to enhance overall understanding of how *B. bacteriovorus* interact with their environment, including prey cells, and aid in their future application industrially and/or medically.

4.2 Future work

There is a variety of future work that could be done to build upon the results presented in this thesis, to confirm theories suggested here and to further deepen our understanding of *B. bacteriovorus* motility behaviour.

Further studies will be needed in order to confirm the hypothesis that *B. bacteriovorus* has a run-reverse-flick style of re-orientation. These studies will need to include imaging the flagellum whilst cells are swimming. Ideally, in order to track their relative motion, both the flagellum and the cell body will need to be imaged at the same time. One of the main limitations of the DIHM imaging technique used in this project was that it only enabled the localisation of the cell body, not the flagellum. In order to overcome this issue, other microscopy techniques such as fluorescent staining and imaging could be used. Considering the size of the *B. bacteriovorus* and the membrane-sheathed nature of its flagellum, this may be challenging. However, a previous study has successfully used fluorescent staining and tagging to visualise *Vibrio alginolyticus* flagella which have a similar single

polar sheathed flagella [214]. It may be possible to use a similar technique to stain *B. bacteriovorus* flagella which, in combination with a differently coloured fluorescent cell strain, such as constitutively expressing mCherry cells, may allow simultaneous and relative cell body to flagella imaging.

Considering the previously seen impact of swimming speed on the flicking behaviour of bacterial cells, as well as the known impact of viscosity on *B. bacteriovorus* predation, it would be interesting to further study *B. bacteriovorus* motility characteristics in medically relevant environmental conditions such as in visco-elastic fluids. This is something that would be relatively straightforward to do with the current DIHM set up. Different types of polymer could be added to the imaging buffer and the cells imaged in the same manner as in this project.

More work needs to be done to understand if the changes of behaviour in *B. bacteriovorus* at surfaces confers it any form of predatory advantage. This work could include modelling of this behaviour, similar to that done by Jashnaz et al., but this time taking into account the key characteristics such as the run distributions and pattern of turning angles found by this study [108]. In addition, experiments could be done to compare the predation rates of prey in bulk fluids compared to prey on surfaces (non-motile or otherwise trapped). One of the most time consuming, manual aspects, of the image analysis process for this project, was manually identifying the sample chamber surface depths. As all the sample chambers were made by hand their depth varied slightly between each one. This meant that they all had to be checked during analysis. If a larger study of surface interactions was going to be done using DIHM it would be preferable to change this method. It may be possible to automate the surface identification using some form of algorithm or machine learning software. Alternatively, commercial sample chambers could be sourced, although these will have manufacturing tolerances which may also need checking.

The increase in swimming speed in the presence of live prey cells seen in this study, combined with the previous chemotaxis studies discussed in section 1.3.5 offer mixed evidence of active hunting by *B. bacteriovorus*. The DIHM technique I have used here could be harnessed to do more in depth studies of chemotaxis towards live prey. Firstly, initial studies could be done using known chemo-attractants for *B. bacteriovorus*. This would enable the study of the *B. bacteriovorus* chemotaxis mechanism in terms of changes in swimming characteristics such as biasing of run times in the direction of desired nutrients, as has been seen in other species such as *E. coli*. Experiments with live prey could then

be performed, using non-motile prey on surfaces, or a range of prey cell types trapped in agar plugs. I did begin experiments with live prey cells trapped within agar plugs. However I found that *B.bacteriovorus* was attracted to the agar plugs alone perhaps due to impurities. If these experiments were performed it would be critical to find a neutral medium within which the prey cells could be suspended. Comparisons could be made between baseline swimming characteristics, known chemotaxis characteristics and any motility changes in the presence of live prey cells. These studies combined would give a comprehensive understanding of *B. bacteriovorus* hunting behaviour.

Beyond the further work in understanding *B. bacteriovorus*, it is interesting to consider the implications of the technique used in section 3.6 to identify cell types from motility characteristics. Whilst the criteria used in this study were relatively simple, it is possible to suggest that if combined with advanced computing techniques, such as machine learning, it could be applied to other more complex samples containing more than two cells types. This technique has wide reaching application possibilities including in medical diagnostics.

APPENDIX A

THE FREEDMAN-DIACONIS RULE

The Freedman-Diaconis rule is a statistical technique developed by David Freedman and Persi Diaconis. It can be used for determining the optimum bin width for histograms particularly for unusual distributions, such as those with long tails or multiple peaks.

The rule approximately minimises the integral of the squared difference between the relative frequency density (i.e. the histogram) and the density of the theoretical probability distribution. In practical terms, it attempts to select the bin width which most appropriately displays the data distribution.

The general equation for the rule is:

$$Binwidth = 2\frac{IQR(x)}{\sqrt[3]{n}} \tag{A.1}$$

where IQR is the interquartile range, n is the number of samples in the data set x [215].

APPENDIX B

BDELLOVIBRIO BACTERIOVORUS CULTURING PROTOCOL

Adapted from published procedure by Carey Lambert and Liz Sockett [193].

B.1 Introduction

This procedure outlines how to culture host dependent *Bdellovibrio bacteriovorus HD100* (*B.bacteriovorus*) including reviving them from frozen frozen stocks, onto plates and into liquid media and general culturing. It also includes the instructions for making the necessary media and plates.

B.2 Media preparation

B.2.1 Media needed:

1. YT media
2. $CaCl_2.2H_2O$ (Calcium chloride dihydrate) stock solution
3. YPSC media
4. Calcium/HEPES free acid buffer

B.2.2 Media descriptions:

- YT media is standard microbial growth medium. It is nutrient rich, and contains peptides and amino acids in a low salt formulation. It is typically used to grow *E.coli* cells.
- YPSC media is specialised microbial growth medium used for growing *E.coli* cells for *B. bacteriovorus* predation. It is low nutrient but does contain peptides and amino acids and is high in calcium salts.
- Calcium/HEPES free acid buffer is used for growing *B.bacteriovorus* cells. This buffer is nutrient free. It is used to maintain the ion levels and therefore the pH of the cell culture.

B.2.3 Media recipes:

YT media

- $5gL^{-1}$ sodium chloride
- $5gL^{-1}$ peptone
- $8gL^{-1}$ tryptone

Dissolve all ingredients in appropriate volume of water. Adjust to pH 7.5 using 2M NaOH. Autoclave to sterilise.

$CaCl_2.2H_2O$ (Calcium chloride dihydrate) stock solution

- $25gL^{-1}$ $CaCl_2.2H_2O$
- MilliQ water

Dissolve $CaCl_2.2H_2O$ in appropriate amount of water. Filter sterilise solution. Store at room temperature. ***Do not heat stock solution or any media once $CaCl_2.2H_20$ has been added as it will precipitate.**

YPSC media

- $0.125 gL^{-1}$ magnesium sulphate
- $0.25 gL^{-1}$ sodium acetate
- $0.5 gL^{-1}$ bacto peptone
- $0.5 gL^{-1}$ yeast extract
- $CaCl_2.2H_2O$ stock solution

Dissolve all ingredients except $CaCl_2.2H_2O$ in appropriate volume of water. Autoclave to sterilise. If using as liquid media add $CaCl_2.2H_2O$ stock solution to achieve $0.25 gL^{-1}$.

Calcium/HEPES buffer

- $5.94 gL^{-1}$ HEPES free acid
- $0.284 gL^{-1}$ calcium chloride dihydrate

Dissolve all ingredients in appropriate volume of water. Adjust to pH 7.6 using 2M NaOH. Autoclave to sterilise.

B.3 Culturing procedure

B.3.1 Reviving from frozen stocks

Equipment needed

- Autoclave
- Water bath set to 55°C
- Pipettes and tips
- Flow hood
- Test tubes
- Petri dishes
- Agar

NB. Prepare all media and buffers prior to starting culturing process.

Day 1: Prepare an overnight culture of prey cells:

1. Inoculate 20ml of LB or YT media with frozen *E.coli*.
2. Incubate overnight at 37°C, 150rpm shaking.

Day 2: Make YPSC overlay plates:

1. Prepare media for plates: 1% (w/v) agar YPSC and 0.6% (w/v) agar YPSC. Allow approximately 10ml of each concentration for each plate.
2. Add the appropriate amount of agar to the YPSC media, stir, autoclave and place into the water bath.
3. Inside the flow hood, add $CaCl_2.2H_2O$ stock solution to achieve $0.25gL^{-1}$ to the 1% (w/v) agar YPSC, pour into plates and allow to set.
4. The next stage need to be done as quickly as possible: to a test tube, add 200µl of overnight prey cell culture, 10ml of 0.6% (w/v) agar YPSC at 55°C and 100µl of $CaCl_2.2H_2O$ stock solution. Pour straight on top of the 1% (w/v) agar bottom layer. Repeat for every plate.
5. Leave plates for at least 5min undisturbed to allow the agar to set smoothly.
6. Spot approximately 50µl of *B.bacteriovorus* frozen stocks onto the centre of the YPSC overlay plate.
7. Seal the plates with parafilm and wrap with clingfilm to prevent drying out over long incubation period.
8. Incubate plate upright (0.6% (w/v) agar layer facing upwards) at 29°C overnight until a lawn of prey cells is observed.

Day 3: Incubate for predation:

1. Turn plate the upside down and incubate for another 1-5 days at 29°C or until clearing of the prey lawn is observed - see appendix for example photos.

Day 8: Prepare an overnight culture of prey cells:

1. Inoculate 20ml of LB or YT media with frozen *E.coli*.
2. Incubate overnight at 37°C, 150rpm shaking.

Day 9 (morning): Make mini lysate:

1. Place 2ml of Calcium/HEPES buffer and 150µl of overnight prey culture into a test tube.
2. Using a P1000 pipette set to 300µl, pick some of the cleared agar off the top layer of the plates and add to the buffer-prey mix in the test tube.
3. Incubate at 29°C, 150rpm for 1-2 days until you can see *B.bacteriovorus* swimming under darkfield microscopy.

Day 9 (evening): Prepare an overnight culture of prey cells:

1. Inoculate 20ml of LB or YT media with frozen *E.coli*.
2. Incubate overnight at 37°C, 150rpm shaking.

Day 10: Make main prey lysate:

1. Add the below to a sterile 250ml conical flask:
   a) 50ml sterile Calcium/HEPES buffer
   b) 3ml of overnight prey cell culture
   c) 1ml of mini lysate
2. Incubate overnight at 29°C with shaking at 200rpm for 24h.

Day 11: Check lysate for cells:

1. Check for *B.bacteriovorus* under darkfield microscope.

Note: YPSC overlay plates can be stored at room temperature for up to 2 weeks, with the *B.bacteriovorus* remaining viable. This is better than storing at 4°C.

B.3.2 Sub-culturing of *B.bacteriovorus* on *E.coli* prey lysates

Day 1: Prepare an overnight culture of prey cells:

1. Inoculate 20ml of LB or YT media with frozen *E.coli*.
2. Incubate overnight at 37°C, 150rpm shaking.

Day 2: Make main prey lysate:

1. Add the below to a sterile 250ml conical flask:
   a) 50ml sterile Calcium/HEPES buffer
   b) 3ml of overnight prey cell culture
   c) 1ml of prey lysate
2. Incubate overnight at 29°C with shaking at 200rpm for 24h.

Day 3: Check lysate for cells:

1. Check for *B.bacteriovorus* cells under darkfield microscope.

BIBLIOGRAPHY

[1] Marianne Frieri, Krishan Kumar, and Anthony Boutin. Antibiotic resistance. *Journal of infection and public health*, 10(4):369–378, 2017.

[2] Tomislav Mestrovic, Gisela Robles Aguilar, Lucien R Swetschinski, Kevin S Ikuta, Authia P Gray, Nicole Davis Weaver, Chieh Han, Eve E Wool, Anna Gershberg Hayoon, Simon I Hay, et al. The burden of bacterial antimicrobial resistance in the who european region in 2019: A cross-country systematic analysis. *The Lancet Public Health*, 7(11):e897–e913, 2022.

[3] Mathieu F Chellat, Luka Raguž, and Rainer Riedl. Targeting antibiotic resistance. *Angewandte Chemie International Edition*, 55(23):6600–6626, 2016.

[4] Rebecca Sugden, Ruth Kelly, and Sally Davies. Combatting antimicrobial resistance globally. *Nature microbiology*, 1(10):1–2, 2016.

[5] Centers for Disease Control and Prevention:. *Report on Antibiotic resistance threats in the United States, 2019*. Atlanta GA: US Department of Health and Human Services, Centres for Disease Control and Prevention, 2019.

[6] Roseann Velez, Elizabeth Sloand, et al. Combating antibiotic resistance, mitigating future threats and ongoing initiatives. *J. Clin. Nurs*, 25(13-14):1886–1889, 2016.

[7] Jim O'Neill. Tackling drug-resistant infections globally: final report and recommendations. The review on antimicrobial resistance chaired by Jim O'Neill. *Wellcome Collection*, 2016.

[8] Christian JH Von Wintersdorff, John Penders, Julius M Van Niekerk, Nathan D Mills, Snehali Majumder, Lieke B Van Alphen, Paul HM Savelkoul, and Petra FG Wolffs. Dissemination of antimicrobial resistance in microbial ecosystems through horizontal gene transfer. *Frontiers in microbiology*, 7:173, 2016.

[9] Alison H Holmes, Luke SP Moore, Arnfinn Sundsfjord, Martin Steinbakk, Sadie Regmi, Abhilasha Karkey, Philippe J Guerin, and Laura JV Piddock. Understanding the mechanisms and drivers of antimicrobial resistance. *The Lancet*, 387(10014):176–187, 2016.

[10] Mario Juhas, Jan Roelof Van Der Meer, Muriel Gaillard, Rosalind M Harding, Derek W Hood, and Derrick W Crook. Genomic islands: tools of bacterial horizontal gene transfer and evolution. *FEMS microbiology reviews*, 33(2):376–393, 2009.

[11] Richard J Fair and Yitzhak Tor. Antibiotics and bacterial resistance in the 21st century. *Perspectives in medicinal chemistry*, 6:PMC–S14459, 2014.

[12] Michael A Kohanski, Daniel J Dwyer, and James J Collins. How antibiotics kill bacteria: from targets to networks. *Nature Reviews Microbiology*, 8(6):423–435, 2010.

[13] Elizabeth M Darby, Eleftheria Trampari, Pauline Siasat, Maria Solsona Gaya, Ilyas Alav, Mark A Webber, and Jessica MA Blair. Molecular mechanisms of antibiotic resistance revisited. *Nature Reviews Microbiology*, pages 1–16, 2022.

[14] Elaine Larson. Community factors in the development of antibiotic resistance. *Annu. Rev. Public Health*, 28:435–447, 2007.

[15] Robert Gaynes. The discovery of penicillin,Äînew insights after more than 75 years of clinical use. *Emerging infectious diseases*, 23(5):849, 2017.

[16] Eili Y Klein, Thomas P Van Boeckel, Elena M Martinez, Suraj Pant, Sumanth Gandra, Simon A Levin, Herman Goossens, and Ramanan Laxminarayan. Global increase and geographic convergence in antibiotic consumption between 2000 and 2015. *Proceedings of the National Academy of Sciences*, 115(15):E3463–E3470, 2018.

[17] Edwin D Charlebois, David R Bangsberg, Nicholas J Moss, Matthew R Moore, Andrew R Moss, Henry F Chambers, and Françoise Perdreau-Remington. Population-based community prevalence of methicillin-resistant staphylococcus aureus in the urban poor of san francisco. *Clinical Infectious Diseases*, pages 425–433, 2002.

[18] Ana C Silva, Paulo Jorge Nogueira, and José-Artur Paiva. Determinants of antimicrobial resistance among the different european countries: more

than human and animal antimicrobial consumption. *Antibiotics*, 10(7):834, 2021.

[19] Thomas P Van Boeckel, Charles Brower, Marius Gilbert, Bryan T Grenfell, Simon A Levin, Timothy P Robinson, Aude Teillant, and Ramanan Laxminarayan. Global trends in antimicrobial use in food animals. *Proceedings of the National Academy of Sciences*, 112(18):5649–5654, 2015.

[20] Katie Tiseo, Laura Huber, Marius Gilbert, Timothy P Robinson, and Thomas P Van Boeckel. Global trends in antimicrobial use in food animals from 2017 to 2030. *Antibiotics*, 9(12):918, 2020.

[21] Carl Llor and Lars Bjerrum. Antimicrobial resistance: risk associated with antibiotic overuse and initiatives to reduce the problem. *Therapeutic advances in drug safety*, 5(6):229–241, 2014.

[22] Aidan Hollis and Ziana Ahmed. Preserving antibiotics, rationally. *New England Journal of Medicine*, 369(26):2474–2476, 2013.

[23] Sara Hernando-Amado, Teresa M Coque, Fernando Baquero, and José L Martínez. Defining and combating antibiotic resistance from one health and global health perspectives. *Nature microbiology*, 4(9):1432–1442, 2019.

[24] Marisa Haenni, Christophe Dagot, Olivier Chesneau, Delphine Bibbal, Jérôme Labanowski, Michèle Vialette, Damien Bouchard, Fabrice Martin-Laurent, Louisiane Calsat, Sylvie Nazaret, et al. Environmental contamination in a high-income country (france) by antibiotics, antibiotic-resistant bacteria, and antibiotic resistance genes: Status and possible causes. *Environment international*, 159:107047, 2022.

[25] Evelina Tacconelli, Elena Carrara, Alessia Savoldi, Stephan Harbarth, Marc Mendelson, Dominique L Monnet, Céline Pulcini, Gunnar Kahlmeter, Jan Kluytmans, Yehuda Carmeli, et al. Discovery, research, and development of new antibiotics: the who priority list of antibiotic-resistant bacteria and tuberculosis. *The Lancet infectious diseases*, 18(3):318–327, 2018.

[26] Christopher JL Murray, Kevin Shunji Ikuta, Fablina Sharara, Lucien Swetschinski, Gisela Robles Aguilar, Authia Gray, Chieh Han, Catherine Bisignano, Puja Rao, Eve Wool, et al. Global burden of bacterial antimicrobial resistance in 2019: a systematic analysis. *The Lancet*, 2022.

[27] Rene S Hendriksen, Patrick Munk, Patrick Njage, Bram Van Bunnik, Luke McNally, Oksana Lukjancenko, Timo Röder, David Nieuwenhuijse, Susanne Karlsmose Pedersen, Jette Kjeldgaard, et al. Global monitoring of antimicrobial resistance based on metagenomics analyses of urban sewage. *Nature communications*, 10(1):1–12, 2019.

[28] A Dashiff, RA Junka, M Libera, and DE Kadouri. Predation of human pathogens by the predatory bacteria micavibrio aeruginosavorus and bdellovibrio bacteriovorus. *Journal of applied microbiology*, 110(2):431–444, 2011.

[29] Yair Shemesh and Edouard Jurkevitch. Plastic phenotypic resistance to predation by bdellovibrio and like organisms in bacterial prey. *Environmental Microbiology*, 6(1):12–18, 2004.

[30] Robert J Atterbury and Jess Tyson. Predatory bacteria as living antibiotics–where are we now? *Microbiology*, 167(1):001025, 2021.

[31] Heinz Stolp and MP Starr. Bdellovibrio bacteriovorus gen. et sp. n., a predatory, ectoparasitic, and bacteriolytic microorganism. *Antonie Van Leeuwenhoek*, 29(1):217–248, 1963.

[32] Andrew L Lovering and R Elizabeth Sockett. Microbe profile: Bdellovibrio bacteriovorus: a specialized bacterial predator of bacteria. *Microbiology*, 167(4), 2021.

[33] Géraldine Laloux. Shedding light on the cell biology of the predatory bacterium bdellovibrio bacteriovorus. *Frontiers in microbiology*, 10:3136, 2020.

[34] Richard P Novick. Antibacterial particles and predatory bacteria as alternatives to antibacterial chemicals in the era of antibiotic resistance. *Current Opinion in Microbiology*, 64:109–116, 2021.

[35] Renee Elizabeth Sockett. Predatory lifestyle of bdellovibrio bacteriovorus. *Annual review of microbiology*, 63:523–539, 2009.

[36] Kaitlyn E Kortright, Benjamin K Chan, Jonathan L Koff, and Paul E Turner. Phage therapy: a renewed approach to combat antibiotic-resistant bacteria. *Cell host & microbe*, 25(2):219–232, 2019.

[37] Janis Doss, Kayla Culbertson, Delilah Hahn, Joanna Camacho, and Nazir Barekzi. A review of phage therapy against bacterial pathogens of aquatic and terrestrial organisms. *Viruses*, 9(3):50, 2017.

[38] Luis DR Melo, Hugo Oliveira, Diana P Pires, Krystyna Dabrowska, and Joana Azeredo. Phage therapy efficacy: a review of the last 10 years of preclinical studies. *Critical reviews in microbiology*, 46(1):78–99, 2020.

[39] Oleg Krut and Isabelle Bekeredjian-Ding. Contribution of the immune response to phage therapy. *The Journal of Immunology*, 200(9):3037–3044, 2018.

[40] Andrzej Górski, Ryszard Międzybrodzki, Jan Borysowski, Krystyna Dąbrowska, Piotr Wierzbicki, Monika Ohams, Grażyna Korczak-Kowalska, Natasza Olszowska-Zaremba, Marzena Łusiak-Szelachowska, Marlena Kłak, et al. Phage as a modulator of immune responses: practical implications for phage therapy. *Advances in virus research*, 83:41–71, 2012.

[41] Lasha Gogokhia, Kate Buhrke, Rickesha Bell, Brenden Hoffman, D Garrett Brown, Christin Hanke-Gogokhia, Nadim J Ajami, Matthew C Wong, Arevik Ghazaryan, John F Valentine, et al. Expansion of bacteriophages is linked to aggravated intestinal inflammation and colitis. *Cell host & microbe*, 25(2):285–299, 2019.

[42] Chunhui Yan, Manjun Zhan, Kewei Xv, Siyuan Zhang, Ting Liang, and Ran Yu. Sludge dewaterability enhancement under low temperature condition with cold-tolerant bdellovibrio sp. cll13. *Science of The Total Environment*, 820:153269, 2022.

[43] OM Olanya, BA Niemira, JM Cassidy, Glenn Boyd, and Joseph Uknalis. Pathogen reduction by predatory bacteria and survival of bdellovibrio bacteriovorus and escherichia coli on produce and buffer treated with low-dose gamma radiation. *LWT*, 130:109630, 2020.

[44] Daniel Youdkes, Yael Helman, Saul Burdman, Ofra Matan, and Edouard Jurkevitch. Potential control of potato soft rot disease by the obligate predators bdellovibrio and like organisms. *Applied and environmental microbiology*, 86(6):e02543–19, 2020.

[45] Monique Waso, S Khan, Anukriti Singh, Stuart McMichael, W Ahmed, Pilar Fernandez-Ibanez, JA Byrne, and Wesaal Khan. Predatory bacteria in combination with solar disinfection and solar photocatalysis for the treatment of rainwater. *Water research*, 169:115281, 2020.

[46] Emma B Saxon, Robert W Jackson, Shobita Bhumbra, Tim Smith, and R Elizabeth Sockett. Bdellovibrio bacteriovorus hd100 guards against

pseudomonas tolaasii brown-blotch lesions on the surface of post-harvest agaricus bisporus supermarket mushrooms. *BMC microbiology*, 14(1):1–12, 2014.

[47] Sonal Dharani, Dong Hyun Kim, Robert MQ Shanks, Yohei Doi, and Daniel E Kadouri. Susceptibility of colistin-resistant pathogens to predatory bacteria. *Research in microbiology*, 169(1):52–55, 2018.

[48] Daniel Kadouri and George A O'Toole. Susceptibility of biofilms to bdellovibrio bacteriovorus attack. *Applied and Environmental Microbiology*, 71(7):4044–4051, 2005.

[49] Yao Sun, Jianzhong Ye, Yuanbo Hou, Huale Chen, Jianming Cao, and Tieli Zhou. Predation efficacy of bdellovibrio bacteriovorus on multidrug-resistant clinical pathogens and their corresponding biofilms. *Japanese Journal of Infectious Diseases*, 70(5):485–489, 2017.

[50] Divakar Sharma, Lama Misba, and Asad U Khan. Antibiotics versus biofilm: an emerging battleground in microbial communities. *Antimicrobial Resistance & Infection Control*, 8(1):1–10, 2019.

[51] Benjamin R Wucher, Mennat Elsayed, James S Adelman, Daniel E Kadouri, and Carey D Nadell. Bacterial predation transforms the landscape and community assembly of biofilms. *Current Biology*, 31(12):2643–2651, 2021.

[52] Susana Merino and Juan M Tomás. Bacterial capsules and evasion of immune responses. *eLS*, pages 1–10, 2010.

[53] Mark A Schembri, Dorte Dalsgaard, and Per Klemm. Capsule shields the function of short bacterial adhesins. *Journal of bacteriology*, 186(5):1249–1257, 2004.

[54] Sana Rehman, Zahid Ali, Momna Khan, Nazish Bostan, and Saadia Naseem. The dawn of phage therapy. *Reviews in medical virology*, 29(4):e2041, 2019.

[55] Simon J Labrie, Julie E Samson, and Sylvain Moineau. Bacteriophage resistance mechanisms. *Nature Reviews Microbiology*, 8(5):317–327, 2010.

[56] Susan F Koval and Manfred E Bayer. Bacterial capsules: no barrier against bdellovibrio. *Microbiology*, 143(3):749–753, 1997.

[57] David Negus, Chris Moore, Michelle Baker, Dhaarini Raghunathan, Jess Tyson, and R Elizabeth Sockett. Predator versus pathogen: how does

predatory bdellovibrio bacteriovorus interface with the challenges of killing gram-negative pathogens in a host setting? *Annual Review of Microbiology*, 71:441–457, 2017.

[58] Valerio Iebba, Valentina Totino, Floriana Santangelo, Antonella Gagliardi, Luana Ciotoli, Alessandra Virga, Cecilia Ambrosi, Monica Pompili, Riccardo V De Biase, Laura Selan, et al. Bdellovibrio bacteriovorus directly attacks pseudomonas aeruginosa and staphylococcus aureus cystic fibrosis isolates. *Frontiers in microbiology*, 5:280, 2014.

[59] Gitte Loozen, Nico Boon, Martine Pauwels, Vera Slomka, Esteban Rodrigues Herrero, Marc Quirynen, and Wim Teughels. Effect of bdellovibrio bacteriovorus hd100 on multispecies oral communities. *Anaerobe*, 35:45–53, 2015.

[60] Alexandra R Willis, Christopher Moore, Maria Mazon-Moya, Sina Krokowski, Carey Lambert, Robert Till, Serge Mostowy, and R Elizabeth Sockett. Injections of predatory bacteria work alongside host immune cells to treat shigella infection in zebrafish larvae. *Current Biology*, 26(24):3343–3351, 2016.

[61] Kenneth Shatzkes, Richard Chae, Chi Tang, Gregory C Ramirez, Somdatta Mukherjee, Liana Tsenova, Nancy D Connell, and Daniel E Kadouri. Examining the safety of respiratory and intravenous inoculation of bdellovibrio bacteriovorus and micavibrio aeruginosavorus in a mouse model. *Scientific reports*, 5(1):1–12, 2015.

[62] Eric G Romanowski, Nicholas A Stella, Kimberly M Brothers, Kathleen A Yates, Martha L Funderburgh, James L Funderburgh, Shilpi Gupta, Sonal Dharani, Daniel E Kadouri, and Robert MQ Shanks. Predatory bacteria are nontoxic to the rabbit ocular surface. *Scientific reports*, 6(1):1–9, 2016.

[63] Shilpi Gupta, Chi Tang, Michael Tran, and Daniel E Kadouri. Effect of predatory bacteria on human cell lines. *PLoS One*, 11(8):e0161242, 2016.

[64] Laura Hobley, John R King, and R Elizabeth Sockett. Bdellovibrio predation in the presence of decoys: three-way bacterial interactions revealed by mathematical and experimental analyses. *Applied and Environmental Microbiology*, 72(10):6757–6765, 2006.

[65] Khaled K Mahmoud and Susan F Koval. Characterization of type iv pili in the life cycle of the predator bacterium bdellovibrio. *Microbiology*, 156(4):1040–1051, 2010.

[66] Nedal Said, Antonis Chatzinotas, and Matthias Schmidt. Have an ion on it: The life-cycle of bdellovibrio bacteriovorus viewed by helium-ion microscopy. *Advanced Biosystems*, 3(1):1800250, 2019.

[67] Carey Lambert, Laura Hobley, Chien-Yi Chang, Andrew Fenton, Michael Capeness, and Liz Sockett. A predatory patchwork: membrane and surface structures of bdellovibrio bacteriovorus. *Advances in microbial physiology*, 54:313–361, 2008.

[68] Ryan M Chanyi and Susan F Koval. Role of type iv pili in predation by bdellovibrio bacteriovorus. *PLoS One*, 9(11):e113404, 2014.

[69] Carey Lambert, Karen A Morehouse, Chien-Yi Chang, and R Elizabeth Sockett. Bdellovibrio: growth and development during the predatory cycle. *Current opinion in microbiology*, 9(6):639–644, 2006.

[70] Carey Lambert, Chien-Yi Chang, Michael J Capeness, and R Elizabeth Sockett. The first bite,Äîprofiling the predatosome in the bacterial pathogen bdellovibrio. *PloS one*, 5(1):e8599, 2010.

[71] Snjezana Rendulic, Pratik Jagtap, Andrea Rosinus, Mark Eppinger, Claudia Baar, Christa Lanz, Heike Keller, Carey Lambert, Katy J Evans, Alexander Goesmann, et al. A predator unmasked: life cycle of bdellovibrio bacteriovorus from a genomic perspective. *Science*, 303(5658):689–692, 2004.

[72] Ewa Bukowska-Faniband, Tilde Andersson, and Rolf Lood. Studies on bd0934 and bd3507, two secreted nucleases from bdellovibrio bacteriovorus, reveal sequential release of nucleases during the predatory cycle. *Journal of bacteriology*, 202(18):e00150–20, 2020.

[73] AK Fenton, M Kanna, RD Woods, S-I Aizawa, and RE Sockett. Shadowing the actions of a predator: backlit fluorescent microscopy reveals synchronous nonbinary septation of predatory bdellovibrio inside prey and exit through discrete bdelloplast pores. *Journal of bacteriology*, 192(24):6329–6335, 2010.

[74] Miles C Duncan, Rebecca K Gillette, Micah A Maglasang, Elizabeth A Corn, Albert K Tai, David W Lazinski, Robert MQ Shanks, Daniel E Kadouri, and Andrew Camilli. High-throughput analysis of gene function in the bacterial predator bdellovibrio bacteriovorus. *MBio*, 10(3):e01040–19, 2019.

[75] Navish Wadhwa and Howard C Berg. Bacterial motility: machinery and mechanisms. *Nature Reviews Microbiology*, pages 1–13, 2021.

[76] Howard C Berg. *Random walks in biology, New, expanded edition*. Princeton University Press, 1993.

[77] David B Dusenbery. *Living at micro scale: the unexpected physics of being small*. Harvard University Press, 2009.

[78] Erik J Anderson, Wade R Mcgillis, and Mark A Grosenbaugh. The boundary layer of swimming fish. *Journal of Experimental Biology*, 204(1):81–102, 2001.

[79] Edward M Purcell. Life at low reynolds number. *American journal of physics*, 45(1):3–11, 1977.

[80] Navish Wadhwa and Howard C Berg. Bacterial motility: machinery and mechanisms. *Nature Reviews Microbiology*, 20(3):161–173, 2022.

[81] Philip Nelson. *Biological physics: Energy, Information, Life*. WH Freeman New York, 2008.

[82] Mehdi Molaei, Ehsan Atefi, and John C Crocker. Nanoscale rheology and anisotropic diffusion using single gold nanorod probes. *Physical review letters*, 120(11):118002, 2018.

[83] Joseph S Beckwith and Haw Yang. Sub-millisecond translational and orientational dynamics of a freely moving single nanoprobe. *The Journal of Physical Chemistry B*, 125(49):13436–13443, 2021.

[84] Koji Yonekura, Saori Maki-Yonekura, and Keiichi Namba. Complete atomic model of the bacterial flagellar filament by electron cryomicroscopy. *Nature*, 424(6949):643–650, 2003.

[85] Michael D Manson, Pat Tedesco, Howard C Berg, Franklin M Harold, and Chris Van der Drift. A protonmotive force drives bacterial flagella. *Proceedings of the National Academy of Sciences*, 74(7):3060–3064, 1977.

[86] Haidai Hu, Mònica Santiveri, Navish Wadhwa, Howard C Berg, Marc Erhardt, and Nicholas MI Taylor. Structural basis of torque generation in the bi-directional bacterial flagellar motor. *Trends in Biochemical Sciences*, 47(2):160–172, 2022.

[87] Yoshiyuki Sowa and Richard M Berry. Bacterial flagellar motor. *Quarterly reviews of biophysics*, 41(2):103–132, 2008.

[88] Howard C Berg. The rotary motor of bacterial flagella. *Annual review of biochemistry*, 72(1):19–54, 2003.

[89] Eli J Cohen, Daisuke Nakane, Yoshiki Kabata, David R Hendrixson, Takayuki Nishizaka, and Morgan Beeby. Campylobacter jejuni motility integrates specialized cell shape, flagellar filament, and motor, to coordinate action of its opposed flagella. *PLoS pathogens*, 16(7):e1008620, 2020.

[90] Roman Stocker. Reverse and flick: Hybrid locomotion in bacteria. *Proceedings of the National Academy of Sciences*, 108(7):2635–2636, 2011.

[91] Kwangmin Son, Jeffrey S Guasto, and Roman Stocker. Bacteria can exploit a flagellar buckling instability to change direction. *Nature physics*, 9(8):494–498, 2013.

[92] Judith P Armitage and Robert M Macnab. Unidirectional, intermittent rotation of the flagellum of rhodobacter sphaeroides. *Journal of Bacteriology*, 169(2):514–518, 1987.

[93] Ursula Attmannspacher, Birgit Scharf, and Rüdiger Schmitt. Control of speed modulation (chemokinesis) in the unidirectional rotary motor of sinorhizobium meliloti. *Molecular microbiology*, 56(3):708–718, 2005.

[94] Birgit Scharf and Rudiger Schmitt. Sensory transduction to the flagellar motor of sinorhizobium meliloti. *Journal of molecular microbiology and biotechnology*, 4(3):183–186, 2002.

[95] Daniel B Kearns. A field guide to bacterial swarming motility. *Nature Reviews Microbiology*, 8(9):634–644, 2010.

[96] Alexey J Merz, Magdalene So, and Michael P Sheetz. Pilus retraction powers bacterial twitching motility. *Nature*, 407(6800):98–102, 2000.

[97] Mark J McBride. Bacterial gliding motility: multiple mechanisms for cell movement over surfaces. *Annual Reviews in Microbiology*, 55(1):49–75, 2001.

[98] Howard C Berg and Douglas A Brown. Chemotaxis in escherichia coli analysed by three-dimensional tracking. *Nature*, 239(5374):500–504, 1972.

[99] Steven H Larsen, Robert W Reader, Edward N Kort, Wung-Wai Tso, and Julius Adler. Change in direction of flagellar rotation is the basis of the chemotactic response in escherichia coli. *Nature*, 249(5452):74–77, 1974.

[100] George H Wadhams and Judith P Armitage. Making sense of it all: bacterial chemotaxis. *Nature reviews Molecular cell biology*, 5(12):1024–1037, 2004.

[101] P Varuni, Shakti N Menon, and Gautam I Menon. Phototaxis as a collective phenomenon in cyanobacterial colonies. *Scientific reports*, 7(1):1–10, 2017.

[102] Paul D Frymier, Roseanne M Ford, Howard C Berg, and Peter T Cummings. Three-dimensional tracking of motile bacteria near a solid planar surface. *Proceedings of the National Academy of Sciences*, 92(13):6195–6199, 1995.

[103] Mehdi Molaei, Michael Barry, Roman Stocker, and Jian Sheng. Failed escape: solid surfaces prevent tumbling of escherichia coli. *Physical review letters*, 113(6):068103, 2014.

[104] Allison P Berke, Linda Turner, Howard C Berg, and Eric Lauga. Hydrodynamic attraction of swimming microorganisms by surfaces. *Physical Review Letters*, 101(3):038102, 2008.

[105] Andrew L Hook, James L Flewellen, Jean-Frédéric Dubern, Alessandro M Carabelli, Irwin M Zaid, Richard M Berry, Ricky D Wildman, Noah Russell, Paul Williams, and Morgan R Alexander. Simultaneous tracking of pseudomonas aeruginosa motility in liquid and at the solid-liquid interface reveals differential roles for the flagellar stators. *MSystems*, 4(5):e00390–19, 2019.

[106] Guanglai Li, James Bensson, Liana Nisimova, Daniel Munger, Panrapee Mahautmr, Jay X Tang, Martin R Maxey, and Yves V Brun. Accumulation of swimming bacteria near a solid surface. *Physical Review E*, 84(4):041932, 2011.

[107] Eric Lauga, Willow R DiLuzio, George M Whitesides, and Howard A Stone. Swimming in circles: motion of bacteria near solid boundaries. *Biophysical journal*, 90(2):400–412, 2006.

[108] Hossein Jashnsaz, Mohammed Al Juboori, Corey Weistuch, Nicholas Miller, Tyler Nguyen, Viktoria Meyerhoff, Bryan McCoy, Stephanie Perkins, Ross Wallgren, Bruce D Ray, et al. Hydrodynamic hunters. *Biophysical journal*, 112(6):1282–1289, 2017.

[109] Guanglai Li and Jay X Tang. Accumulation of microswimmers near a surface mediated by collision and rotational brownian motion. *Physical review letters*, 103(7):078101, 2009.

[110] Jinglei Hu, Adam Wysocki, Roland G Winkler, and Gerhard Gompper. Physical sensing of surface properties by microswimmers–directing bacterial motion via wall slip. *Scientific reports*, 5(1):1–7, 2015.

[111] Jeungeun Park, Yongsam Kim, Wanho Lee, and Sookkyung Lim. Modeling of lophotrichous bacteria reveals key factors for swimming reorientation. *Scientific Reports*, 12(1):6482, 2022.

[112] Sebastian Bubendorfer, Mihaly Koltai, Florian Rossmann, Victor Sourjik, and Kai M Thormann. Secondary bacterial flagellar system improves bacterial spreading by increasing the directional persistence of swimming. *Proceedings of the National Academy of Sciences*, 111(31):11485–11490, 2014.

[113] Michelle Baker, David Negus, Dhaarini Raghunathan, Paul Radford, Chris Moore, Gemma Clark, Mathew Diggle, Jess Tyson, Jamie Twycross, and R Elizabeth Sockett. Measuring and modelling the response of klebsiella pneumoniae kpc prey to bdellovibrio bacteriovorus predation, in human serum and defined buffer. *Scientific reports*, 7(1):1–18, 2017.

[114] A James, MJ Plank, and R Brown. Optimizing the encounter rate in biological interactions: ballistic versus lévy versus brownian strategies. *Physical Review E*, 78(5):051128, 2008.

[115] Vladas Skakauskas, Pranas Katauskis, Remigijus Šimkus, and Feliksas Ivanauskas. Phenomenological model of bacterial aerotaxis with a negative feedback. *Nonlinear Analysis: Modelling and Control*, 18(2):227–249, 2013.

[116] PV Bayly and KS Wilson. Analysis of unstable modes distinguishes mathematical models of flagellar motion. *Journal of the Royal Society Interface*, 12(106):20150124, 2015.

[117] Kevin M Passino. Biomimicry of bacterial foraging for distributed optimization and control. *IEEE control systems magazine*, 22(3):52–67, 2002.

[118] Andy M Reynolds. Current status and future directions of lévy walk research. *Biology open*, 7(1):bio030106, 2018.

[119] Jean-Philippe Bouchaud and Antoine Georges. Anomalous diffusion in disordered media: statistical mechanisms, models and physical applications. *Physics reports*, 195(4-5):127–293, 1990.

[120] Carlos Mejía-Monasterio, Ralf Metzler, and Jürgen Vollmer. Anomalous transport: Applications, mathematical perspectives, and big data, 2020.

[121] Ralf Metzler, Jae-Hyung Jeon, Andrey G Cherstvy, and Eli Barkai. Anomalous diffusion models and their properties: non-stationarity, non-ergodicity, and ageing at the centenary of single particle tracking. *Physical Chemistry Chemical Physics*, 16(44):24128–24164, 2014.

[122] Paul Lévy. *Théorie de l'addition des variables aléatoires*. Gauthier-Villars, 1954.

[123] Michael F Shlesinger and Joseph Klafter. Lévy walks versus lévy flights. *On growth and form: Fractal and non-fractal patterns in physics*, pages 279–283, 1986.

[124] Haiyan Huo, Rui He, Rongjing Zhang, and Junhua Yuan. Swimming escherichia coli cells explore the environment by lévy walk. *Applied and environmental microbiology*, 87(6):e02429–20, 2021.

[125] Frederic Bartumeus, M G E da Luz, Gandhimohan M Viswanathan, and Jordi Catalan. Animal search strategies: a quantitative random-walk analysis. *Ecology*, 86(11):3078–3087, 2005.

[126] Gandhimohan M Viswanathan, Vsevolod Afanasyev, Sergey V Buldyrev, Eugene J Murphy, Peter A Prince, and H Eugene Stanley. Lévy flight search patterns of wandering albatrosses. *Nature*, 381(6581):413–415, 1996.

[127] RPD Atkinson, CJ Rhodes, DW Macdonald, and RM Anderson. Scale-free dynamics in the movement patterns of jackals. *Oikos*, 98(1):134–140, 2002.

[128] Gabriel Ramos-Fernández, José L Mateos, Octavio Miramontes, Germinal Cocho, Hernán Larralde, and Barbara Ayala-Orozco. Lévy walk patterns in the foraging movements of spider monkeys (ateles geoffroyi). *Behavioral ecology and Sociobiology*, 55:223–230, 2004.

[129] Friedrich Lenz, Thomas C Ings, Lars Chittka, Aleksei V Chechkin, and Rainer Klages. Spatiotemporal dynamics of bumblebees foraging under predation risk. *Physical review letters*, 108(9):098103, 2012.

[130] Andy M Reynolds and Mark A Frye. Free-flight odor tracking in drosophila is consistent with an optimal intermittent scale-free search. *PloS one*, 2(4):e354, 2007.

[131] Franziska Matthäus, Mario S Mommer, Tine Curk, and Jure Dobnikar. On the origin and characteristics of noise-induced lévy walks of e. coli. *PloS one*, 6(4):e18623, 2011.

[132] Gil Ariel, Amit Rabani, Sivan Benisty, Jonathan D Partridge, Rasika M Harshey, and Avraham Be'Er. Swarming bacteria migrate by lévy walk. *Nature communications*, 6(1):8396, 2015.

[133] Siddhartha Mukherjee, Rahul K Singh, Martin James, and Samriddhi Sankar Ray. Anomalous diffusion and lévy walks distinguish active from inertial turbulence. *Physical Review Letters*, 127(11):118001, 2021.

[134] Frederic Bartumeus, Francesc Peters, Salvador Pueyo, Celia Marrasé, and Jordi Catalan. Helical lévy walks: adjusting searching statistics to resource availability in microzooplankton. *Proceedings of the National Academy of Sciences*, 100(22):12771–12775, 2003.

[135] Frederic Bartumeus and Simon A Levin. Fractal reorientation clocks: Linking animal behavior to statistical patterns of search. *Proceedings of the National Academy of Sciences*, 105(49):19072–19077, 2008.

[136] Andy Reynolds. Liberating lévy walk research from the shackles of optimal foraging. *Physics of life reviews*, 14:59–83, 2015.

[137] Carey Lambert, Katy J Evans, Rob Till, Laura Hobley, Michael Capeness, Snjezana Rendulic, Stephan C Schuster, Shin-Ichi Aizawa, and R Elizabeth Sockett. Characterizing the flagellar filament and the role of motility in bacterial prey-penetration by bdellovibrio bacteriovorus. *Molecular microbiology*, 60(2):274–286, 2006.

[138] Linda S Thomashow and Sydney C Rittenberg. Isolation and composition of sheathed flagella from bdellovibrio bacteriovorus 109J. *Journal of bacteriology*, 163(3):1047–1054, 1985.

[139] Yoshiko Iida, Laura Hobley, Carey Lambert, Andrew K Fenton, R Elizabeth Sockett, and Shin-Ichi Aizawa. Roles of multiple flagellins in flagellar formation and flagellar growth post bdelloplast lysis in bdellovibrio bacteriovorus. *Journal of molecular biology*, 394(5):1011–1021, 2009.

[140] Linda S Thomashow and Sydney C Rittenberg. Waveform analysis and structure of flagella and basal complexes from bdellovibrio bacteriovorus 109J. *Journal of bacteriology*, 163(3):1038–1046, 1985.

[141] Rajesh Sathyamoorthy, Anat Maoz, Zohar Pasternak, Hansol Im, Amit Huppert, Daniel Kadouri, and Edouard Jurkevitch. Bacterial predation under changing viscosities. *Environmental microbiology*, 21(8):2997–3010, 2019.

[142] Hansol Im, Heeun Kwon, Gayoung Cho, Jisoo Kwon, Seong Yeol Choi, and Robert J Mitchell. Viscosity has dichotomous effects on bdellovibrio bacteriovorus hd100 predation. *Environmental microbiology*, 21(12):4675–4684, 2019.

[143] Aruthur G LaMarre, Susan C Straley, and SF Conti. Chemotaxis toward amino acids by bdellovibrio bacteriovorus. *Journal of bacteriology*, 131(1):201–207, 1977.

[144] Susan C Straley and SF Conti. Chemotaxis in bdellovibrio bacteriovorus. *Journal of Bacteriology*, 120(1):549–551, 1974.

[145] Susan C Straley, Arthur G LaMarre, Lowell J Lawrence, and SF Conti. Chemotaxis of bdellovibrio bacteriovorus toward pure compounds. *Journal of bacteriology*, 140(2):634–642, 1979.

[146] Carey Lambert, Margaret CM Smith, and R Elizabeth Sockett. A novel assay to monitor predator–prey interactions for bdellovibrio bacteriovorus 109 j reveals a role for methyl-accepting chemotaxis proteins in predation. *Environmental Microbiology*, 5(2):127–132, 2003.

[147] Carey Lambert, Andrew K Fenton, Laura Hobley, and R Elizabeth Sockett. Predatory bdellovibrio bacteria use gliding motility to scout for prey on surfaces. *Journal of bacteriology*, 193(12):3139–3141, 2011.

[148] Susan C Straley and SF Conti. Chemotaxis by bdellovibrio bacteriovorus toward prey. *Journal of bacteriology*, 132(2):628–640, 1977.

[149] Michael W Davidson. Pioneers in optics: Zacharias janssen and johannes kepler. *Microscopy Today*, 17(6):44–47, 2009.

[150] Huib J Zuidervaart and Douglas Anderson. Antony van leeuwenhoek's microscopes and other scientific instruments: new information from the delft archives. *Annals of science*, 73(3):257–288, 2016.

[151] JR Porter. Antony van leeuwenhoek: tercentenary of his discovery of bacteria. *Bacteriological reviews*, 40(2):260–269, 1976.

[152] Zeiss. Education in microscopy and digital imaging: Zeiss microscopy online campus. `http://zeiss-campus.magnet.fsu.edu/articles/basics/kohler.html`. Accessed: 2019-05-30.

[153] Michael T Madigan and Martinko. *Brock biology of microorganisms 11th edn*. Upper Saddle Rive, NJ, Prentice Hall, 11 edition, 2006.

[154] Adam JM Wollman, Richard Nudd, Erik G Hedlund, and Mark C Leake. From animaculum to single molecules: 300 years of the light microscope. *Open biology*, 5(4):150019, 2015.

[155] Nikon. Microscopy u: The source for microscopy education. `https://www.microscopyu.com/`. Accessed: 2019-05-30.

[156] D.B. Murphy. *Fundamentals of Light Microscopy and Electronic Imaging*. Wiley, 2001.

[157] Michael L Davis, Leslie C Mounteer, Lindsey K Stevens, Charles D Miller, and Anhong Zhou. 2d motility tracking of pseudomonas putida kt2440 in growth phases using video microscopy. *Journal of bioscience and bioengineering*, 111(5):605–611, 2011.

[158] Roseanne M Ford and Ronald W Harvey. Role of chemotaxis in the transport of bacteria through saturated porous media. *Advances in Water Resources*, 30(6-7):1608–1617, 2007.

[159] Michael Morse, Remy Colin, Laurence G Wilson, and Jay X Tang. The aerotactic response of caulobacter crescentus. *Biophysical journal*, 110(9):2076–2084, 2016.

[160] Willow R DiLuzio, Linda Turner, Michael Mayer, Piotr Garstecki, Douglas B Weibel, Howard C Berg, and George M Whitesides. Escherichia coli swim on the right-hand side. *Nature*, 435(7046):1271–1274, 2005.

[161] Mingming Wu, John W Roberts, Sue Kim, Donald L Koch, and Matthew P DeLisa. Collective bacterial dynamics revealed using a three-dimensional population-scale defocused particle tracking technique. *Applied and environmental microbiology*, 72(7):4987–4994, 2006.

[162] Howard C Berg. How to track bacteria. *Review of Scientific Instruments*, 42(6):868–871, 1971.

[163] Roland Thar, Nicholas Blackburn, and Michael KuÃàhl. A new system for three-dimensional tracking of motile microorganisms. *Applied and Environmental Microbiology*, 66(5):2238–2242, 2000.

[164] G Corkidi, B Taboada, CD Wood, A Guerrero, and A Darszon. Tracking sperm in three-dimensions. *Biochemical and biophysical research communications*, 373(1):125–129, 2008.

[165] Mingming Wu, John W Roberts, and Mark Buckley. Three-dimensional fluorescent particle tracking at micron-scale using a single camera. *Experiments in Fluids*, 38(4):461–465, 2005.

[166] Matthew R Edwards, Rika Wright Carlsen, Jiang Zhuang, and Metin Sitti. Swimming characterization of serratia marcescens for bio-hybrid microrobotics. *Journal of Micro-Bio Robotics*, 9(3):47–60, 2014.

[167] KM Taute, S Gude, SJ Tans, and TS Shimizu. High-throughput 3D tracking of bacteria on a standard phase contrast microscope. *Nature communications*, 6(1):1–9, 2015.

[168] Evgeniya V Pankratova, Alena I Kalyakulina, Mikhail I Krivonosov, Sergei V Denisov, Katja M Taute, and Vasily Yu Zaburdaev. Chemotactic drift speed for bacterial motility pattern with two alternating turning events. *PloS one*, 13(1):e0190434, 2018.

[169] Marianne Grognot and Katja M Taute. A multiscale 3D chemotaxis assay reveals bacterial navigation mechanisms. *Communications biology*, 4(1):1–8, 2021.

[170] Nicola E Farthing, Rachel C Findlay, Jan F Jikeli, Pegine B Walrad, Martin A Bees, and Laurence G Wilson. Simultaneous two-color imaging in digital holographic microscopy. *Optics express*, 25(23):28489–28500, 2017.

[171] SK Jericho, P Klages, J Nadeau, EM Dumas, MH Jericho, and HJ Kreuzer. In-line digital holographic microscopy for terrestrial and exobiological research. *Planetary and Space Science*, 58(4):701–705, 2010.

[172] HJ Kreuzer and Manfred H Jericho. Holographic microscopy gives new tool for biology and microfluidics. *The International Society for Optical Engineering, SPIE Newsroom*, pages 1–4, 2006.

[173] Anna Wang, Rees F Garmann, and Vinothan N Manoharan. Tracking e. coli runs and tumbles with scattering solutions and digital holographic microscopy. *Optics express*, 24(21):23719–23725, 2016.

[174] Mehdi Molaei and Jian Sheng. Succeed escape: Flow shear promotes tumbling of escherichia colinear a solid surface. *Scientific reports*, 6(1):1–10, 2016.

[175] Rachel C Findlay, Mohamed Osman, Kirstin A Spence, Paul M Kaye, Pegine B Walrad, and Laurence G Wilson. High-speed, three-dimensional

imaging reveals chemotactic behaviour specific to human-infective leishmania parasites. *Elife*, 10:e65051, 2021.

[176] Katie L Thornton, Jaimi K Butler, Seth J Davis, Bonnie K Baxter, and Laurence G Wilson. Haloarchaea swim slowly for optimal chemotactic efficiency in low nutrient environments. *Nature communications*, 11(1):1–9, 2020.

[177] Dennis Gabor. A new microscopic principle. *Nature*, 161:777–778, 1948.

[178] Nobel Prize Outreach. The nobel prize in physics 1971. `https://www.nobelprize.org/prizes/physics/1971/summary/`. Accessed: 2022-02-08.

[179] TH Maiman. Stimulated optical radiation in ruby. *Nature*, 4736:493–494, 1960.

[180] V Michael Bove and Nicole A Reader. Holography and the luxury industry. In *Photonics*, volume 8, page 219. Multidisciplinary Digital Publishing Institute, 2021.

[181] Sam Davies, Yubing Hu, Nan Jiang, Jeff Blyth, Monika Kaminska, Yunzheng Liu, and Ali K Yetisen. Holographic sensors in biotechnology. *Advanced Functional Materials*, 31(47):2105645, 2021.

[182] Myung K Kim. Principles and techniques of digital holographic microscopy. *SPIE reviews*, 1(1):018005, 2010.

[183] D Gabor. Dennis gabor - nobel lecture. `https://www.nobelprize.org/uploads/2018/06/gabor-lecture.pdf`. Accessed: 2022-02-10.

[184] Camila B Giuliano, Rongjing Zhang, and Laurence G Wilson. Digital inline holographic microscopy (dihm) of weakly-scattering subjects. *JoVE (Journal of Visualized Experiments)*, (84):e50488, 2014.

[185] F Saglimbeni, S Bianchi, A Lepore, and R Di Leonardo. Three-axis digital holographic microscopy for high speed volumetric imaging. *Optics express*, 22(11):13710–13718, 2014.

[186] Andreas Erik Gejl Madsen, Mohammad Aryaee Panah, Peter Emil Larsen, Frank Nielsen, and Jesper Glückstad. On-axis digital holographic microscopy: Current trends and algorithms. *Optics Communications*, page 129458, 2023.

[187] Sang-Hyuk Lee, Yohai Roichman, Gi-Ra Yi, Shin-Hyun Kim, Seung-Man Yang, Alfons Van Blaaderen, Peter Van Oostrum, and David G Grier. Characterizing and tracking single colloidal particles with video holographic microscopy. *Optics express*, 15(26):18275–18282, 2007.

[188] Laurence Wilson. Wilson lab website: Biophysical imaging and spectroscopy. `https://sites.google.com/a/york.ac.uk/bis_lab/research-techniques/eukaryotes-and-holography`. Accessed: 2022-02-10.

[189] Laurence Wilson and Rongjing Zhang. 3D localization of weak scatterers in digital holographic microscopy using rayleigh-sommerfeld back-propagation. *Optics Express*, 20(15):16735–16744, 2012.

[190] Marco J Kühn, Felix K Schmidt, Nicola E Farthing, Florian M Rossmann, Bina Helm, Laurence G Wilson, Bruno Eckhardt, and Kai M Thormann. Spatial arrangement of several flagellins within bacterial flagella improves motility in different environments. *Nature communications*, 9(1):1–12, 2018.

[191] Zhaoning Zhang, Yujie Wang, Rafael Piestun, and Zhen-Li Huang. Characterizing and correcting camera noise in back-illuminated scmos cameras. *Optics Express*, 29(5):6668–6690, 2021.

[192] Sang-Hyuk Lee and David G Grier. Holographic microscopy of holographically trapped three-dimensional structures. *Optics Express*, 15(4):1505–1512, 2007.

[193] Carey Lambert and R Elizabeth Sockett. Laboratory maintenance of bdellovibrio. *Current protocols in microbiology*, 9(1):7B–2, 2008.

[194] Howard C Berg. *E. coli in Motion*. Springer, 2004.

[195] Jonathan Saragosti, Pascal Silberzan, and Axel Buguin. Modeling e. coli tumbles by rotational diffusion. implications for chemotaxis. *PloS one*, 7(4):e35412, 2012.

[196] John F Staropoli and Uri Alon. Computerized analysis of chemotaxis at different stages of bacterial growth. *Biophysical Journal*, 78(1):513–519, 2000.

[197] Uri Alon, Laura Camarena, Michael G Surette, Blaise Aguera y Arcas, Yi Liu, Stanislas Leibler, and Jeffry B Stock. Response regulator output in bacterial chemotaxis. *The EMBO journal*, 17(15):4238–4248, 1998.

[198] Nicholas C Darnton, Linda Turner, Svetlana Rojevsky, and Howard C Berg. On torque and tumbling in swimming escherichia coli. *Journal of bacteriology*, 189(5):1756–1764, 2007.

[199] Miqiu Kong, Yan Wu, Guangxian Li, and Ronald G Larson. A bead-spring model for running and tumbling of flagellated swimmers: Detailed predictions compared to experimental data for e. coli. *Soft Matter*, 11(8):1572–1581, 2015.

[200] Jananee Jaishankar and Preeti Srivastava. Molecular basis of stationary phase survival and applications. *Frontiers in microbiology*, 8:2000, 2017.

[201] Juana María Navarro Llorens, Antonio Tormo, and Esteban Martínez-García. Stationary phase in gram-negative bacteria. *FEMS microbiology reviews*, 34(4):476–495, 2010.

[202] Hideki Makinoshima, Shin-Ichi Aizawa, Hideo Hayashi, Takeyoshi Miki, Akiko Nishimura, and Akira Ishihama. Growth phase-coupled alterations in cell structure and function of escherichia coli. *Journal of bacteriology*, 185(4):1338–1345, 2003.

[203] CD Amsler, Myungsun Cho, and P Matsumura. Multiple factors underlying the maximum motility of escherichia coli as cultures enter post-exponential growth. *Journal of Bacteriology*, 175(19):6238–6244, 1993.

[204] Karen A Morehouse, Laura Hobley, Michael Capeness, and R Elizabeth Sockett. Three motab stator gene products in bdellovibrio bacteriovorus contribute to motility of a single flagellum during predatory and prey-independent growth. *Journal of bacteriology*, 193(4):932–943, 2011.

[205] Nazli Maki, Jason E Gestwicki, Ellen M Lake, Laura L Kiessling, and Julius Adler. Motility and chemotaxis of filamentous cells of escherichia coli. *Journal of Bacteriology*, 182(15):4337–4342, 2000.

[206] Li Xie, Tuba Altindal, Suddhashil Chattopadhyay, and Xiao-Lun Wu. Bacterial flagellum as a propeller and as a rudder for efficient chemotaxis. *Proceedings of the National Academy of Sciences*, 108(6):2246–2251, 2011.

[207] Tuba Altindal, Li Xie, and Xiao-Lun Wu. Implications of three-step swimming patterns in bacterial chemotaxis. *Biophysical Journal*, 100(1):32–41, 2011.

[208] Marianne Grognot, Anisha Mittal, Mattia Mah‚Äômoud, and Katja M Taute. Vibrio cholerae motility in aquatic and mucus-mimicking environments. *Applied and Environmental Microbiology*, 87(20):e01293–21, 2021.

[209] Rajesh Sathyamoorthy, Yuval Kushmaro, Or Rotem, Ofra Matan, Daniel E Kadouri, Amit Huppert, and Edouard Jurkevitch. To hunt or to rest: prey depletion induces a novel starvation survival strategy in bacterial predators. *The ISME Journal*, 15(1):109–123, 2021.

[210] Shashank Kamdar, Seunghwan Shin, Premkumar Leishangthem, Lorraine F Francis, Xinliang Xu, and Xiang Cheng. The colloidal nature of complex fluids enhances bacterial motility. *Nature*, 603(7903):819–823, 2022.

[211] Jonathan Leach, H Mushfique, S Keen, R Di Leonardo, G Ruocco, JM Cooper, and MJ Padgett. Comparison of Faxens correction for a microsphere translating or rotating near a surface. *Physical Review E*, 79(2):026301, 2009.

[212] Julia A Schwartzman, Ali Ebrahimi, Grayson Chadwick, Yuya Sato, Benjamin RK Roller, Victoria J Orphan, and Otto X Cordero. Bacterial growth in multicellular aggregates leads to the emergence of complex life cycles. *Current Biology*, 32(14):3059–3069, 2022.

[213] Miles C Duncan, John C Forbes, Y Nguyen, Lauren M Shull, Rebecca K Gillette, David W Lazinski, Afsar Ali, Robert MQ Shanks, Daniel E Kadouri, and Andrew Camilli. Vibrio cholerae motility exerts drag force to impede attack by the bacterial predator bdellovibrio bacteriovorus. *Nature communications*, 9(1):1–9, 2018.

[214] Meiting Chen, Ziyi Zhao, Jin Yang, Kai Peng, Matthew AB Baker, Fan Bai, and Chien-Jung Lo. Length-dependent flagellar growth of vibrio alginolyticus revealed by real time fluorescent imaging. *Elife*, 6:e22140, 2017.

[215] David Freedman and Persi Diaconis. On the histogram as a density estimator: L 2 theory. *Zeitschrift für Wahrscheinlichkeitstheorie und verwandte Gebiete*, 57(4):453–476, 1981.